Trinity College Dublin
Coláiste na Tríonóide, Baile Átha Cliath
The University of Dublin

The Role of Contemporary CO_2 Sublimation as a Geomorphic Agent on Mars

by

Lauren Eve Mc Keown

A thesis submitted in partial fulfilment for the degree of Doctor of Philosophy

in the

School of Natural Sciences

supervised by

Dr. Mary Bourke

September 2019

Declaration of Authorship

I, Lauren Mc Keown, declare that this thesis titled, 'The Role of Contemporary CO_2 Sublimation as a Geomorphic Agent on Mars' has not been submitted as an exercise for a degree at this or any other university and it is entirely my own work.

I agree to deposit this thesis in the University's open access institutional repository or allow the library to do so on my behalf, subject to Irish Copyright Legislation and Trinity College Library conditions of use and acknowledgement. I confirm:

- This work was done wholly while in candidature for a research degree at this University.
- Where I have consulted the published work of others, this is always clearly attributed.
- Where I have quoted from the work of others, the source is always given. With the exception of such quotations, this thesis is entirely my own work.
- I have acknowledged all main sources of help.
- Where the thesis is based on work done by myself jointly with others, I have made clear exactly what was done by others and what I have contributed myself.

Signed: _____

Date: _____

"Do what is necessary to be resilient. You will get knocked down. What matters is that you get back up."

Hillary Rodham Clinton

Abstract

The Martian surface is geomorphologically active, with a variety of mass–wasting, erosional and depositional features that form and change in the current climate. Many of these features have analogues on Earth (e.g. Alcove–Channel–Apron (ACA) gullies, dust devil tracks) and therefore there is a long history of observational studies of the processes which may have shaped them. Conversely, some features differ from Terrestrial scales and morphologies and others are completely unlike any seen on Earth. These include linear dune gullies, the dendritic araneiform terrain and associated fans and spots of the southern high latitudes and the faint sand furrows etched across polar dunes. All of these features have been attributed to seasonal carbon dioxide sublimation. While elegant numerical and conceptual models have attempted to elucidate their specific formation mechanisms, the dynamics of CO_2 sublimation and its interaction with sediment is still weakly understood. This thesis chronicles a four year long campaign to provide for the first time, quantitative empirical data on CO_2 sublimation and its interaction with granular material. This work documents and quantifies sediment mobilisation styles and morphological change when a granular bed is subject to CO_2 sublimation and sand furrows, pits and araneiforms develop. A survey of high resolution images and topographic models of morphologically analogous features on Mars is presented and laboratory results are synthesised in the context of the Martian scale. This work subsumes a rigorous tool which can be used by future studies to advance our understanding of the Martian surface and the processes which shape it today and concludes that CO_2 sublimation is an efficient and dynamic agent of change to the contemporary Martian surface over short timescales.

Acknowledgements

This PhD has been the most challenging but formative journey I have experienced in my life and therefore I don't think a brief Acknowledgements section would communicate all that I want to say. Apart from broadening my knowledge on the Martian environment and stimulating my passion for its active surface processes in a country where planetary science is only emerging, the greatest gift this PhD has given me has been that of personal growth. I went from a self–deprecating student who really did not believe in herself very much and definitely could not give a talk even to a room of close peers, to someone capable of speaking confidently to a room of NASA scientists about her recently published Nature journal paper.

I have my supervisor, Dr. Mary Bourke to thank for all of this and I am not sure what words I can place on paper to describe my gratitude for her guidance and unwavering support throughout this PhD. Mary's challenging but omnipresent encouragement transformed who I am as a person. I approached her in 2014 after my supervisor in Physics left the university and she gave me a chance to retrain in geomorphology. I look back on that awful period of uncertainty and panic now and see it truly as a blessing in disguise. A Ph.D. is never worth it unless you are totally committed to the subject and are passionate about what you do. Mary afforded me the opportunity to study what I have always wanted to study in my home country and I am eternally grateful for that. I am sure my sensitivity has been difficult to manage, but I know that beneath it all she accepts me for who I am. Her endless encouragement, belief in and respect for me and my (oftentimes ambitious!) thoughts, were blessings I am not sure where I would be today without. As well as a supervisor, she has been a friend I can count on 100%. Mary is the greatest role model I have been fortunate to meet in my career thus far and it has been an honour and pleasure to work under her guidance.

Along with my supervisor, I would like to thank my parents who have believed in me from day one. At age 13 when I expressed an interest in planetary science, my Mom arranged a private tour of Kennedy Space Center for me while on a family holiday and since then, I have been fascinated by planetary science. My parents have been stalwart supporters of my ambitions and always taught me I can be anything I want to be if I just try hard enough. Through the many tough times during the last five years, my Mom has been my number one source of support, advice or a lending ear and I am so fortunate that she has not gotten fed up listening to me by now. Dad would and has drop(ped) everything to be there when I have needed him and I am very grateful for that. I would also like to thank my Aunts Therese and Nancy for their continuous support and belief in me. Therese and Nancy are family. They once dropped everything and flew to California to be with me during a difficult time and I will never, ever forget that. I thank my sister for her humour and company and the rest of my extended family for their support throughout the years. In particular, I remember the strong influence my late grandparents had on my development, with Grandma teaching me to read, write and paint at an early age and Papa sparking my imagination with stories - one about a spider, funny that I ended up working on 'spiders on Mars!'.

I have been fortunate to meet some incredible people within the planetary science community whose companionship, advice and support has not gone unnoticed. I would like to thank my colleagues at the Open University, in particular Frances and Jack who have provided support, lifted me up when down and are always encouraging of me. I know you will be lifelong conference buddies at the annual LPSC and I'm grateful that our shared love of the inner planets has brought us together. To all of my UK colleagues Chris, Laura, Peter, Joel, Rhian, Susan, Matt B. et al. thank you also for some wonderful conference memories and interesting discussions! Here's to many more. To Pete, my new mentor - thank you for trusting me to transition to a slightly new area of planetary science, and for being a totally supportive manager who is a pleasure to work for! Matt S. and his wife Onedia - thank you for giving me

a place to stay when completing my experiments. It has been wonderful getting to know you both and my two furry friends across the pond. I am grateful to Manish for letting me overstay my welcome at the Open University Mars Simulation Chamber when I got excited with more ideas to explore and so kindly providing the funding for me to do so. I am grateful to my co–supervisor, Jim for lending his expertise and for all of his compassion, encouragement and input during the review process of my first paper. I very much enjoyed our time working in the lab in Arizona and the U.K. together. In particular I'd like to thank Richard for always checking in on me and seeing how my writing is going. I would also like to thank Serina who has been a great source of guidance and encouragement to me. Serina kindly took the time to review Chapter 3 and 6 of this thesis and to lend her expertise where necessary.

I am grateful to the Irish Research Council for funding this PhD (project 204432, award 13626) as well as my internship at NASA Ames. Their support has opened many doors for me and the opportunities they have given me have been incredible. I thank Europlanet for giving me the opportunity to perform the experiments detailed in this thesis at the Open University Mars Simulation Chamber. Additionally, I am grateful to the Planetary Science Institute for awarding me the Pierazzo International Student Travel Award which gave me the platform to present my research at the 49th annual Lunar and Planetary Science Conference in March of 2018.

To the friends that never left me when I wasn't so freely available, when I was writing through the night and when I wasn't very much myself–thank you. To those that did–thank you for teaching me to love myself first.

Sam, who despite the small obstacle of the Irish Sea, has managed to check in almost every day, thank you for being my twin soul and a shining light in my life. You have the most beautiful heart. Sam went as far as to send a care package over to me with

little notes of encouragement on the second round of major revisions of my first paper. Julie, who is a little further away in France, thank you for all of the long chats and for believing in me since we were four years old. You know me better than I know myself and so it has been so helpful to get your perspective on any difficulties I may have faced while conducting this research. Killian, you could rival Julie in knowing me better than myself. Thank you for being a true, honest and dedicated friend. Scott, thank you for the deep chats, endless belief in me and for the giggles. I have never come away from seeing you not feeling remarkably better than before I met with you. Mark - possibly one of my greatest champions. Thanks for always believing in me. I could write a thesis with all of our Whatsapp voice messages musing about trying to improve science communication and various other things. Ashling, I am so glad we have grown so close this year. We are so alike and I adore spending time with you. Thank you for always being there when I need you and for talking sense into me when I am thinking the worst. Olwyn, a true friend since secondary school who no matter how long it has gone since we have seen each other, it never feels like time has passed. Thank you as always for your support. Britt and Stephen; two wonderful friends who have only come into my life recently but have been so supportive. Thank you for trusting me to teach at Paint by the Pints and encouraging me to pursue a hobby which has been dormant for the last few years. You have given me the courage to teach art to rooms of people, something I never dreamt possible only last year. Exciting times ahead for you both - I can't wait! Dan, thank you for your support and just even for the lovely foodie times we have shared over the last few years – especially the times where you have cooked for me. Orla, thank you for being a true friend I can rely on and for the evenings we have shared watching terrible documentaries. Joe, thank you for being a source of wisdom and support during my PhD, having gone through the process yourself. To the rest of my undergraduate group of friends; Dani, Tian, Cormac, Conor, et al., thank you for providing humour, fun and banter. To the friends I met through my year in the Trinity Astrophysics Research Group–thank you for all the fun and mutual rants about PhD life over pints of a Friday in Kennedy's.

Going through a disaster of a first PhD attempt in physics was worth it, if only to have met you guys. I loved handing in this thesis with Aoife and cannot wait to graduate together. To my friends across the atlantic–KP, Josie and Alex; it is always a pleasure to stop by on the way to conferences. These friends were truly wonderful to have around during my internship at NASA Ames which unfortunately was also a very difficult personal time. I am grateful to my NASA supervisors Dr. Yuri Griko and Dr. Chris McKay and to Desi Bridges for their guidance and encouragement to follow my dreams of one–day working at NASA. Conor, you were there for me through some of the most difficult periods of my life when we were interning at Ames and ever since you have been a friend that never fails to check in on me, even when I'm so terrible at contact. I would like to thank my colleagues in the Earth and Planetary Surface Processes Group–Niamh and Ankit, who it has been great to go through this journey with. I am also so grateful to my friends and colleagues in the Department of Geography–particularly Maria–Teresa and Chris with whom I have grown so close to in the last couple of years. This PhD experience has been made so much better having you around. To my flatmate and incredibly good friend Duncan, thank you for making my time post-PhD and the move to Cambridge so memorable. To new friends who I feel I've known a lot longer - especially Nadine - thank you for making me feel like Cambridge is home, for being a wonderful friend and for encouraging me to finish the edits on this thesis!

To the people who I wish I could mention here, who have encouraged me, celebrated with me and cheered me on through even small milestones, you know who you are. I miss you, I think of you often and I thank you.

To Leo, who was introduced to the Mc Keown family household early in 2016 as a very timid, anxious rescue dog, thank you for trusting us, for being my best friend and for bringing our family so much joy. You don't know what a PhD is, but thank

you for sitting at my feet at 5am while I was making edits on my first paper and providing writing break cuddles despite me keeping you from sleeping. You have been a source of support I never knew was possible from an animal. I hope that one day I can pay you back with enough walks and treats.

Humour and cuteness aside, the completion of this thesis would not be possible without the support systems available at Trinity College Dublin. A formal acknowledgements section may not be the most conventional place to be so open, but I really want to thank all of the people who got me here and leave no stone unturned in doing so. I am so grateful to the Student Counselling Service for their endless support– in particular Mark, Helen and the ongoing group. These strangers–turned friends were my cheerleaders when coping with a year of negative review comments on my first paper. I owe a lot of that first paper (which is now framed on my wall!) to their tireless encouragement and I feel we got there together. More than anything, I want to thank these wonderful compassionate, empathetic people for teaching me that personal worth is not measured by grades or publications and for guiding me on a continuous journey to loving myself more than someone who is only valuable if they attain the near–unattainable. I would like to thank Martin from the Postgraduate Advisory Service for all of his support with the obstacles in completing the final chapter of this thesis. In particular I want to thank Sandra whose advice, kindness and understanding throughout the last few months has taken me from a place of wanting to give up on my PhD entirely last November to submitting this thesis. Sandra–who had never even met me months ago, has insisted on meeting me just before handing in this thesis for a celebratory cup of tea.

I want to take this opportunity to urge any PhD student who may ever read this thesis to use the resources available to you and to be kind to yourself. Academic people often place a large amount of self worth on academic success and at the top where

rejections, pitfalls and disappointments are all part and parcel of PhD life, that is a very risky game. I don't know a peer at postgraduate level who has not needed strong emotional support at some point. It's normal. This thesis was written during some of the toughest months of my life personally and so I want to thank the tiny reserve of strength I had left within me that got me over the line. PhD life is tough, but even tougher when life outside of it isn't exactly a reprieve from the work. On that note, I am extremely grateful to my research topic itself which at one point kept me moving forward. I feel so lucky to have pursued a topic I love and am so passionate about and I hope the essence of this thesis communicates that.

Contents

List of Figures

List of Tables

Abbreviations

HiRISE	**H**igh **R**esolution **I**maging **S**cience **E**xperiment
MOC	**M**ars **O**rbiter **C**amera
MRO	**M**ars **R**econnaissance **O**rbiter
DTM	**D**igital **T**errain **M**odel (3D model of Martian surface)
DEM	**D**igital **E**levation **M**odel (3D model of lab-scale surface)
SfM	**S**tructure **f**rom **M**otion
OMEGA	**O**bservatoire pour la **M**inéralogie, l'**E**au, les **G**laces et l'**A**ctivité
SHARAD	**SHA**llow **RAD**ar sounder
CRISM	**C**ompact **R**econnaissance **I**maging **S**pectrometer for **M**ars
MY	**M**ars **Y**ear
DLA	**D**iffusion **L**imited **A**ggregation
MOLA	**M**ars **O**rbiter **L**aser **A**ltimeter

Physical Constants

Acceleration due to Gravity on Earth	g	=	$9.81\,ms^{-2}$
Acceleration due to Gravity on Mars	g_M	=	$3.71\,ms^{-2}$

Symbols

$\mu\, m$	$1 \times 10^{-6}\, m$
CO_2	Carbon Dioxide
H_2O	Water

For my Mom. My best friend, greatest confidante and unwavering champion on completing this thesis. Thank you for believing in me even when I didn't believe in myself.

Chapter 1

Introduction

1.1 Scope of the Thesis

Sublimation of the seasonal carbon dioxide (CO_2) ice deposit is recognised as an active and dynamic driver of surface modification on Mars today. Linear gullies of the southern mid–latitudes, sand furrows ubiquitous on northern hemisphere dunes and araneiform terrain native to the southern polar region have all been proposed to form by the action of sublimating CO_2 ice (Bourke, 2013; Diniega et al., 2013; Kieffer et al., 2006; Piqueux et al., 2003). However, though the theoretical framework for these processes is well–developed, there is a paucity of empirical evidence to support models of CO_2 sublimation.

This thesis seeks to advance our present understanding of the role of sublimating carbon dioxide ice as a geomorphic agent on Mars. The central research question motivating this work is; can sublimating CO_2 ice interact with granular material to form features morphologically similar and are their morphometries scalable to those that are active on Mars today?

1.2 Structure and Layout

This thesis is structured around three published or submitted first–authored research papers. Chapter Two reviews the literature surrounding CO_2 sublimation studies with regard to active surface features on Mars and specifically discusses research campaigns which contextualise the research presented in this thesis. The aims and associated objectives of the work contained in this thesis are outlined in Chapter Two. Chapters Three, Four and Five have been prepared for publication in selected academic journals and therefore the abstract, introduction and conclusion of each of these core chapters are self-contained. Chapter Six synthesises the over–arching findings of the research and discusses the wider implications of the findings to the study of carbon dioxide

sublimation on Mars as an agent of geomorphic change. This conclusion chapter also highlights open questions the state of the art has not yet answered which will motivate future work.

1.3 Author Contributions

The three research chapters presented in this thesis (3-5) are based on published or submitted academic papers and therefore are co–authored. The author of this thesis led each research effort and wrote each of these chapters in its entirety. All co–authors contributed to editing and revising the original draft in each case and specific individual contributions are outlined below.

1.3.1 Chapter 3: Experiments On Sublimating Carbon Dioxide Ice And Implications For Contemporary Surface Processes On Mars

Status: **published** in Nature *Scientific Reports*.

Authors: Mc Keown, L.E., Bourke, M.C., McElwaine, J.N.

Contributions: L.E.M. wrote the main chapter text with significant input from M.C.B. and J.N.M. J.N.M. completed the calculations discussed in "Experimental Scaling". A pilot laboratory experimental approach was conceived by M.C.B. and J.N.M. and was designed by J.N.M. The low humidity environment employed in the laboratory experiments reported in this chapter was designed by L.E.M. and M.C.B. L.E.M. conceived the idea of displacing air within the chamber with CO_2 gas to minimise humidity. M.C.B. conceived the idea of using a sealed, low humidity environment and suggested the equipment with which to monitor humidity and block sublimation. Experiments were performed by L.E.M. DEMs were developed by L.E.M. Experimental analysis was completed through input from all authors, with a significant contribution

from M.C.B. on furrow analysis. The hypothesis for detached pit formation at linear gully termini was conceived by L.E.M. All figures and plots were prepared by L.E.M. Table 3.1 and Table 3.2 were prepared by J.N.M. All authors contributed to the ideas discussed and the preparation of the chapter.

1.3.2 Chapter 4: The Formation of Araneiforms by Carbon Dioxide Venting and Vigorous Sublimation Dynamics Under Martian Conditions

Status: **Under peer review** at Nature *Scientific Reports*.

Authors: Mc Keown, L.E., Bourke, M.C., McElwaine, J.N., Sylvest, M.E., Patel, M.R.

Contributions: L.E.M., M.C.B. and J.N.M. developed the research aims, objectives and methodology involved in the experiments. L.E.M. carried out the experiments with extensive input from M.E.S and M.R.P. M.E.S. conceived the idea and constructed the pulley used to lower the CO_2 blocks. M.E.S. and M.R.P. led chamber operation and maintenance. Table 4.1 and the plots in Figure 4.3 were developed by L.E.M. Analysis of araneiform morphometry was carried out by L.E.M. with significant input from M.C.B. L.E.M wrote this chapter with input from all authors.

1.3.3 Chapter 5: Morphometric Trends and Implications for the Formation of Araneiforms

Status: **submitted** to *Icarus*

Authors: Mc Keown, L.E., Bourke, M.C.

Contributions: L.E.M. wrote the chapter with input from M.C.B. L.E.M. conducted the HIgh Resolution Imaging Science Experiment (HiRISE) survey of araneiforms.

L.E.M. analysed the data and generated the plots in Figures 5.3 and 5.4 and all figures. L.E.M. illustrated the schematic which classifies araneiforms in Figure 5.1.

Chapter 2

Chapter 2: A Review of Martian Sublimation Geomorphology

2.1 An Overview of Mars

The planet Mars has long been a source of great attraction for scientific exploration, with its earliest reputed observation dating back to Ancient Greece when Aristotle described an occultation of Mars by the Moon. Present–day studies of the planet now benefit from decades of orbital data collected on the Martian environment. Mars (Figure 2.1) is currently occupied by seven operational remote sensing platforms. These include six orbiters; ESA's ExoMars Trace Gas Orbiter (TGO) and Mars Express (MEx), NASA's Mars Atmosphere and Volatile EvolutioN (MAVEN), 2001 Mars Odyssey and Mars Reconnaissance Orbiter (MRO), the Indian Space Agency's Mars Orbiter Mission (MOM) and one rover; NASA's Mars Science Laboratory (Curiosity). Collectively, these missions have returned datasets which have led to a deeper understanding of present and past Martian geology, surface processes, orbital mechanics and atmospheric dynamics and composition. The following introductory section reviews the Martian environment as studied by this team of instruments and their predecessors. This thesis homes in on the very present day environment on Mars, and thus the review of the geological history of the planet is non-exhaustive and serves to place the study area of present-day surface activity, along with CO_2 sublimation into context.

The advent of high resolution multi–wavelength imagery of the Martian surface (Malin and Edgett, 2001; McEwen et al., 2007) revealed that the surface of Mars preserves signals of a complex geological, atmospheric and climatic past. Observations showed a surface defined by a complicated stratigraphy, comprising a patchwork of layered surfaces of different ages (Christensen et al., 2003), each a vestige of relic climatic conditions on Mars. Based on mapping of geological terrains and crater density counting, Martian geochronology is divided into three main epochs; the Noachian, Hesperian and Amazonian periods (Scott and Carr, 1978). The Noachian (4.1-3.7 Ga) represents a period of heavy bombardment by asteroids and comets, creating the largest

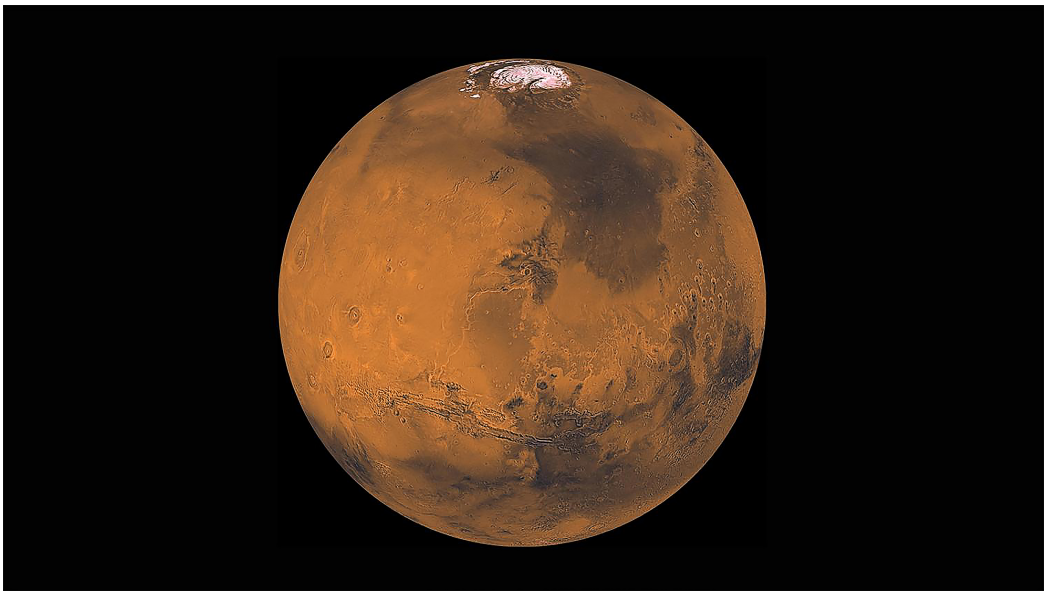

FIGURE 2.1: Mars as viewed by the Viking orbiter. Source: NASA/JPL/Caltech

impact structures seen on Mars today; the Hellas, Argyre and Isidis basins. Also pertinent to this period was the loss of the Martian magnetosphere after its interior cooled and its magnetic dynamo slowed down $\sim 4\,Ga$ (Acuña et al., 1999) leaving the planet vulnerable to much of its ionosphere being stripped over time (Jakosky et al., 2018). The Noachian was a period of intense volcanic activity, and a putatively warm and wet environment, represented today by imprints of valley networks, lakes, and even a debated ocean in the Northern hemisphere. Home to Olympus Mons, the largest shield volcano in the Solar System, the northern plains house regions which are sheathed by lava flows. The Martian crust in the northern lowlands is dramatically lower by 1-3 km than the southern rugged, cratered highlands. This *Martian dichotomy* is likely to have arisen from an early giant impact (Andrews-Hanna et al., 2008).

During the Hesperian (3.7-2.9 Ga), volcanic activity continued, reworking about 30% of the Martian terrain. The climate became colder, and it is thought that much of the water became frozen as permafrost or sequestered ice deposits. Despite this, subsurface ice was released catastrophically through heating during bombardment, resulting in outflow channels such as those in Hellas Planitia. The Amazonian (2.9 Ga-present)

period experienced less violent activity in comparison, defined by aeolian or wind activity eroding and depositing material in the form of polar dunes and sand seas and recent glaciation, resulting in the emplacement of water-rich mantling deposits equatorward (Conway, S.J. and Mangold, N., 2013; Head et al., 2003). The Amazonian time period is also represented by putatively periglacial activity; for example within the Utopia Planitia basin in the northern hemisphere, lie candidate pingos (Burr et al., 2009; Soare, R.J. and Conway, S.J. and Williams, J.-P. and Gallagher, C. and Mc Keown, L.E., 2019), polygonally patterned ground (Soare, R.J. and Conway, S.J. and Godin, E. and Hawkswell, J. and Osinski, G. and Bina, A., 2018) and scalloped terrain hypothesised to have formed by permafrost degradation (Lefort et al., 2009; Morgenstern et al., 2007; Séjourné et al., 2012).

The Martian north and south poles are covered by permanent ice caps which too, are thought to have modified in extent and composition over time. Both are comprised mainly of water ice (Byrne and Ingersoll, 2003; Kieffer et al., 1976). However, the caps are compositionally distinct in that the south polar ice deposits are topped by a residual layer of CO_2 (Kieffer, 1979; Leighton and Murray, 1966) which is 2–10 m thick (Byrne and Ingersoll, 2003; Thomas et al., 2000) and is concentrated between 84° S and 89° S latitude, and between 220° E and 50° E longitude. Together, these are native to a general region known as the South Polar Layered Deposits (SPLD). Mars Orbiter Camera (MOC) images showed that the polar regions differ vastly in metre to decametre–scale morphology between hemispheres, again indicative of a difference in recent climate history (Thomas et al., 2000). The North Polar Layered Deposits (NPLD) are landscaped by pitted and rugged buttes while the SPLD display a vast array of surface expressions including a pattern of circular depressions among arcuate mesas known as "Swiss Cheese Terrain" (Malin et al., 2001). The km-thick polar ice caps contain thousands of distinct layers, which are thought to represent periodic variations in climate.

Although relative timelines of the formation of distinct features are difficult to constrain observationally without wide uncertainty margins, modelling efforts have provided a potential conciliation with these morphological signatures of climate change on Mars. The main orbital parameters that concern climate change on Mars are eccentricity and obliquity. Eccentricity concerns the level of deviation of a body's orbit from circular (e=0) to elliptical (e<1). Obliquity is defined as the angle between a body's orbital axis and its rotational axis, otherwise known as axial tilt. Mars lacks a large moon to stabilise it, so over the course of history, the planet has been subjected to perturbations induced mainly by the relatively massive and nearby Jupiter, causing its obliquity and eccentricity to vary much more than those of the Earth. Models of climate forcing on Mars have revealed a complicated history of Martian orbital mechanics whereby over 5Ga, the planet's chaotic obliquity has increased from 0°–82° (Laskar et al., 2004). In just the past 5 Ma, the obliquity of Mars has changed by 10-15° and orbital eccentricity varied from 0 to 0.12 (Laskar, J. and Robutel, P., 1993; Touma and Wisdom, 1993). Such excursions of orbital parameters would have governed the global distribution and seasonal intensity of solar insolation over time, inducing considerable variations in climate and hence the extent of the polar caps (Ward et al., 1974). As obliquity increased, insolation receipt at the poles would have increased. As obliquity reduced, the poles received less insolation. A diagram of the predicted effect on the polar caps with changing obliquity is included in Figure 2.3 (Forget et al., 2017).

Mars today is cold and dry, with diurnal temperatures near the equator ranging from 293 K to 223 K (Gómez-Elvira et al., 2014) and average atmospheric pressure ranges between 6.5 and 10 mbar (Hess et al., 1979). The present-day rarefied Martian atmosphere is comprised predominantly of $\sim$ 96% CO_2, with 1.93% Ar, 1.89% N and trace gases including water and oxygen (Nier and McElroy, 1977). Much like Earth, Mars experiences seasons due to its axial tilt of 25.19° with respect to its spin axis. However, the seasonal interchanges between the Martian atmosphere and its surface

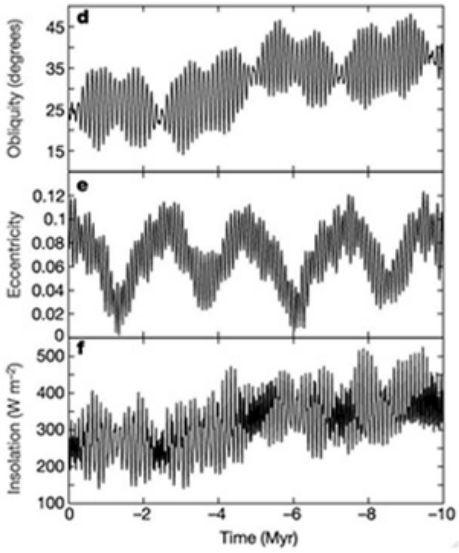

FIGURE 2.2: Variations in obliquity, eccentricity and insolation receipt over time on Mars. Source: Mars Climate Group, adapted from Laskar et al. (2004)

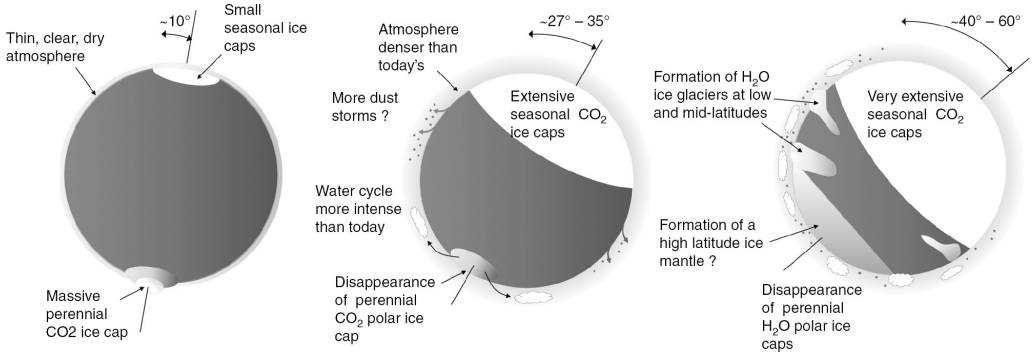

FIGURE 2.3: Quasi-periodic climate change on Mars. Diagram source: Forget et al. (2017)

are far removed from those on Earth. Current climate conditions are not conducive to sustaining any of the Martian atmospheric volatiles in their liquid phase (Figures 2.5, 2.6), and thus phase changes are restricted to those between solid and gas. During the Martian winter, a layer of CO_2 ice blankets both perennial polar ice caps and the terrain surrounding them in thicknesses ranging from the metre scale poleward (Aharonson et al., 2004; Nier and McElroy, 1977) to a few millimetres down to latitudes between $\sim 30 - 50°$ (Mangold, 2011). In the spring, this seasonal ice layer converts from ice to gas and is returned to the Martian atmosphere in a process known as the CO_2 cycle.

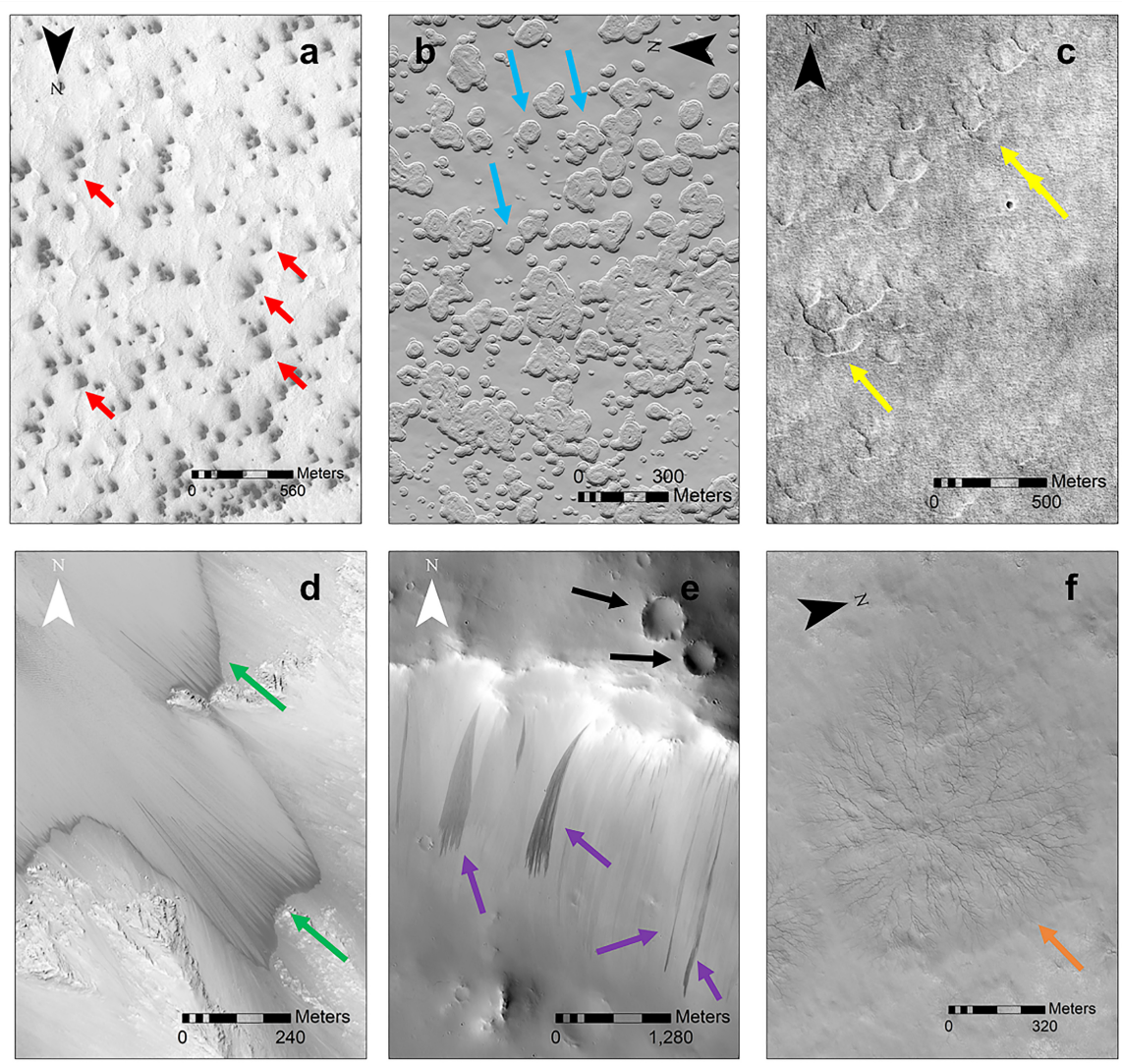

FIGURE 2.4: The dynamic Martian surface: examples of surface features on Mars. (a) HiRISE image *ESP*_011351_0945 shows dark fans on ice in the high southern latitudes at lat = −85.22°, lon = 181.55°, taken at L_s = 181.2°. Red arrows indicate implied wind direction. (b) HiRISE image *ESP*_012271_0940 shows swiss cheese terrain at lat = −85.95°, lon = 272.9°, taken at L_s = 224.0°. Blue arrows point to flat–floored depressions. (c) HiRISE image *ESP*_019884_2305 shows scalloped terrain (yellow arrows) at lat = 49.43°, lon = 90.04°, taken at L_s = 169.0°. (d) HiRISE image *ESP*_034830_1835 shows Recurring Slope Linae (RSL) at lat = −12.93°, lon = 295.42°, taken at L_s = 70.0°. Green arrows point to RSL. (e) HiRISE image *ESP*_012410_1835 shows dark slope streaks (purple arrows) in Arrabia Terra at lat = 3.68°, lon = 26.07°, taken at L_s = 230.8°. Black arrows indicate craters. (f) HiRISE image *ESP*_013147_0980 shows a starburst araneiform (orange arrow) at lat = −81.82°, lon = 76.15°, taken at L_s = 267.2°. HiRISE image credit: NASA/JPL/University of Arizona

Despite the slowing-down of geological and geomorphological activity on Mars, the present-day surface of the planet is far from quiescent. The discovery that the Martian surface is modified in today's climate was a major paradigm shift in our understanding

of contemporary extraterrestrial physical processes. Many of these processes and their consequent geomorphological features have Earth analogues; Dunes are widespread on Mars (Hayward et al., 2007), covering $\sim 70,000\,km^2$ of the Martian surface (Hayward et al., 2007) and have been found to migrate in the present day (Bridges et al., 2012), indicating active wind regimes. Dust storms engulf the Martian atmosphere on regional to global scales and dust devil activity forms spectacular dark albedo streaks across the surface of the planet. Adding to the diversity of the Martian surface came the discovery of features upon these dunes which are morphologically similar to those formed by water on Earth such as gullies (Malin and Edgett, 2001). Other features posited to be triggered by liquid water–driven activity are Recurring Slope Linae (RSL) which are recurring flow–like features mainly on equator–facing slopes (Chevrier and Rivera-Valentin, 2012; McEwen et al., 2013) (Figure 2.4 d) and slope streaks (Figure 2.4 e) (Bhardwaj et al., 2017; Ferris et al., 2002; Kreslavsky and Head, 2009; Miyamoto et al., 2004; Schorghofer et al., 2002) which are streaks darker and sometimes brighter than their surroundings that brighten over decade timescales and gradually disappear (Schorghofer et al., 2007). While many of these features are observed to be modified in the present day (Chevrier and Rivera-Valentin, 2012; Diniega et al., 2013; Dundas et al., 2012; McEwen et al., 2013), the low atmospheric pressure and diurnal temperature ranges of the current climate on Mars hamper the availability of water in the liquid state (Figures 2.5 (Hess et al., 1979), 2.6). Therefore, reconciling morphology and formation process for many features on Mars is confounded by the issue of equifinality. Moreover, many active surface features including sand furrows which form in spring and subsequently fade Bourke (2013); Bourke and Cranford (2011), linear dune gullies which form, fade and extend inter-annually (Diniega et al., 2013; Pasquon et al., 2016) and araneiforms, from which relatively dark fans and spots emanate annually (Hansen et al., 2010), have no analogue features sharing their likeness on Earth. When considering *active* Martian surface processes, it is important to understand geomorphic processes specific to the present-day climate conditions on Mars.

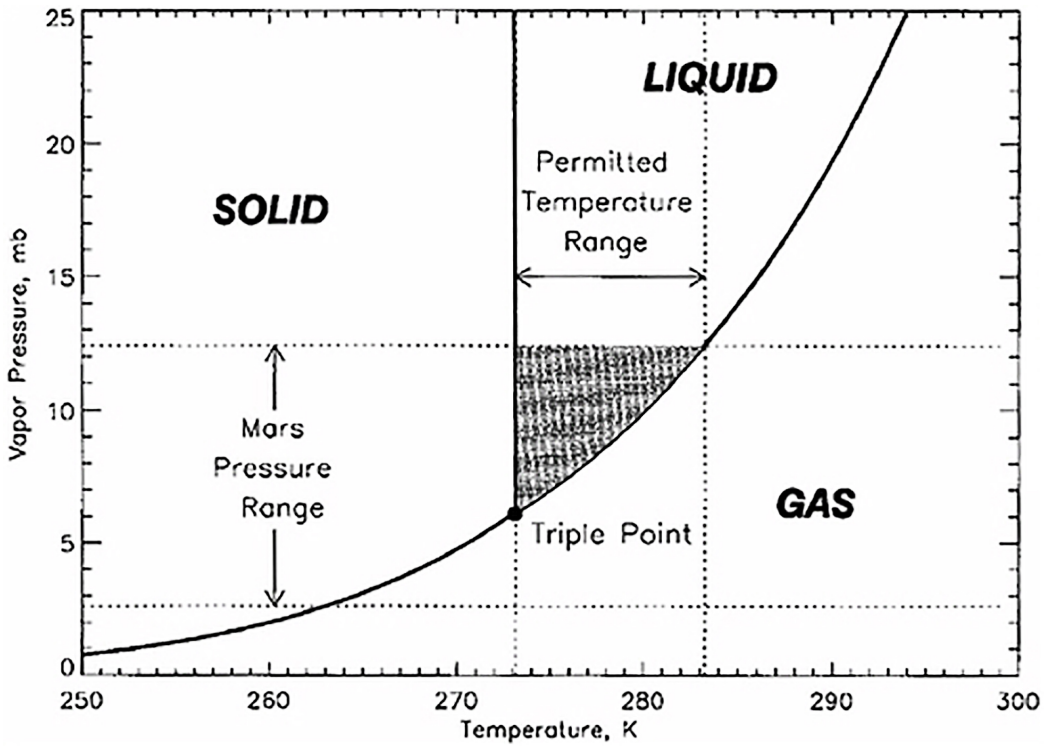

FIGURE 2.5: Water phase diagram for Mars. Diagram showing that current Martian atmospheric conditions straddle the triple point of water where water is stable as liquid, solid and gas. Hatched area represents conditions where water can exist as a liquid. Source: Haberle et al. (2001).

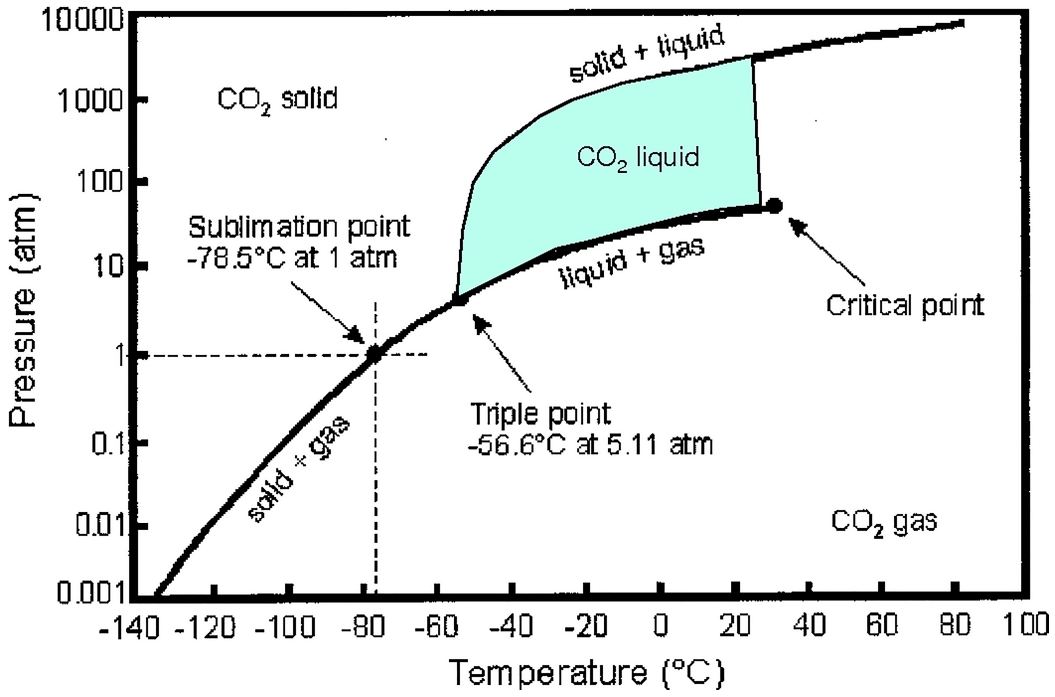

FIGURE 2.6: CO_2 phase diagram indicating that for Martian temperature and pressure ranges, the only possible phase transitions for CO_2 are deposition and sublimation. Source: Hrubes (2001).

2.2 Active Martian CO_2 Sublimation Processes and Features

Our understanding of the genesis of many Martian landforms evolved with the introduction of volatile sublimation as a geomorphic process. Sublimation, or the direct phase change from ice to gas, is proposed to modify the Martian surface in the present day over short to medium timescales (Hansen et al., 2010; Hansen et al., 2011; Kieffer et al., 2006; Mangold, 2011). Sublimation is now recognised as an important process by which the Martian surface is modified, and yet there is a lack of empirical data to accurately constrain the influence it has on the Martian terrain. Our understanding of the geomorphic efficacy of sublimation has implications for wider context studies on Mars such as the identification of features formed by liquid water, potential biosignatures and potentially hazardous landing sites for future missions to Mars, as well as considering sublimation–driven mass movement on other terrestrial planetary bodies. The remainder of this chapter reviews the advances made in understanding the role of CO_2 sublimation as a geomorphic agent on Mars, and identifies the outstanding questions from this recent published research on active Martian surface processes.

2.2.1 Swiss Cheese Terrain

Swiss cheese terrain (Figure 2.4 b) is unique to the SPRC and is attributed to collapse and erosion of CO_2 ice (Thomas et al., 2000). The features comprise a $< 15\,m$ thick CO_2 ice unit embayed by mesas (or small pieces of CO_2 detached from the main surface), troughs, ridges, circular depressions and quasi–circular pits (Thomas et al., 2000) which reveal water ice exposures (Bibring et al., 2004; Byrne and Ingersoll, 2003; Titus et al., 2003). These circular depressions range from metres to hectometres in scale, have flat floors and sloped side walls and are all $\sim 8\,m$ deep (Byrne and Ingersoll, 2003). The deposit is composed of two individual units which

were deposited at different times following a period of degradation (Thomas et al., 2005); one comprising 4–6 layers $\sim 2\,m$ thick with a surface landscaped by polygonal troughs (Byrne and Ingersoll, 2003; Mangold, 2011). The younger layer is comprised of 3 sub–layers $\sim 1\,m$ thick (Thomas et al., 2005).

Both units are found to erode at a prodigious rate by scarp retreat of 3.6 m/MY and 2.2 m/MY respectively, which is faster than any change identified on Mars at the metre scale (Malin et al., 2001). By this observation and given the density of the ice, it seems plausible that the swiss cheese features should be removed completely within a century and that the climate is changing on Mars by a measurable rate (Malin et al., 2001). However, observations of local CO_2 ice without circular depressions suggests that the terrain undergoes a renewal process (Mangold, 2011). A landscape evolution model of accumulation and ablation of condensed CO_2 on varying surface roughness has also proposed that climate change may not be responsible for the formation of swiss cheese terrain (Byrne et al., 2015). The model suggests that the differing elevation regions and resultant differential energy budgets from location to location, cause steeper regions to receive more solar insolation and hence sublimate locally and that the features may wax and wane over timescales of $\sim$ 100 years (Byrne et al., 2015). Additionally, the model suggests that global dust storms may sustain the SPRC as dust is an effective heat emitter and hence snowfall has been modelled to increase in the winter following a global dust storm (Hayne et al., 2014). Observations of global dust storms over the next century will determine whether or not this theory is correct and will ascertain whether climate change on Mars is occurring as rapidly as previously thought.

On seasonal timescales, the swiss cheese features have displayed bright haloes (Becerra et al., 2015) which have only ever appeared during observational monitoring of the SPRC in MY 28. The haloes are suggested to be caused by a combination of

summertime sublimation of CO_2 on the inner slopes of the swiss cheese features and contemporaneous dust settling from a global dust storm that occurred during MY 28 (Becerra et al., 2015). This is proposed to have resulted in a sublimation wind that diverted settling dust particles from the very edges of the slopes, keeping the outer rims of the swiss cheese circular depressions brighter than the rest of the icy surface (Becerra et al., 2016). Close monitoring of the SPRC in light of the recent 2018 global dust storm will shed further insight into the role of dust in sublimation dynamics and resultant morphologies of the swiss cheese terrain.

2.2.2 Fans and Spots and Araneiform Terrain

The Mars Global Surveyor mission captured the Martian surface in detail, notably revealing mid–latitude gullies, high latitude linear gullies, exhumed surface terrain, glacial and periglacial features and spectacular fans and spots of the polar regions (Malin and Edgett, 2001) (Figure 2.4 a). Time–sensitive analysis with MOC and later in greater detail the HIgh Resolution Imaging Science Experiment (HiRISE), revealed that these dark albedo fans and spots appear particularly at the south polar regions in spring and summer (Kieffer et al., 2006; Malin et al., 1998) and that these features were not at the same brightness temperature as soil, but rather just below that of CO_2 ice (Kieffer et al., 2006). The surroundings of the fans and spots were thus colloquially referred to as "cryptic" (Kieffer et al., 2006). The disparity between albedo and temperature suggests that the dark material must be either composed of, or in intimate contact with CO_2 ice (Kieffer et al., 2006). Many dark spots and elongate fans are in spatial proximity or concurrence with dendritic, ragged, tortuous negative topography features in the substrate now known as araneiform terrain (Kieffer et al., 2006; Piqueux et al., 2003). However, many are not and so their relationship with these features is stochastic in nature.

Araneiforms (Figure 2.4 f) are colloquially referred to as "spiders" as their morphologies comprise of radial branched "legs" or troughs emanating from a central depression which are torturous and anastomose in some cases (Piqueux et al., 2003). They are located on the Martian South Polar Layered Deposits and have a range of sub–types based on their observed morphologies (Hansen et al., 2010). Their concurrence with the dark albedo seasonal fans and spots which are recognised as transported fines originating beneath seasonal CO_2 ice (Kieffer et al., 2006) has placed them among the growing inventory of Martian features attributed to seasonal CO_2 sublimation.

Kieffer's hypothesis (Figure 2.7) for subsurface CO_2 jetting at the south polar cryptic region (Kieffer et al., 2006) spurred a paradigm shift in our understanding of active Martian surface processes and inspired a progeny of models of CO_2 sublimation proposed to modify the Martian surface in the present–day. The model notes that as temperatures decrease in winter, CO_2 deposits out of the atmosphere seasonally onto the Martian surface. The ice is proposed to be large–grained (Kieffer et al., 2000; Titus et al., 2001) and thus translucent to broad–spectrum radiation (Kieffer et al., 2006; Kieffer et al., 2000). This radiation will penetrate the ice, reaching the loose, unconsolidated fines beneath the ice overburden and become trapped, increasing the temperature of the regolith in a phenomenon coined the Solid State Greenhouse Effect (Matson and Brown, 1989). Once the terrain becomes sufficiently warm, the ice overburden will sublimate from its base and levitate before rupturing due to the CO_2 gas pressure surmounting cryostatic pressure. This high velocity gas will travel towards the vent, entraining dust and deposit the dark albedo material on the ice surface, often in a circular shape surrounding the vent (Kieffer et al., 2006). These are referred to as spots. Surface winds, which may often be Katabatic that occurs during venting, will direct the sediment downwind and the deposit will take the form of fans, rather than spots.

This conceptual model for fan, spot and associated araneiform formation is generally accepted. It is also proposed for other contemporary surface landforms (Bourke, 2013; Bourke and Cranford, 2011; Portyankina et al., 2017b). However, the process has never been directly observed in satellite images (Hansen et al., 2010). Additionally, the relationship between spot and fan appearance and araneiform terrain requires further understanding. While spots and fans are observed to occur year to year, the existing araneiforms have not been observed to expand in any dimension over the last 6 Mars Years (Portyankina et al., 2017b). Though it is generally held that araneiforms evolved via a connection of individual troughs over time (Hansen et al., 2010; Portyankina et al., 2017b), the specifically radial araneiforms of the South Polar Cryptic Region and surroundings have not been observed to form in the present day.

There are many questions regarding araneiforms and their associated fans and spots– specifically:

1. It remains unexplained why individual troughs would organise in a radial symmetry through multiple venting events.

2. Furthermore, why fans and spots appear in locations devoid of araneiforms as well as clearly emanating from their centres or depressions in their troughs (Hansen et al., 2010), is uncertain.

3. Additionally, it is unclear why while dark albedo material is emitted from their locations annually, the araneiforms have not been observed to change in dimension by a resolvable quantity in the last 6 MY.

4. It is entirely possible that the high latitude araneiforms developed in a relic period of high obliquity. However, further understanding of the limits that ice thickness and insolation properties play on this extant process is necessary in order to place constraints on geological timescales attributed to araneiform formation.

FIGURE 2.7: Artistic impression of Kieffer's hypothesis for spot and fan formation. Source: Gordon McBryde, Featherwax Post Production

2.2.3 Furrows and Dendritic Troughs

Sand furrows (Figure 2.8 c) are narrow ($\sim 2\,m$ wide), shallow ($< 0.5\,m$ deep) etchings around 100 m long on dunes in both the Martian northern and southern hemispheres (Bourke and Cranford, 2011). Their network types range from dendritic to rectilinear and their patterns tend to extend upslope, rendering a gravity–driven formation process unlikely. Furrows are proposed to form by a similar process to that described in Kieffer's model known as a CO_2 *cryoventing* process (Bourke, 2013) whereby solar insolation causes the seasonal ice veneer to fracture. High–velocity gas conduits are proposed to travel towards vents and entrain sediment in their paths to erode the surface (Bourke, 2013) and deposit fans in a plume of material. Furrows are detected on over 95% of north polar dunes (Bourke, 2013; Bourke and Cranford, 2011) and lesser so on dunes between 40° S and 72° S in the southern hemisphere (Nash and Bourke, 2015). The features appear on the same dunes each year, but in different forms and locations. They are erased by winds in summer and are not observed to grow annually due to their short lifespan (Bourke and Cranford, 2011).

Recently, perennial features known as dendritic troughs (Figure 2.8 a, b) were identified in the southern hemisphere (Portyankina et al., 2017b). Similar to dendritic furrows in morphology, dendritic troughs are distinguished by their endurance and inter–annual growth (Portyankina et al., 2017b). The disparity in lifespan of furrows and dendritic troughs is attributed to the environmental differences between the hemispheres on Mars. Much of the northern polar regions are populated by large dunes. Dune sediment here is loose and dust covered. Therefore ripple migration in summer will easily erase furrows in the time during which the dunes are not ice-covered (Portyankina et al., 2017b). Dunes in the southern hemisphere are less abundant and many are located inside large craters. Other factors such as compositional differences in the substrate between the young northern terrain and older southern landscapes and extent of sediment induration with water ice are expected to influence the morphological distinction between dendritic troughs and furrows (Portyankina et al., 2017b) but the cardinal influence on the distinction has not yet been elucidated.

Some authors have reasoned that the dendritic troughs will eventually grow into araneiforms (Portyankina et al., 2017b; Schwamb et al., 2018). However, this seems unlikely due to three factors: (i) the distinct radial organisation of individual troughs over time would be highly coincidental given the abundance of radial araneiforms, (ii) the radial araneiforms of the high southern latitudes have not been observed to change in dimension during the last 6 MY of observational campaigns and (iii) dendritic troughs are not observed to form in radial araneiform locations in polar regions. It remains plausible that while formation processes may be similar between furrows, dendritic troughs and radial araneiforms, cryoventing or cryo "jetting" is a process which is sensitive to slope and hence pressure gradient, ice thickness, regolith consolidation, dust abundance, and presence or lack thereof of interstitial pore ice in regolith material, among others. These factors are all clearly very different for sloped dunes, interdune material and relatively flat unconsolidated fines.

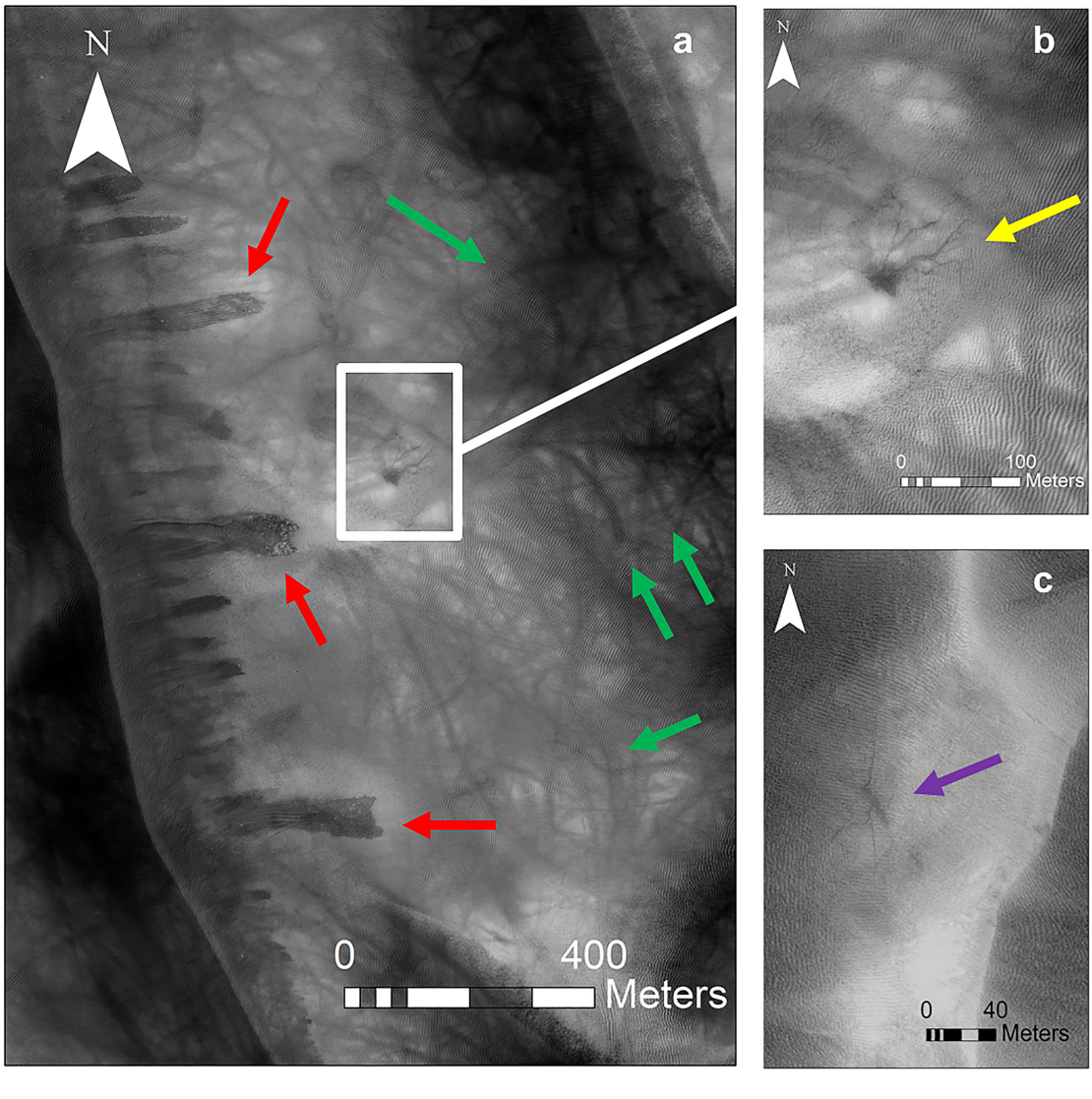

FIGURE 2.8: Examples of furrows and dendritic troughs. (a) HiRISE image *ESP*_039912_1095 at lat = −70.34°, lon = 178.2° taken at L_s = 282.6°, shows a dynamic dune surface marked by active linear dune gullies surrounded by recurring diffusive flows (red arrows), dust devil tracks (green arrows) and a dendritic trough which was observed to grow inter–annually (Portyankina et al., 2017b) (white box). (b) shows a zoomed–in section of (a) detailing the dendritic trough (yellow arrow). (c) HiRISE image *ESP*_026851_2590 at lat = 78.64°, lon = 308.49° taken at L_s = 98.7° shows a dendritic furrow on a dune south of the mouth of Chasma Boreale (purple arrow). Such furrows are erased seasonally. HiRISE image credit: NASA/JPL/University of Arizona

Although both furrows and dendritic troughs are observed to form during the annual retreat of the seasonal CO_2 ice layer, the formation model has not been tested. Specific gaps in the theory surrounding furrow formation remain:

1. The physical constraints on furrow morphometry as well as pattern type remain theoretical.

2. It is unclear why furrows are more prevalent on northern hemisphere dunes than southern hemisphere dunes and why dendritic troughs endure in the southern hemisphere.

3. Furthermore, the debate on whether dendritic troughs would radially organise to form araneiforms needs to be challenged as so far there has been little convincing evidence to support their origin from dendritic troughs and yet many have relied on this proposed development to date the features (Piqueux et al., 2003; Portyankina et al., 2017b).

Empirical studies of dendrites on granular substrate of a wide variety of grain sizes and extrapolation of conditions to the vast scale on Mars via a numerical model will be vital tools to distinguish between the genesis of dendritic troughs, furrows and araneiforms, and to close the many open ended questions circulating these exotic features.

2.2.4 Gullies

Martian gullies (Figure 2.9) were first identified in high resolution images taken by MOC in 1999 (Malin and Edgett, 2001). Occurring two and a half times more often on poleward facing slopes than on equator facing slopes (Malin and Edgett, 2001), these archetypal gullies were defined as having a "theatre–shaped" alcove comprised of head and sidewall escarpments, main and secondary V–shaped channels which taper downslope and distally, and depositional aprons (Malin and Edgett, 2001). Gullies

are predominantly located in the southern hemisphere, mostly in the mid–latitudes or in polar pits near 70° S (Balme et al., 2006; Heldmann et al., 2007; Malin and Edgett, 2001). Those at lower latitudes (30-40° are located mainly on pole-facing slopes, while those concentrated near the mid latitudes (generally >40°) have a variety of orientations (Conway et al., 2017; Dundas et al., 2012). Gullies are mainly found on inner and outer crater walls and on sand dunes, south polar pits and two of the larger Martian valleys; Nirgil Vallis and Dao Vallis and a variety of mesas. Only one apron out of all gully features imaged by MOC was observed to have any visible superposed craters (Malin and Edgett, 2001) and so combined with their fresh appearance and superposition relationships on putatively late amazonian landforms such as polygons, dunes and transverse aeolian ridges (Reiss et al., 2004), it was conceded that gullies were geologically young (Dickson and Head, 2009; Malin and Edgett, 2001; Reiss et al., 2010; Schon et al., 2009) (less than a few million years).

Martian gullies resemble landforms formed by liquid water driven mass–wasting processes on Earth (Hartmann et al., 2003; Marchant and Head, 2007), and based on their similar morphology it has been suggested that kilometre scale Martian gullies were formed by the action of surficial liquid water e.g. (Conway and Balme, 2016; Heldmann et al., 2001, 2007; Malin and Edgett, 2001; Védie et al., 2008). If confirmed, the role of surficial liquid water in gully formation on Mars would be significant because ongoing seasonal gully activity has been recorded in the present day (Diniega et al., 2010; Dundas et al., 2012; Pasquon et al., 2016; Raack et al., 2015; Reiss et al., 2010) and liquid water could indicate a potential habitable environment. However, the apparent water–driven morphologies of gullies on Mars combined with their activity in the present–day is paradoxical. It is difficult to reconcile recent gully formation with surficial liquid water given that water is unstable in the liquid phase under atmospheric pressure ranges between 6.5 and 10 mbar (Hess et al., 1979) and is available in extremely limited amounts (Ingersoll, 1970).

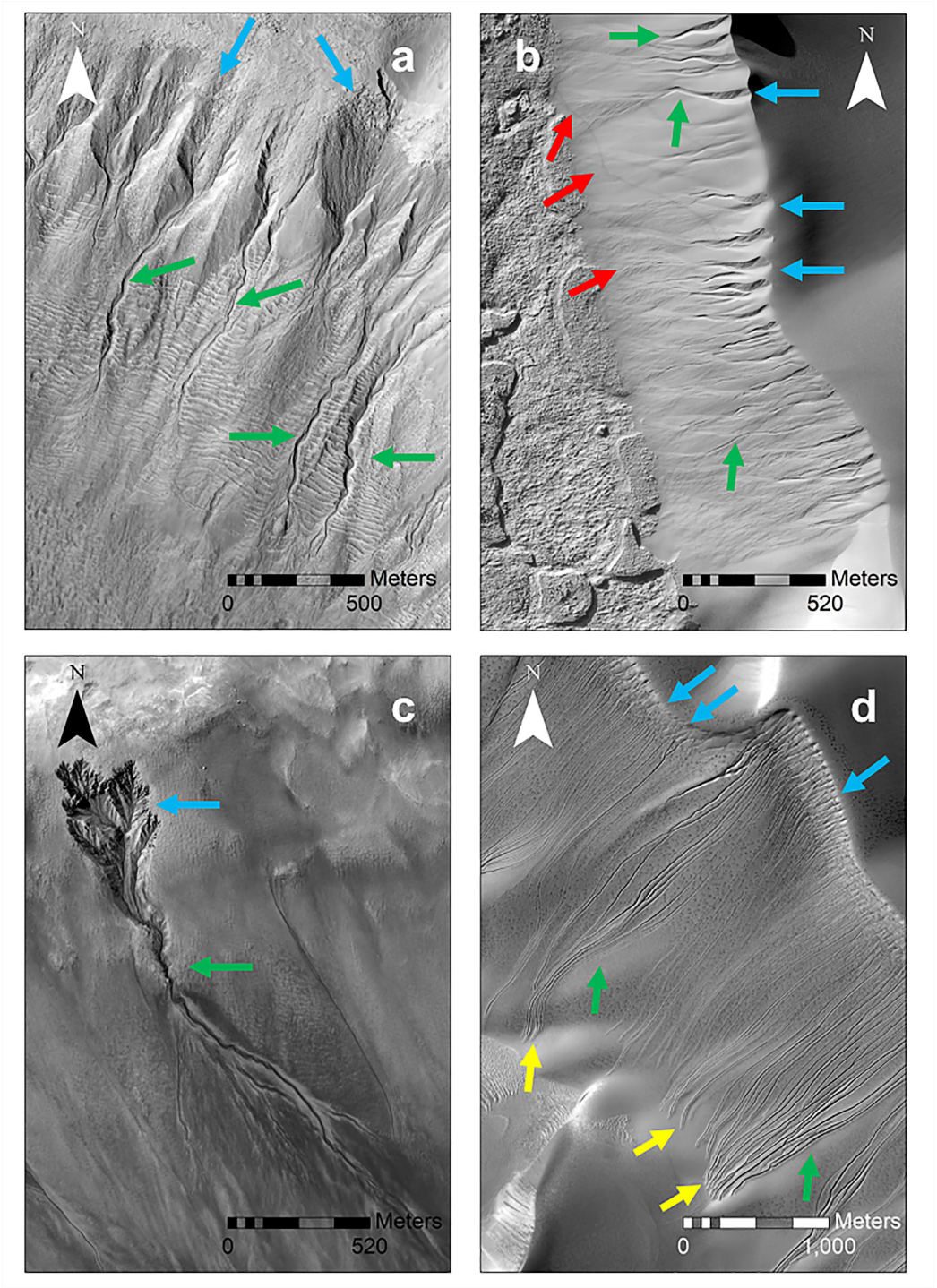

FIGURE 2.9: Examples of different Martian gully morphologies. Blue arrows indicate alcoves, red arrows indicate aprons, green arrows indicate channels and yellow arrows indicate terminal pits. (a) HiRISE image ESP_011995_1410 shows gullies on a pole–facing slope at lat = −38.82°, lon = 201.43°, taken at L_s = 210.8°. These gullies have large alcoves and meandering channels. (b) HiRISE image ESP_016907_1330 shows smaller gullies on a Kaiser crater dune at lat = −46.74°, lon = 20.15°, taken at L_s = 60.1°. (c) HiRISE image ESP_022472_1285 shows a gully with prounounced sidewall escarpments within its theatre–shaped alcove at lat = −51.26°, lon = 6.82°, taken at L_s = 291.8°. (d) HiRISE image ESP_018872_1255 shows some of the longest linear dune gullies on Russell Crater megadune at lat = −54.27°, lon = 12.95°, taken at L_s = 128.8°. HiRISE image credit: NASA/JPL/University of Arizona

Several hypotheses have since been offered to account for the putative role of liquid water in gully formation on Mars. These include melting of near–surface snow or ice (Costard et al., 2002; Jouannic et al., 2015; Schon et al., 2009; Védie et al., 2008) in the recent past, melting of surface snow or ice in the present–day (Christensen, 2003; Head et al., 2008), and liquid water aquifer activity (e.g. (Gaidos, 2001; Gilmore and Phillips, 2002; Mellon and Phillips, 2001)). Some authors have suggested the involvement of perchlorates, or other salts, which are abundant on the surface of Mars (Brass, 1980; Hecht et al., 2009; Martín-Torres et al., 2015) and can lower the freezing point of liquid water allowing episodic flow activity Massé et al. (2016); Ojha et al. (2015); P.L. and Burt (2002). Experimental data show that on the laboratory scale, limited quantities of transient boiling liquid water under Martian pressure (6.5–10 mbar) and temperature ranges (274–281 K) can produce significant geomorphic change Herny et al. (2018); Raack et al. (2015). However, temperatures only exceed 285 K locally on Mars (Haberle et al., 2001; McEwen et al., 2013; Reiss and Jaumann, 2003) and so this process is unlikely to apply to gullies in the high polar latitudes or those which receive minimal insolation. Other hypotheses have not invoked liquid water including dry granular flows (Pelletier et al., 2008; Shinbrot et al., 2004; Treiman, 2003) and CO_2 enabled flows (Cedillo-Flores et al., 2011; Dundas et al., 2012; Dundas et al., 2012; Hoffman, 2002; Musselwhite et al., 2001; Pilorget and Forget, 2016). Laboratory studies have shown that when CO_2 is condensed onto a granular surface under Martian pressure and allowed to sublimate, slope failure occurs resulting in measurable geomorphic change (Sylvest et al., 2016; Sylvest et al., 2018) and modelling efforts have indicated that fluidisation of a sloped granular surface by CO_2 sublimation can produce channel morphologies (Pilorget and Forget, 2016) However, none of these hypotheses have been able to explain the timing of activity (Diniega et al., 2013; Dundas et al., 2012; Pasquon et al., 2016; Pasquon et al., 2018), distribution and all of the morphological components of the discrete types of gullies on Mars (Conway and Balme, 2016).

Gully morphologies on Mars are often treated as a single group of geomorphic features, and this warrants caution because synonymity is then often made with liquid water. In addition, it is imperative to consider the distinction between "recent" and present–day. It is possible that the classic mid–latitude gullies formed in the recent geological past, or the aforementioned water–driven hypotheses are reasonable for present–day activity under certain conditions. In addition, while hydrated salt spectra detected at RSL locations may infer brine activity (Ojha et al., 2015), there has been no unequivocal evidence of flowing surficial liquid water ubiquitous among *gully* locations on present–day Mars. For this reason, and noticing the diverse range of gully morphologies, a gully classification system (Table 2.1) was proposed by Auld and Dixon (Auld and Dixon, 2016) based on a HiRISE image survey of distinct morphologies of gully sub–types. The three components used to classify over 7500 gullies surveyed were the presence and shape of an alcove, the presence and shape of the apron and channel geometry.

2.2.4.1 Timing and Types of Activity for Active Dune Gullies

This thesis concerns active surface features on Mars in relation to CO_2 sublimation processes and so this discussion of gullies homes in on those which are active today. Dune gullies are the most active gully type on present-day Mars, showing measurable interannual and even inter-seasonal change Diniega et al. (2010, 2013); Dundas et al. (2012); Pasquon et al. (2016); Pasquon et al. (2018). Dune gullies include classic 'alcove-channel-apron' gullies, (re-named 'large apron' gullies to account for those that don't include a distinct channel by Pasquon et al. (2018)) and 'linear dune' gullies. These are often co-located on the same dune slipfaces (e.g. Kaiser crater dunefield gullies Pasquon et al. (2018) and on gentle slopes between ∼12 and 16° Pasquon et al. (2016), but differ in the timing of their activity. Classic-type dune gullies show activity in local mid-late autumn and winter Diniega et al. (2010); Pasquon et al. (2018). This activity is spread across the seasons and includes metre-scale material

Gully Classification			
Gully Class	**Alcove**	**Channel**	**Apron**
Classic gully	Single alcove narrowing down slope	V-shaped erosional channel that may divert around topography	Alluvial apron or lobate fan
Complex gully	One or more alcoves feeding into a single channel	One or more V-shaped erosional channels that may exhibit braiding. Channel often dissects the developing apron	One or more alluvial aprons that often exhibit braiding
Channel gully	No alcove	V-shaped channel that exists only in the colluvium above any local bedrock layers	Small alluvial apron-sor lobate fans
Alcove-apron feature	Single alcove narrowing down slope	No V-shaped channel	Alluvial apron or lobate fan
Abbreviated alcove gully	Single alcove narrowing down slope and abbreviated upslope by an obvious layer within the subsurface	V-shaped erosional channel that may divert around topography	Alluvial apron or lobate fan
Linear gully	No alcove or extremely small triangular alcove	Narrow U-shaped channel that maintains its width and will divert around topography	No apron
Mantled gully	Alcove often filled by collapse or aeolian deposition	Channel obscured by infilling or aeolian deposition	Aprons that have been covered by subsequent deposits or mantling or that have edges that have ben eroded

TABLE 2.1: Classification of Martian gullies. Source: Auld and Dixon, 2016.

collapse into gully alcoves as CO_2 condenses, mass flows in late winter and conspicuous appearance of flows on gully fans in channels in autumn and winter and have been found to form over hundreds of Mars Years Pasquon et al. (2016). In contrast, the activity of linear dune gullies is ephemeral and restricted to late winter and early spring, exactly when the CO_2 frost disappears. Linear dune gully activity is marked by the extension of channels, development of pits and the darkening of the surface surrounding them to form digate features lateral to their channels known as RDFs Pasquon et al. (2016). Linear dune gullies are likely to form within one to tens of Martian years Pasquon et al. (2018) and the specific timing of their activity has

strongly advocated for CO_2 sublimation as a driver of their activity and formation mechanism Diniega et al. (2013); Pasquon et al. (2016).

2.2.4.2 Formation Mechanism Hypotheses for Active Gullies on Mars

Based on timing and morphology, several formation hypotheses have been offered in order to explain active gullies on Mars. Due to the low pressure and temperatures on Mars today, the mechanisms offered are generally processes which do not invoke liquid water. The Frosted Granular Flow model Hugenholtz (2008) suggests that a rare Terrestrial type of granular flow detected in Québec, Canada, could be applied to Mars. In this type of flow regime, dry flows can occur even on the very gentle slopes where active gully activity occurs today. Frost coated grains experience less dynamic inter-particle friction and thus flow is more lubricated than dry granular flows which only occur on very steep slopes (35-41°) Hugenholtz (2008). However for application on Mars, this kind of flow needs to be triggered by rockfall Hugenholtz (2008). It is therefore unlikely that this process is applicable to all gullies.

Using a thermo-physical numerical model of seasonal sublimation dynamics Pilorget and Forget (2016), suggested a mechanism whereby insolation triggers basal sublimation-driven debris flows beneath the seasonal CO_2 ice layer. Applied to the Russell Megadune gullies, the model simultaneously solves the heat conduction and radiative transfer through the seasonal CO_2 ice layer, as well as the diffusion, condensation and sublimation of CO_2 and the related latent heat exchanges. Via this process, insolation penetrates translucent slab ice causing the ice to sublimate from its base. Some CO_2 sublimates and diffuses down to keep the porous regolith sandwiched between the overlying CO_2 layer and the impermeable permafrost in vapour pressure equilibrium with the CO_2 ice slab. The gas is thus trapped and pressure rises significantly. The pressure eventually surpasses the cryostatic pressure of the ice and lifts it. Eventually the ice will rupture and the pressure within the regolith pores

then reduces rapidly to atmospheric pressure. The CO_2 ice that is present within the pores and at the base of the slab sublimates rapidly and this can trigger debris flows Pilorget and Forget (2016) 2.10. Results of this simulation are in agreement with the temporal activity of Russell Crater linear gullies and suggest that such basal sublimation can carve channels similar to the scale of those observed on Russell Crater Megadune Pilorget and Forget (2016). However, the model does not explain the enigmatic pits at linear gully termini and surrounding detached pits.

Cedillo-Flores et al. (2011) proposed a mechanism whereby polar gullies can be eroded by fluidisation of sediment *overlying* CO_2 ice. However, this scenario would require the deposition of a thin layer of sediment on top of a seasonal frost layer overlying a dune. This constraint can only be met under restricted conditions, where a pole-facing slope is covered by CO_2 ice, while a nearby equator-facing slope is bare. Wind would then deposit material from the bare slope onto the ice-covered slope and insolation will eventually cause the underlying ice to sublimate. The rapid sublimation of the underlying CO_2 would trigger mass movement on the dune slope. Heat induced by friction causes more CO_2 gas to be produced and hence fluidises the flow, carving a channel. However, such a situation is likely to be rare and thus while conceivable, cannot account for all gully activity. In a similar vein, Hoffman (2002) proposed that active gullies may be formed by fluidised CO_2 flow, but that fluidisation occurs *beneath* the seasonal CO_2 layer, resulting in an avalanche. Insolation penetrates translucent ice and heats the regolith from its base. CO_2 vapor will destabilise the snowpack, resulting in avalanching. The mixture of cold snowpack and warm entrained debris will then tumble downslope. The mechanical churning of warm granular material and cold snowpack fragments results in further degassing of CO_2. This results in a brief CO_2 gas-lubricated flow which may erode gully channels. However, such a flow is limited to steep slopes and cannot account for the very gentle slopes upon which many active gullies are found Dundas et al. (2012); Pasquon et al. (2016).

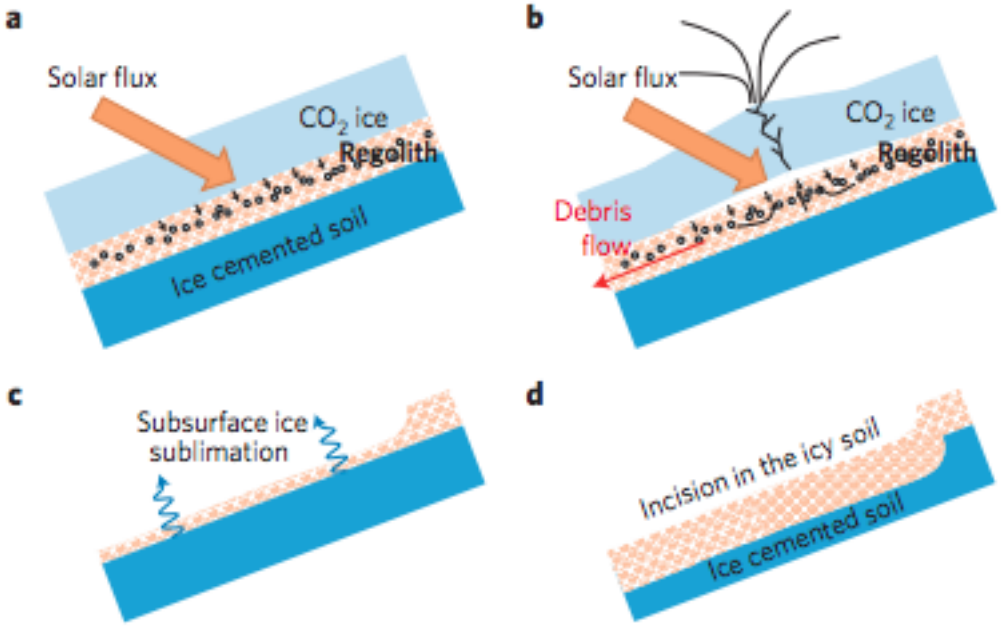

FIGURE 2.10: The Pilorget basal-sublimation-driven debris flow model. Source: Pilorget and Forget (2016)

Ishii and Sasaki (2004) proposed that CO_2 frost avalanches during spring/summer could be responsible for carving gully channels by solid chunks of frost "scratching" into the regolith. However, because such avalanches would not include a sublimation or melting phase, they tend to travel in straight lines, instead of being deflected by surface topography. Observations of erosional features on Earth caused by avalanches have very straight, wide channels with wide levées, with little comparative morphology to the sometimes sinuous, narrow gully channels observed on Mars Kochel and Trop (2008). In the same vein, the suggestion put forth that dry granular flow may be responsible for active gully formation by Treiman (2003), has largely been rejected, again due to inconsistencies in the morphology of active gullies on Mars and straight flow features formed by dry granular flow on Earth. Furthermore, dry granular flows require steep slopes and many active gullies occur on dune slopes below the angle of repose Pasquon et al. (2016).

2.2.5 Linear Gullies

Linear dune gullies (Figure 2.9 d) on the lee slope of Russell Crater Megadune were first reported by Mangold et al. (2002a) and later distinguished nominally from other gully forms (Auld and Dixon, 2016; Dundas et al., 2012; Védie et al., 2008). They are the most spatially restricted of all gully forms, occurring only on large dunes in latitudinal bands between 36.3° S and 54.35° S and 64.6° S and 70.4° S and comprising ∼ 5% of the total gully population (Pasquon et al., 2016). Linear gullies are long (relative to their width), narrow systems which consist of small alcoves and linear though sometimes sinuous channels which are bounded by lateral levées. Many of these forms are also accompanied by seasonally appearing and disappearing low albedo digitate flows lateral to their channels known as *Recurring Diffusive Flows* (Pasquon et al., 2016). These are dark patches which sometimes are surrounded by bright "haloes" Pasquon et al. (2016). The origin of these flows remains unclear. Unlike all other gully subtypes, linear gullies have a paucity of terminal deposits, meaning that none of them have a depositional apron indicative of downslope mass transport. A striking morphological feature associated with linear gullies is known as the terminal pit. Terminal pits are small (<1 m–19 m in diameter), shallow circular depressions often encircled by levées, which punctuate the distal end of the linear gully channel. These are often surrounded by multiple smaller detached pits.

The primary terminal pits found at all linear gully termini distinguish these features from gullies found on Earth. The lack of deposited material associated with them pose a difficulty for Terrestrial type water–enabled debris flow formation hypotheses which have been proposed in the past (Mangold et al., 2002b; Reiss and Jaumann, 2003; Reiss et al., 2010). Additionally, while it is plausible that basal sublimation of the seasonal CO_2 ice layer (Pilorget and Forget, 2016) can destabilise granular material on dune slopes sufficiently to form a dry debris flow, it is not clear what aspect of

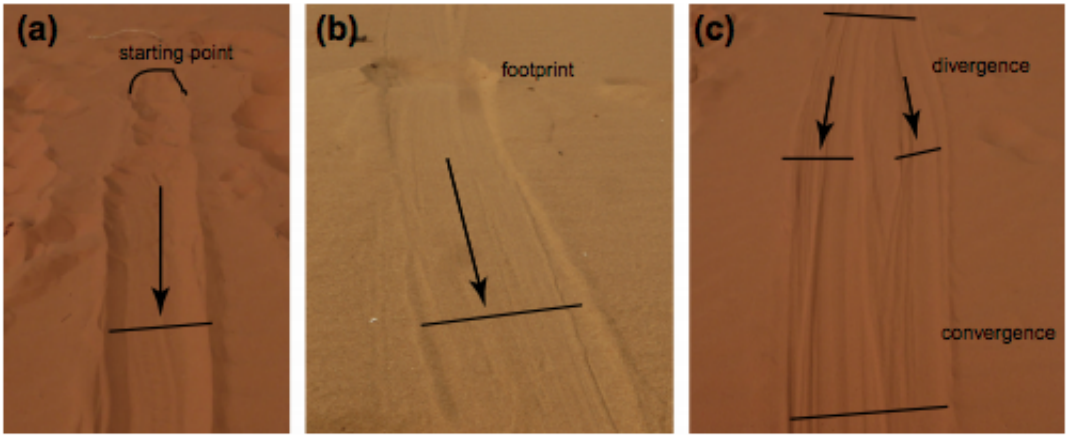

FIGURE 2.11: Field tests of the sublimating block hypothesis in Utah showing the generation of channel morphology by sliding blocks Diniega et al. (2013).

this formation process would be responsible for the clear deposition of lateral levées and erosion of a terminal pit.

The only hypothesis that can account for the formation of all morphological components of the linear gully system including pits is the Sliding CO_2 Block Hypothesis (Diniega et al., 2013). The hypothesis proposes that in spring when dunes are partially defrosted, solar insolation destabilises and fractures the CO_2 ice sufficiently for blocks of CO_2 ice to fall from dune brinks, explaining the absence of or presence of very small alcoves. The blocks will traverse the defrosted dune lee slope assisted by a lubricative layer brought about by an effect similar to the *Leidenfrost Effect* Leidenfrost (1966). This effect occurs when a substance reaches thermal contact with a surface which is at a temperature far higher than its boiling or sublimation point. The substance will become encapsulated in a "vapor prison" and the surface of the block in contact with the dune slope will levitate on this vapor layer, negating solid friction in its path. The joint effect of the bulldozing force of the block sliding downwards by the force of gravity and the pressure of the sublimating gas mobilising sediment to the sides of the block, is proposed to erode the almost uniform channel width of the linear gully and deposit lateral levées. The erosion of the terminal pit is posited to be caused by the in–situ sublimation of the CO_2 block which has come to rest at the distal end of the slope (Diniega et al., 2013). Linear gully activity and morphological

change has been detected to occur in the Martian spring (Diniega et al., 2013; Dundas et al., 2012; Pasquon et al., 2016). In addition, field tests were conducted on sand dunes in Arizona and Utah in order to investigate whether sliding CO_2 blocks would form morphologies similar to linear gullies. Shallow channels and lateral lev'es were generated by the downslope movement of CO_2 ice blocks and it was found that the CO_2 ice blocks continued movement downslope unhindered by surface friction. It was inferred from this work that even under Terrestrial gravity, CO_2 blocks in contact with relatively warmer substrate will sublimate and levitate and that the combined action of downslope block movement is capable of eroding channel and levée morphologies 2.11. However:

1. Though this hypothesis has been developed and tested in the context of linear gully channel formation in the field and a mathematical model has extrapolated the process to Martian conditions (Diniega et al., 2013), there has been a deficiency of empirical evidence that stationary block sublimation can erode linear gully pits and in turn deposit the lateral levées that surround them.

2. Additionally, though the numerical model describing this process is robust under normal Earth conditions where fluid dynamic regimes are well–understood, it needs to be tested under ambient Martian pressure in order to establish its stability under extant conditions.

Investigating the potential role of sublimation in gully formation on Mars will have wider implications to the field of planetary science. Gully landforms have been detected on planetary bodies which have scant or non–existent atmospheres which are even less conducive to hosting liquid water than Mars, such as the Moon (Bart, 2007) and even the massive asteroid Vesta (Scully et al., 2015). Understanding the role of sublimation is therefore integral to guiding a non–biased interpretation of data from future planetary missions within the Solar System.

2.3 Aims of the Thesis

CO_2 sublimation–driven hypotheses have existed in the literature on Martian surface processes for the past two decades and yet whether sublimating CO_2 ice is responsible for some features, is still a subject of ongoing debate. Understanding the dynamics of seasonal CO_2 ice will result in a more robust inventory of current active surface processes and related potential hazards for planned human missions to Mars. With a recent advent of Earth and Mars chamber based laboratory experiments (Chinnery et al., 2018; Kaufmann and Hagermann, 2017; Sylvest et al., 2016; Sylvest et al., 2018), numerical modelling (Diniega et al., 2013; Pilorget and Forget, 2016) and fieldwork (Diniega et al., 2013), we are now testing these concepts and quantifying to what extent and timescales this agent of surface modification may be at play. Additionally, temporal high–resolution imaging of the Martian surface has provided a lens through which we can study these processes and how the Martian surface is being modified seasonally. The aims of this thesis are:

1. To determine if CO_2 block sublimation can form linear gully primary terminal pits, associated levées and detached pits.

2. To determine if pressurised escaping CO_2 gas can erode sand furrow morphologies.

3. To determine if pressurised escaping CO_2 is capable of forming radial araneiform morphologies.

2.3.1 To Determine if CO_2 Block Sublimation can form Linear Gully Primary Terminal Pits, Associated Levées and Detached Pits.

Objectives:

1. To perform low–humidity experiments on granular substrate under Earth conditions of sliding and hence partially buried CO_2 blocks in order to document the response of the granular bed and quantitatively measure the features produced

2. To conduct a survey of linear gully pits in Russell, Proctor and Matara Crater in order to (a) characterise the different terminal pit morphologies (b) investigate if there is evidence of a relationship between the morphometries of these terminal pits and the observed presence of detached pits and (c) to investigate the range of block sizes which may be reactivating and widening linear gully channels and pits seasonally and compare these measurements with the documented lab–generated granular bed response to given CO_2 block dimensions

3. To perform experiments under Earth conditions and Martian atmospheric pressure in order to quantify gas pressure of a vapor layer and heat transfer between sublimating CO_2 ice blocks and granular beds of a range of grain sizes in order to (a) generate empirical data to feed into the semi–analytic model and (b) test the model output

2.3.2 To Determine if Pressurised Escaping CO_2 Gas Can Erode Sand Furrow Morphologies.

Objectives:

1. To document and measure the erosion patterns resulting from the interaction between a gently placed CO_2 block and granular substrate and compare these features to a pre-existing Martian furrow network classification (Bourke, 2013)

2. To identify the potential physical factors which control furrow pattern type and furrow density when a CO_2 block is gently placed on granular substrate

2.3.3 To Determine if Pressurised Escaping CO_2 is Capable of Forming Radial Araneiform Morphologies.

Objectives:

1. To study the erosion patterns resulting from the interaction between a gently placed CO_2 block containing a central vent and granular substrate under Martian atmospheric pressure

2. To investigate the relationship between radial araneiform morphometry observed in the laboratory and (a) grain size and (b) vent diameter

3. To conduct a survey of araneiforms in the southern high latitudes on Mars and (a) extend the existing morphometric classification of araneiform sub–types, (b) investigate whether there is a feedback between araneiform spacing and their level of branching and (c) investigate whether there is a feedback between the ratio of araneiform full extent to central depression and the level of branching of araneiforms

Chapter 3

Experiments On Sublimating Carbon Dioxide Ice And Implications For Contemporary Surface Processes On Mars

Abstract

Carbon dioxide is Mars's primary atmospheric constituent and is an active driver of Martian surface evolution. CO_2 ice sublimation mechanisms have been proposed for a host of features that form in the contemporary Martian climate. However, there has been very little experimental work or quantitative modelling to test the validity of these hypotheses. Here we present the results of the first laboratory experiments undertaken to investigate if the interaction between sublimating CO_2 ice blocks and a warm, porous, mobile regolith can generate features similar in morphology to those forming on Martian dunes today. We find that CO_2 sublimation can mobilise grains to form (i) pits and (ii) furrows. We have documented new detached pits at the termini of linear gullies on Martian dunes. Based on their geomorphic similarity to the features observed in our laboratory experiments, and on scaling arguments, we propose a new hypothesis that detached pits are formed by the impact of granular jets generated by sublimating CO_2. We also study the erosion patterns formed underneath a sublimating block of CO_2 ice and demonstrate that these resemble furrow patterns on Mars, suggesting similar formation mechanisms.

3.1 Introduction

The Martian atmosphere, which is comprised of over 95% CO_2 (Nier and McElroy, 1977), interacts seasonally with the planetary surface. As temperatures fall between late autumn and early winter, a CO_2 deposit covers the surface (Leighton and Murray, 1966) in thicknesses ranging from around a metre in the polar regions (Aharonson et al., 2004; Nier and McElroy, 1977) to a few millimetres towards the equator (Vincendon, 2015). The distribution of this dry ice is governed primarily by solar insolation (Smith et al., 2001). In the early spring, as insolation increases, the dry ice begins to sublimate. This process is now recognised as an important agent in the formation of contemporary surface features on Mars. These features include the dendritic

araneiform terrain of the south polar cryptic region (Hansen et al., 2010; Malin and Edgett, 2001; Piqueux et al., 2003), linear gullies, their associated pits (Dundas et al., 2012; Mangold et al., 2002a) and sand furrows (Bourke and Cranford, 2011). In this study we focus on linear gully pits and sand furrows; both active features which are observed to form and evolve on dunes under the current Martian climate. These features have no Earth analogues and the specific mechanisms responsible for their formation have yet to be fully understood and quantified.

3.1.1 Furrows

Furrows are shallow (∼0.25 m) and narrow (∼1.5 m) negative relief (Bourke, 2013; Bourke and Cranford, 2011) features which are observed on over 95% of the northern polar dunes (Bourke and Cranford, 2011) and are also found between 40° S and 72° S (Nash and Bourke, 2015). Their network patterns range from rectilinear, to dendritic and radial, tributary and distributary and their planforms can be linear or sinuous (Bourke, 2013) (Figure 3.1), though it is unclear what factors control this variety of patterns. Appearing to "defy gravity", furrows extend upslope and transect existing aeolian ripples, and so while their patterns may resemble those eroded by fluvial activity on Earth, gravity-driven processes are unlikely to form them (Bourke, 2013).

3.1.1.1 Furrow Formation Hypotheses

Furrows frequently form after the appearance of polygonal cracks in CO_2 ice and relatively dark fans and spots sometimes appear close to them in spring. This led Bourke (Bourke, 2013) to hypothesise that they were caused by cryoventing; that is, basal sublimation of CO_2 and consequent erosion. This is similar to Kieffer's model for the dark spots and fans in the southern hemisphere (Kieffer et al., 2006), but applied in the context of dunes. The cryoventing model proposes that in the spring, gas pressures increase at the ice-substrate interface until the overlying ice cracks. Gas

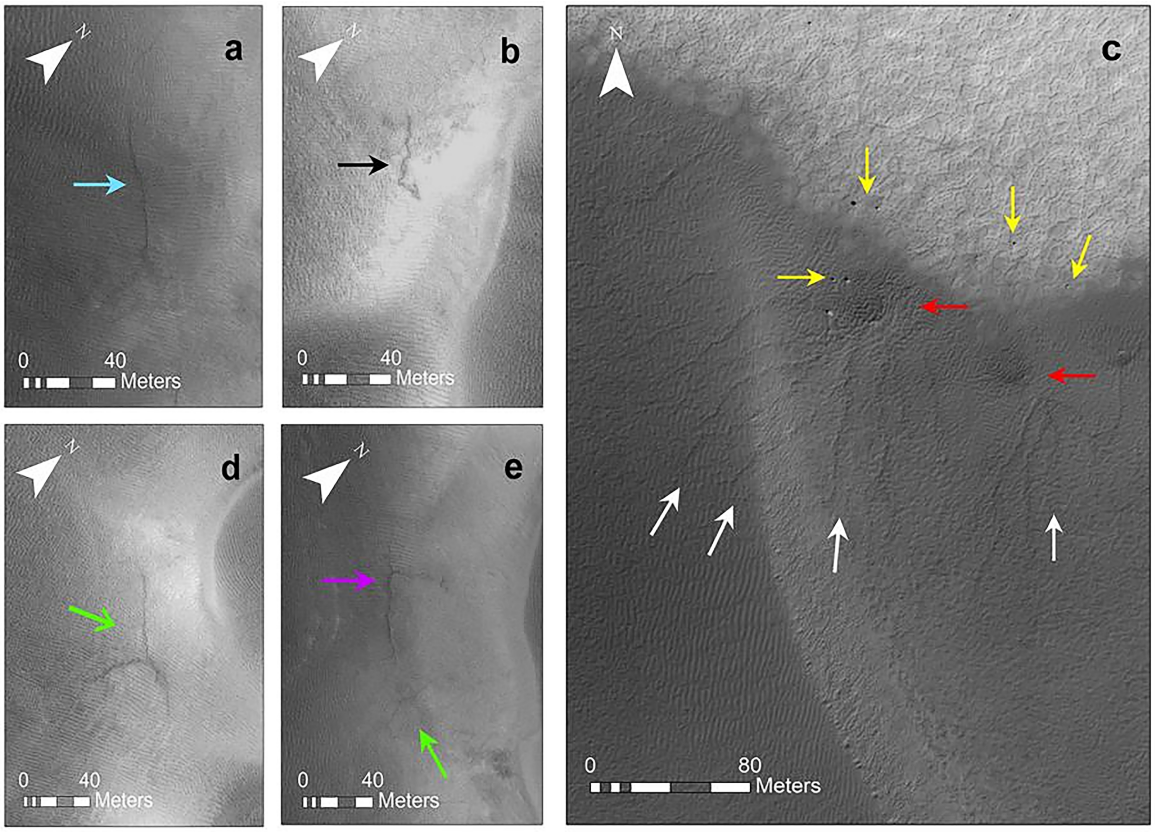

FIGURE 3.1: Examples of sand furrows on Martian Dunes (a) Linear (blue arrow) and curvilinear (pink arrow) furrows on sand dune in Chasma Boreale (all Chasma Boreale furrows are taken from HiRISE image ESP_026851_2590, latitude 78.65°, longitude 308.494°, solar incidence angle 56° with the Sun ∼ 34° above the horizon). (b) sinuous (black arrow) furrow on sand dune in Chasma Boreale, (c) dendritic furrows (white arrows) on sand dunes at latitude -67.607°, 185.343° in the southern hemisphere (HiRISE image ESP_023270_1120. Solar incidence angle is 60° with the sun ∼ 30° above the horizon). Yellow arrows point to boulders, red arrows point to dark fans and highlight their proximity to the furrows. (d) radial (green arrow) furrow on sand dune in Chasma Boreale. (e) rectilinear (purple arrow) and radial (green arrow) furrows on sand dune in Chasma Boreale. Images have been stretched to improve contrast as furrows are narrow, shallow and thus subtle features. HiRISE image credit: NASA/JPL/University of Arizona

rapidly exits, eroding material below the ice sheet to form furrows. A plume then deposits the sediment to form fans on the surface of the seasonal ice. The thickness of the overlying ice and dune topography are thought to have a strong influence on this process (Bourke and McGaley-Towle, 2014a). Close spacing of vents has also been noted to reduce cryoventing efficacy, with fewer furrows forming in locations where ice cracks are closer together (Bourke, 2013).

Recent work has drawn a distinction between furrows in the northern hemisphere and

dendritic troughs in the southern hemisphere (Portyankina et al., 2017b). While both show similar morphologies, furrows in the northern hemisphere are ephemeral features which disappear every year (Bourke and McGaley-Towle, 2014b). The dendritic troughs on south polar dunes endure, with new tributaries adding to the networks annually (Portyankina et al., 2017b). This study (Portyankina et al., 2017b) has drawn a potential link in formation process between the highly dendritic araneiform terrain of the south polar cryptic region and furrows/dendritic troughs. It has been suggested that araneiform terrain (dubbed "spiders" in the literature) may develop over many years by a gradual connection of dendritic networks into a radial network, rather than forming in one event (Portyankina et al., 2017b). Noting the difference in environmental conditions between the hemispheres, it has been argued that furrows in the northern hemisphere do not develop into dendrites because of the high mobility of the material into which they are eroded (Portyankina et al., 2017b). However, the size distribution of the granular substrate in both hemispheres is poorly constrained. For the purpose of our purely morphological laboratory study we refer to all network types as furrows.

Recent experimental work has demonstrated that insolation-driven dust ejecta from within CO_2 ice is a viable process (Kaufmann and Hagermann, 2017) and that pressure driven processes can form dendritic patterns under certain conditions (de Villiers et al., 2012). However, it has not yet been demonstrated that sublimating CO_2 in contact with porous substrate can transport underlying material and create the complex furrow morphologies seen on Mars. Until now, this geomorphic process has been framed in a purely theoretical context.

3.1.2 Linear Gully Pits

Linear gullies (Figure 3.2) form on Martian dunes under current climatic conditions (Diniega et al., 2013; Dundas et al., 2012; Pasquon et al., 2016; Reiss et al., 2010). Recent mapping has shown that they occur between 36.3° S and 54.3° S and from

64.6° S to 70.4° S (Pasquon et al., 2016). They are characterised by long (100–2,500 m), narrow grooves, are bounded by levées and have relatively small source areas. Forming exclusively on south polar and mid latitudinal intra-crater dunes, their activity is seasonal, and has been found to be concurrent with the final stages of sublimation of the CO_2 ice deposit at the end of winter and beginning of spring (Pasquon et al., 2016), rendering a CO_2 sublimation formation mechanism likely. These eponymous features are mostly linear; though they sometimes adopt sinuous patterns and taper down-slope.

3.1.2.1 Terminal Pits

Unlike terrestrial gullies, which are nearly always formed by liquid water, linear gullies do not have associated debris aprons. Instead, their channel termini are invariably punctuated by one (or more) terminal pit(s) (Figure 3.2 a–d). Located at the end of the linear gully channel, the terminal pit is usually slightly wider than the channel (Dundas et al., 2012). Terminal pits are defined by a roughly circular depression encircled by levées, apart from where the channel enters the pit. Most linear gully channels end in a single pit, herein referred to as the primary terminal pit. However, some terminal pits occur as part of a dyadic to triadic sequence known as "pit strings". Secondary and tertiary terminal pits are defined as terminal pits that are in a linear sequence with the primary terminal pit, and are always similar in size to the primary terminal pit. Many linear gullies, particularly the largest in scale, have lower albedo circular depressions *within* the distal region of their channels and/or their primary terminal pits. We refer to these as inset pits.

3.1.2.2 Detached Pits

Some terminal pits or terminal pit strings are surrounded by multiple detached pits (Figure 3.2 a–d). These pits are not connected to (or in line with) channels and are

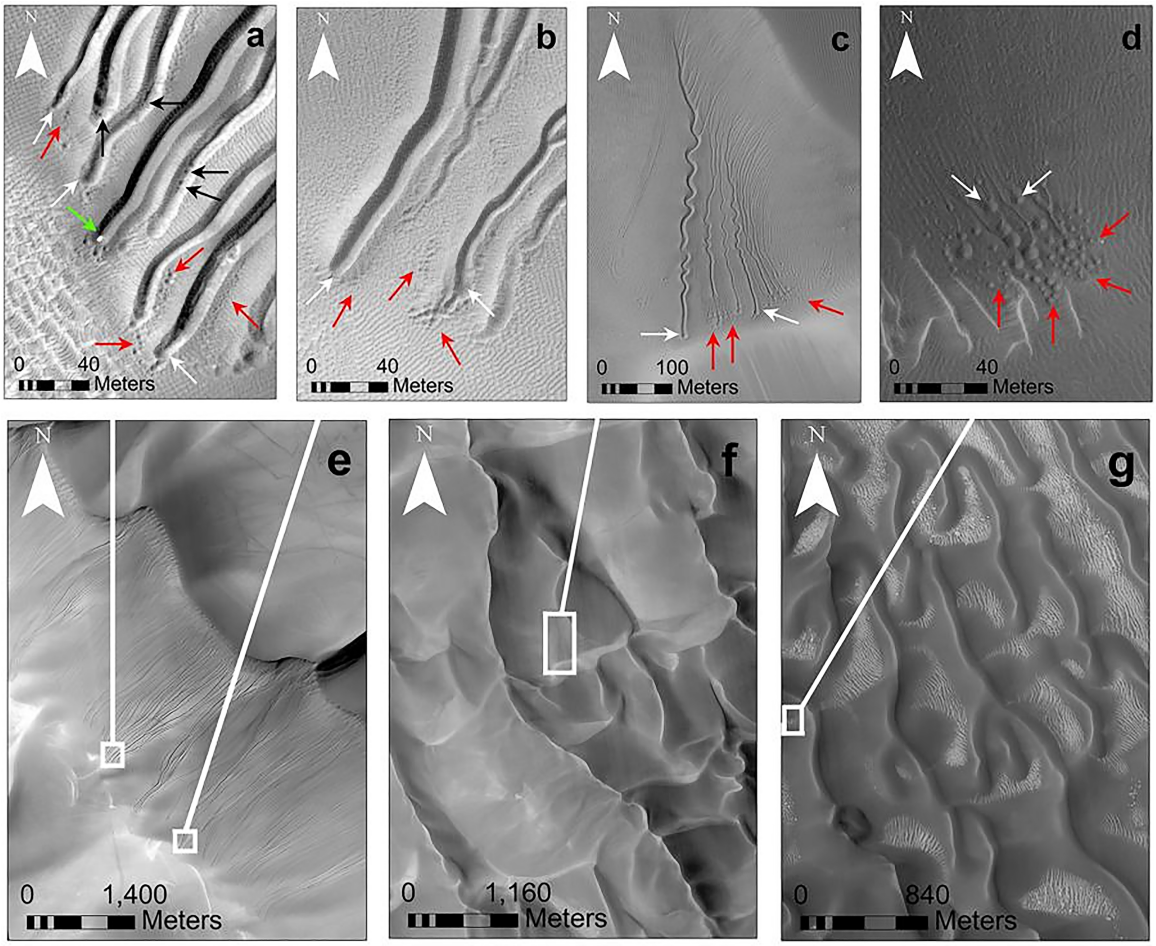

FIGURE 3.2: (a) Terminal and detached linear gully pit morphologies. Terminal pits (white arrows), and detached pits (red arrows) at linear gully termini on Russell Crater Mega-dune (HiRISE image ESP_020784_1255, image centre at -54.3°, 12.9 °, taken at L_s 209.5°). Black arrows point to inset pits within terminal pits. Green arrow indicates a high albedo block which is likely to be a CO_2 block within a pre-existing terminal pit. (b) Terminal pits (white arrows) and detached pits (red arrows) on Russell Crater mega-dune (HiRISE image PSP_007018_1255 taken at L_s 22.5°, image centre at -54.3°, 13° which was used as part of a stereo pair to create the DTM, DTEEC_007018_1255_007229_1255). (c) Example of highly sinuous linear gullies on the west side of Matara Crater dunefield (HiRISE image ESP_030528_1300, image centre at -49.5°, 77.2°, taken at L_s 254.8°). Red arrows point to detached pits, white arrows show terminal pits. (d) "Tadpole" terminal pits in Proctor Crater dunefield (HiRISE image PSP_003800_1325, image centre at -46.9°, 30.7°, taken at L_s 240.9°). These pits (white arrows) are much wider in diameter than their corresponding channels and are surrounded by detached pits (red arrows). (e) Russell Crater Mega-dune (HiRISE image PSP_007018_1255). White boxes show locations of (a) and (b). (f) Matara Crater dunefield. White box shows location of (c). (g) Proctor Crater dunefield (HiRISE image PSP_003800_1325). White box shows location of (d). HiRISE image credit: NASA/JPL/University of Arizona

usually considerably smaller than their associated terminal pit(s). Detached pits are always exclusive to the distal region of the channel and are not found upslope.

3.1.2.3 Pit Formation Hypotheses

Linear gully pits have no terrestrial analogues, and so it is likely that a geomorphic agent that does not occur naturally on Earth may be instrumental in their formation. Originally, terminal pits were proposed to be older flow fronts formed by successive debris flows (Reiss et al., 2010), however this is unlikely as linear gullies are forming today, in a climate which does not currently support liquid water (Dundas et al., 2012).

There are two main schools of thought on the type of CO_2 sublimation activity which might form linear gullies: the CO_2 basal sublimation triggered debris flow hypothesis (Pilorget and Forget, 2016) and the sliding CO_2 block hypothesis (Diniega et al., 2013). The CO_2 basal sublimation triggered debris flow hypothesis (Pilorget and Forget, 2016) suggests a solar-insolation-driven dry debris flow beneath seasonal CO_2 ice on dunes. Successive events have been suggested to carve gully channels in Russell Crater (Pilorget and Forget, 2016). However, while basal sublimation driven debris flows are a plausible mechanism for channel formation, such a process would also deposit material at channel termini. Additionally, the model does not account for the presence of terminal pits or detached pits. The sliding CO_2 block hypothesis (Diniega et al., 2013) is currently the only process that can account for the formation of channels and terminal pits which distinguish linear gullies from other gully morphologies, making this class of gullies exclusive to Mars. The hypothesis proposes that in spring, ice blocks detach from dune brinks. The blocks then descend dune slopes supported by a lubricating layer of CO_2 gas. This gas layer is similar to the Leidenfrost Effect (Leidenfrost, 1966) when a liquid or solid is in thermal contact with a surface that is at a temperature far beyond its boiling or sublimation point. Upon surface contact, the substance (in this case, CO_2 ice), will levitate on a cushion of gas, because the total force exerted by the gas pressure under the block exceeds its weight. This lubricating gas layer eliminates, or reduces, frictional forces so that blocks may move down even very gentle slopes of a few degrees. As it moves it will carve out channels

and deposit lateral levées, until it eventually stops to sublimate at the terminus. This ultimate sublimation explains the formation of a terminal pit. The block is proposed to rest at the base of the channel while sublimating, eroding a depression beneath it and transporting material to the side to form levées. This protracted stationary sublimation may explain why pits are commonly slightly wider than their corresponding channels, which are proposed to form by the rapid movement of blocks downslope (Diniega et al., 2013).

Thus far, alcove, channel, levée and shallow pit morphologies have been observed to form when CO_2 ice blocks were slid onto sand dunes in Utah and Arizona (Bourke et al., 2016a,b). Further evidence consistent with this hypothesis was the detection of high albedo blocks within linear gully channels on Mars. These are most likely CO_2 ice blocks "caught in the act" of sliding through, or stuck within pre-existing linear gully channels (Diniega et al., 2013; Dundas et al., 2012).

It is possible that secondary and tertiary terminal pits may form by blocks that bounce at the channel terminus in the manner observed during field tests on sand dunes in Utah (Bourke et al., 2016a). It has also been proposed that the multiple detached pits which surround many linear gully termini may be formed by smaller parts of blocks which have broken up at the terminus, scattering ice fragments into their surroundings (Diniega et al., 2013). However, the formation mechanism responsible for pronounced terminal pits and detached pits remains uncertain. It is not known if a stationary CO_2 block can erode and deposit material to form the full range of pits identified here. Why detached pits are exclusive to a small fraction of linear gullies and why they are restricted to the lower part of the channel is also not yet clear. If detached pits were formed by broken blocks, it is conceivable that blocks would also break at locations such as sharp bends in the channel, areas of dune surface undulation and locations where channels merge. These are all regions where a block would be subjected to stress and yet detached pits are only found at channel termini. We hypothesise that if stationary sublimating CO_2 blocks have the geomorphic agency to

excavate and deposit material to form pits and circular levées, they must undergo a rapid sublimation process to do so. We reason therefore that blocks which reach the terminus may emit CO_2 jets as they sublimate. If these jets entrain sufficient granular material (Royer et al., 2009) they may then be capable of eroding detached pits when they return to the surface.

Prior to this study, measurements of linear gullies has concentrated on geographical trends (Pasquon et al., 2016) and the linear gully system as a whole (Bourke et al., 2016a; Diniega et al., 2013). Comprehending pit formation is crucial to understanding the formation mechanism responsible for this extra–terrestrial gully type. Therefore, it is important that we test whether sublimating CO_2 ice blocks can form pit morphologies.

3.2 Methods

3.2.1 Objectives

To test the CO_2 block hypothesis, in the context of pit formation, we first conducted a short survey of Martian linear gully terminal pits and detached pits on dunes in Russell, Proctor and Matara Craters. The objectives of this study were to (i) characterise the different terminal pit morphometries, (ii) investigate if there was any evidence of a link between these terminal pit morphometries and detached pits and (iii) investigate the range of block sizes which may be reactivating and widening linear gully channels seasonally.

To further test the CO_2 hypothesis, in the context of pit formation, we performed experiments to examine whether sliding and hence partially buried CO_2 ice blocks would form morphologies comparable to Martian linear gully primary terminal pits and detached pits.

To test the cryoventing hypothesis, in the context of furrow formation, we performed a second set of experiments with two aims: (i) to study the erosion patterns resulting from the interaction between a gently placed CO_2 block and granular substrate and compare these features to a pre-existing Martian furrow network classification (Bourke, 2013); (ii) to study the factors which might constrain furrow pattern type and furrow density.

3.2.2 Survey of Linear Gully Pits in Proctor, Russell and Matara Craters

HiRISE Digital Terrain Models (DTMs) DTEEC_003080_1325_004077 and DTEEC_007018_1255_007229 and corresponding orthophotos were employed to survey linear gully pits in Proctor Crater and Russell Crater, respectively. The polygon tool in ArcMap 10.4 was used to measure the area of individual terminal pits (along the levée apex), taking the diameter of this circle as the pit width. Terminal pit area was calculated by squaring the pit radius and multiplying by π. Pit depths were measured using the Interpolate Line tool, by drawing a line across the pit centre and extending this to the surrounding dune surface. Depth was estimated as the difference in elevation between a pit floor and the surrounding dune surface on each side and averaging these values.

The Russell Crater DTM (DTEEC_007018_1255_007229) has an estimated vertical precision of 1.2 m (Kirk et al., 2008). The relatively low estimated vertical precision is attributed to a low convergence angle (or sum of emission angles) between the stereo pair used to develop the DTM, which reduces vertical precision. Horizontal accuracy of this DTM was given by post spacing, which was 1 m/pixel. The Proctor Crater DTM (DTEEC_003080_1325_004077) has an estimated vertical precision of < 0.5 m (Kirk et al., 2008) and a horizontal accuracy of 1 m/pixel. Pit widths in both locations were generally much wider than 1 m and so horizontal accuracy should not significantly affect our measurements. Both sites were dark dunes and so noise in the

DTMs may have affected our measurements to a small degree. We have estimated an upper limit of this effect by taking 10 linear cross sections close to pit locations in both DTMs. We detrended these cross sections, averaged them and calculated the standard deviation as an estimate of noise (Becerra et al., 2016). In Russell Crater this value was 1.7 m and in Proctor Crater, the value was 1.08 m and so depths < 1.7 m were not reported in Russell Crater and depths less than 1.08 m were not reported in Proctor Crater. Horizontal measurements from orthophotos at both locations may have been affected by atmospheric dust and detector noise which was at the pixel level and would affect our horizontal measurements by one pixel at most.

A time-series of HiRISE images was used to determine whether there may be a link between detached pit and terminal pit formation. We propose that larger pit sizes (that indicate larger ice blocks) have a higher probability of generating detached pits. Terminal pit areas were measured as outlined above and the number of detached pits surrounding them were counted. Detached pits were identified as low albedo depressions. Negative topography was confirmed using the Interpolate Line tool to generate topographic profile data across the feature in the corresponding DTM where possible. Smaller features that may have been artefacts of dune surroundings (*e.g.* shadows in ripples), were not included. HiRISE images taken at the same location (-54.3°, 12.9–13°) on the Russell mega-dune and Matara Crater dunes (-49.5°, 34.7° and -49.5°, 34.6°) allowed us to identify new or widened terminal pits and new detached pits. Suitable data were not available for Proctor Crater.

The Russell Crater observations ranged over 4 MY between MY 29 and 32 and were taken in the Martian southern hemisphere spring. The images used were ESP_012213_1255, ESP_020784_1255, ESP_029764_1 255 and ESP_039153_1255 for MY 29, 30, 31 and 32 respectively. These images have emission angles of 8.2°, 5.1°, 3.8° and 3.8° respectively. Emission angle is the angle between the HiRISE camera and a normal drawn perpendicular to the surface, where 0° is known as *nadir*). Roll directions (obtained by comparing image centre longitude and subspacecraft longitude) were

from west, east, east and west, respectively. For Matara Crater the survey extended over 2 MY between MY 30 and 31 taken in spring (HiRISE images ESP_020414_1300, ESP_029750_1305 for sites at -49.5°, 34.7°. These images have emission angles of 4.7° looking from west and 0.4°looking from east respectively. ESP_021759_1300 and ESP_030528_1300 were examined for sites at -49.5°, 34.6°. These images had emission angles of 9.7° looking from east and 12.2° looking from east, respectively. Differences in lighting were accommodated for by adjusting contrast and brightness in the overlapping images. New detached pits were identified as circular depressions of low albedo that were not in the previous MY image and which surrounded a terminal pit. The extent to which pits were widened (if any) was measured by fitting a circular polygon to the same terminal pit for two consecutive Mars years, calculating area as outlined above, and differencing these data. Early spring images were examined for each location in order to measure high albedo features thought to be CO_2 blocks within channels. This was done by zooming in to optimal pixel resolution and using the Measure tool to record their width and length.

The images were taken at similar L_s, or solar longitude (the Mars/Sun angle, measured from the northern hemisphere spring equinox where $L_s = 0$, a measurement used to quantify Martian seasons). Images were also selected based on the emission angle. To minimise the effect of geometric distortions, single colour RDR images were used in each case. These are radiometrically-corrected images which are map projected. The radiometric correction adjusts for instrument offset, dark current and gain and then converts pixel values to $\frac{Intensity}{Flux}$ reflectance. Geometric processing corrects for optical distortion and projects the image from spacecraft viewing to a map coordinate system. The MOLA (Mars Orbiter Laser Altimeter) DTM is used to improve the camera pointing intercept position on the Martian surface. Orthorectification corrects for distortions that may occur in off-nadir images where the spacecraft roll angle causes pixel foreshortening in the cross-track direction (Cushing et al., 2015). The images we used were not orthorectified, and so disparities may occur when comparing images with different observation geometry. To minimise this effect, images close to nadir

were chosen and care was taken to select images with less than a 5° difference in emission angle. Because such differences are small, we can neglect parallax distortions (Silvestro et al., 2010). A correction was made for any minor deviations however by dividing x-direction measurements by the cosine of the emission angle (Cushing et al., 2015). In each case the distortions are within tens of centimetres and thus fall within errorbars for our measurements.

3.2.3 Experimental Setup

In order to investigate the CO_2 block hypothesis for pit formation (Diniega et al., 2013) and the cryoventing hypothesis for furrow formation (Bourke and Cranford, 2011) we performed laboratory experiments. Initial pilot work, under ambient terrestrial conditions, revealed that water in the atmosphere had a significant effect as it formed frost on the surface of the block and on the bed. This affects the heat budget, the permeability of the bed and the mobility of the grains and must be avoided. Additionally, this frost would later melt and erase the surface microtopography. Therefore, we performed our experiments in a low humidity chamber. The chamber was erected on a level surface in a constant temperature ($\Delta T \approx 3\,\mathrm{K}$) laboratory. A plastic container ($460\times675\times400\,\mathrm{mm}$) was filled with dehumidifying silica gel beads. A smaller plastic container ($300\times520\times370\,\mathrm{mm}$) was placed inside, forming a silica gel bead moat which surrounded the interior container. A perspex lid was fitted on top of the chamber and vacuum bagging gum sealant tape was added at the interface between the container and lid to ensure the chamber was air-tight. A sealed trap door was constructed within the perspex lid in order to minimise exposure to atmospheric water vapour when placing blocks inside.

Prior to each experimental run, three CO_2 ice blocks were placed upon the silica bead moat and were given time to sublimate. These generated dense CO_2 gas which flushed out the original gaseous content, thus removing any water vapour. This reduced the

relative humidity sufficiently so that there was no noticeable frost formation during the experiments on the ∼-80° C CO_2 ice blocks.

Though grain sizes at linear gully and furrow locations on Mars have not been constrained, we used the preliminary data collected by the Curiosity Rover in the Bagnold dune setting on Mars to optimise the range of grain sizes employed in our experiments. We estimated a scale factor of 0.61 (see *Scaling Discussion*) by which to reduce grain size to compensate for the disparity in gravity between Mars and Earth. Grain sizes detected in the Bagnold dunes ranged from fine to coarse sand (Bridges et al., 2016), with many passing through a $<150\,\mu m$ sieve. The average grain size detected in the Bagnold dunes was between 200 and $300\,\mu m$ (Bridges et al., 2016). When scaled, these ranges fall between $<90\,\mu m$ and 122–183 μm, respectively. Therefore, Guyson Honite Glass Spheres of four grain diameter ranges (4–$45\,\mu m$, 45–$90\,\mu m$, 75–$150\,\mu m$ and 160–$212\,\mu m$) were used for sixteen separate experimental runs.

3.2.4 Experimental Protocol

In the low humidity environment, pure CO_2 ice blocks were slid onto beds of glass spheres of each grain size range. We define "sliding" as a gentle motion nudging the block onto the bed surface — sliding is a motion which has enough force to slightly disrupt the granular surface. Sublimation then transports the grains underneath and near the edge of the block. We used Structure from Motion (Westoby et al., 2012) (Sfm) to build Digital Elevation Models (DEMs) of the resultant morphologies from each experiment. We then compared these morphologies and morphometries with Martian terminal and detached pits measured using HiRISE images and DTMs.

A second set of experiments was designed to study the formation of furrows. The blocks were placed as gently as possible on a flat granular bed in order to generate CO_2 gas flow beneath the block. The aim was to investigate whether such a layer of gas at the interface between CO_2 ice and a granular substrate could form furrow networks

on an initially smooth and level bed. SfM was again employed to build high resolution DEMs of the features produced and the resulting furrow morphologies were compared with the well-characterised furrow networks on Martian dunes (Bourke, 2013; Bourke and Cranford, 2011).

Each granular sample was dried and sieved to disaggregate material prior to each experiment. The sample was then poured into the inner container and levelled using a spirit level. A time-lapse camera was positioned inside the chamber to record sublimation rate. A digital hygrometer placed on top of the bed indicated depression of relative humidity in real-time. Once relative humidity decreased sufficiently, the trap door was opened and a CO_2 ice block of mass $< 1\,\text{kg}$ (Table 3.1) was either placed or slid onto the bed. The chamber was immediately sealed and the block in each case was allowed to sublimate and interact with the granular substrate. This sublimation process lasted ∼7–11 hours for each block depending on its mass and whether it burrowed. Videos of the initial sublimation dynamics in each case were recorded with an iPhone 6S 12 megapixel camera from outside the chamber, in order to avoid accumulation of grains on the lens which would hamper video quality.

3.2.5 Digital Elevation Model Development

All features resulting from CO_2 sublimation were modelled in three dimensions by SfM (Westoby et al., 2012) using Agisoft Photoscan. SfM is a technique for reconstructing three dimensional structures from two dimensional image sequences. Agisoft Photoscan is commercially available software which can photogrammetrically process digital images to create 3D spatial data. Each feature produced was imaged at many overlapping positions. In order to establish scale in the DEMs, coded markers were placed within the scene. Agisoft Photoscan finds the exact centre of coded markers enabling the production of highly accurate DEMs and the accurate measurement of features in the scene. Agisoft recommend that three or more scale bars are optimal.

Therefore, a local coordinate system composed of three coded markers at known distances apart from one another, was used for scale definition (Verma and Bourke, 2018) to develop our 3D models. This local coordinate system was composed of three black and white circular 12-bit coded markers which were printed on three 6.8×8 cm sheets of paper. The centres of these markers were positioned on a flat wooden triangle (of 75 cm^2 area) and the markers themselves were laminated with a thin layer of plastic (Verma and Bourke, 2018). The (x, y, z) coordinates of the marker centres were carefully measured with an Engineer's Scale prior to placement in the scene (Verma and Bourke, 2018) and these were later entered in Agisoft Photoscan to develop scale bars for reference within the models. These coordinates (in metres) were: (0, 0, 0), (0.064, 0.115, 0) and (0.131, 0, 0) and these have accuracy < 1 mm. The scale was in a constant location relative to the experimental chamber in each case, the centre of the nearest target on the scale was 15 cm from the chamber. This was close enough so that it could be seen in multiple overlapping images. This served as a reference for scale definition and also helped the processing tool to align images accurately. Constancy was assured by the remote nature of the laboratory — external vibrations were minimised. Care was taken when moving around the region of interest not to cause vibrational disturbances. In order to ensure a vertical orientation of the z-plane, the local coordinate system was placed flat on the laboratory bench during each experiment. The planar arrangement of the coded markers was confirmed using a spirit level to ensure the bench was level and the laminate nature of the markers ensured they did not bend.

The images were captured at a maximum distance of ∼1 m from the bed surface and minimum distance of ∼0.05 m at a variety of angles with respect to the image subject in each case. Camera positions were not recorded, as Agisoft Photoscan can compute accurate estimates. The focal length on the camera and aperture were fixed at 4.15 mm and f2.2 respectively and otherwise, the camera was not calibrated. Between 41 and 100 images were captured for each experiment, depending on whether fine detail such as furrow patterns were to be captured, or whether primary pit dimensions

alone would be measured. The images were then aligned and referenced in Agisoft Photoscan, to build a point cloud, mesh and generate a DEM and corresponding orthophoto of each feature (resolutions in Table 3.1). The dimensions of each pit were then measured in ArcMap 10.4, using the DEM and orthophoto.

Differencing before and after DEMs in order to estimate pit depth was not possible due to the high albedo of the initial flat bed. We approximated the initial level surface by taking an average of 5 linear cross sections of the flat bed surrounding (but farthest from) the pit in ArcMap 10.4. In each case brighter regions where distortions were expected were avoided when taking these transects. A line was interpolated across the primary pit to these locations and the difference in height between the original bed surface and the depression formed by the CO_2 ice block was determined. An average and standard deviation of these values were taken in each case and standard deviations fall within the uncertainty margins outlined in *Laboratory DEM Uncertainty Estimates*. Levées were measured in a similar manner by taking average values of the difference between the average flat surface and levée height. Maximum and minimum levée height were recorded in each case.

The area of furrows produced on each bed surface was recorded using polygonal mapping in ArcMap 10.4. The area of the flat pit floor in each case was determined by zooming in to optimal pixel resolution on the orthophoto overlain above the DEM and using the free-hand tool to mark the line where the inner slope of levées ended and the flat pit floor began. The pit floor is defined as the reasonably flat area directly below where the incident block was for which the perimeter is identified as the line between where the inner levée slope ended at 1 pixel resolution. The area of the space between furrow networks was determined by zooming in to optimal pixel resolution and mapping the outer edge of each furrow. This total area was differenced from the total pit floor area to get the area covered by furrow networks. The area covered by furrows was then expressed as a percentage of the total pit floor area. A

complete discussion of the DEM uncertainties presented in this chapter is available in *Laboratory DEM Uncertainty Estimates*.

3.3 Results and Discussion

3.3.1 Primary Pit and Levée Formation via CO_2 Ice Block Sublimation

Pits, which are visually comparable to Martian linear gully primary terminal pits, were observed to form via both the (i) stationary and (ii) sliding interaction between sublimating CO_2 ice and substrate of all grain sizes. The primary terminal pits which punctuate linear gully channels on Mars are characterised by depressions in the substrate encircled by positive relief levées. The pits observed in our laboratory experiments were negative relief features surrounded by positive relief levées which formed primarily by excavation of material via sublimation. Pits were deepest for finer grain sizes (Table 3.1).

In the cases where material was not transported on top of the block, the resulting pits adopted the shape of the block that formed them (Figure 3.3 a,b). In our experiments, blocks were rectangular. In other cases, the block burrowed into the bed and superposed material sunk as the block moved downward. In all cases, the primary pit which formed was wider than the block forming it.

Upon initial contact with the substrate which was roughly at room temperature, the block in each case underwent rapid sublimation, thus levitating it and mobilising material within its surroundings. This interaction was interpreted by observation to be brought about by the Leidenfrost Effect, as considered in the CO_2 block hypothesis. The force of the escaping gas on the grains, transported grains within the sublimating gas from beneath the block to the side, forming levées. During this initial stage of sublimation, vent apertures developed at gaps between the block and the inner slope

Exp.		Duration (hr:min)	DEM resolution (cm/pixel)	Orthophoto resolution (cm/pixel)	SfM RMS reprojection error (pix)	DEM Noise Uncertainty (cm)	DEM Horizontal Uncertainty (cm)	DEM Vertical uncertainty (cm)	Relative humidity (%)	Gas temperature ()	Block mass (g)	Block thickness (cm)	Pit depth (cm)	Block length (cm)	Pit length (cm)	Block width (cm)	Pit width (cm)	Max levée height (cm)	Min levée height (cm)	Predicted pit width (m)	Predicted pit length (m)	Predicted pit depth (m)	Predicted pit depth error (m)	
Experimental Series 1																								
4–45	**placed**	10h45	0.087	0.011	0.293	0.038	0.079	0.067	12.3	24.2	544	1.5	1.10	19.0	21.8	10.2	14.9	13.4	10.8	1.46	1.15	0.733	0.107	Dendritic, curvilinear
45–90	**placed**	10h48	0.108	0.013	0.240	0.038	0.082	0.100	10.0	23.4	680	1.9	0.66	19.3	21.5	12.0	15.0	9.7	5.7	1.25	1.11	0.347	0.116	Sinuous, linear
75–150	**placed**	9h35	0.101	0.013	0.136	0.020	0.074	0.168	8.9	24.0	832	2.1	0.5	20.0	22.8	12.2	14.1	5.0	2.8	1.16	1.14	0.238	0.052	Dendritic, linear
160–212	**placed**	9h20	0.124	0.016	0.444	0.080	0.071	0.083	5.6	21.7	626	2.0	0.3	20.0	21.0	12.5	13.5	5.3	3.2	1.08	1.05	0.15	0.040	Dendritic, linear
4–45	**slid**	8h00	0.075	0.009	0.261	0.024	0.070	0.209	10.2	24.9	803	2.0	2.0	19.8	32.0	11.1	19.1	17.4	5.4	1.72	1.62	1.000	0.130	None
45–90	**slid**	9h10	0.080	0.010	0.256	0.100	0.070	0.210	9.9	24.7	813	2.2	1.4	20.2	22.6	12.5	14.8	10.3	6.0	1.18	1.12	0.636	0.106	None
75–150	**slid**	9h00	0.083	0.010	0.083	0.038	0.083	0.049	2.7	19.1	761	2.3	0.45	19.8	23.1	11.8	13.4	5.3	3.2	1.14	1.17	0.194	0.027	Sinuous
160–212	**slid**	9h40	0.104	0.013	0.293	0.063	0.073	0.068	6.0	24.1	811	2.3	0.41	20.0	23.6	12.2	14.3	4.0	3.0	1.17	1.18	0.179	0.033	None
Experimental Series 2																								
4–45	**placed**	10h17	0.064	0.017	0.35	0.031	0.078	0.230	13.3	22.3	818	2.2	1.14	19.5	21.6	12.0	14.0	15.0	1.04	1.17	1.11	0.304	0.114	Sinuous, linear
45–90	**placed**	11h25	0.058	0.015	0.77	0.083	0.060	0.290	9.8	20.0	788	2.2	1.33	19.5	23.9	10.6	14.6	9.0	8.0	1.38	1.23	0.6	0.135	Sinuous
75–150	**placed**	10h36	0.065	0.018	0.49	0.068	0.080	0.270	3.0	23.8	712	2.2	0.73	20.0	22.2	11.5	13.9	5.5	1.5	1.21	1.11	0.332	0.157	Linear
160–212	**placed**	7h35	0.064	0.016	0.52	0.035	0.080	0.050	1.0	23.0	626	2.0	0.49	19.2	20.1	11.5	12.4	5.0	3.6	1.08	1.05	0.245	0.117	Dendritic, linear
4–45	**slid**	7h00	0.053	0.013	0.27	0.043	0.079	0.120	13.0	23.2	932	2.5	2.50	20.0	34.2	12.0	19.2	16.5	5.0	1.59	1.71	1.000	0.134	None
45–90	**slid**	8h15	0.110	0.013	0.27	0.092	0.090	0.230	1.0	20.7	726	1.7	1.15	19.5	29.5	12.0	16.7	12.5	3.5	1.39	1.51	0.676	0.082	None
75–150	**slid**	8h00	0.059	0.015	0.26	0.081	0.086	0.090	12.3	21.2	782	2.5	0.82	19.5	21.7	12.0	14.1	3.9	1.3	1.18	1.11	0.328	0.095	Dendritic, linear
160–212	**slid**	9h18	0.138	0.016	0.28	0.043	0.076	0.080	7.1	20.5	832	2.5	0.29	20.0	26.2	12.0	13.8	3.5	1.3	1.15	1.31	0.119	0.033	Linear

TABLE 3.1: Earth laboratory experiment controlled and measured parameters. Duration is the time taken for the block to sublimate fully. Where a block submerged, the end of the experiment was taken as the time when the primary pit was observed to cease sinking. SfM RMS reprojection error is the root mean square reprojection error for the markers. Low reprojection error is indicative of good localisation accuracy of point projections within the model. DEM noise uncertainty denotes errors measured by taking 5 closely spaced linear profiles on a nominally flat region of the granular surface, detrending the vertical profiles and taking the standard deviation. DEM horizontal uncertainty denotes the uncertainty on horizontal measurements as a result of imprecision in target constancy, estimated via a bootstrap method within the SfM models. DEM vertical uncertainty denotes our upper limit vertical uncertainty estimates for any vertical distortions caused by some photos taken at a perpendicular angle to the viewing subject. This error estimate was derived by taking 10 vertical transects along a 1.3 cm section of a ruler in experiment 1 and a 3.3 cm section of the experimental container close to the region of interest in experiment 2, calculating the average of these values and expressing the uncertainty as the difference between the average vertical measurements observed in the model and 1.3 cm or 3.3 cm respectively. Predicted pit dimensions are normalised pit dimensions calculated as the ratio of pit dimensions to corresponding block dimensions. DEM vertical uncertainty was then propagated along with a block measurement uncertainty of 0.2 cm, to get the uncertainty on predicted pit depth (see *Laboratory DEM Uncertainty Estimates*, for further detail.)

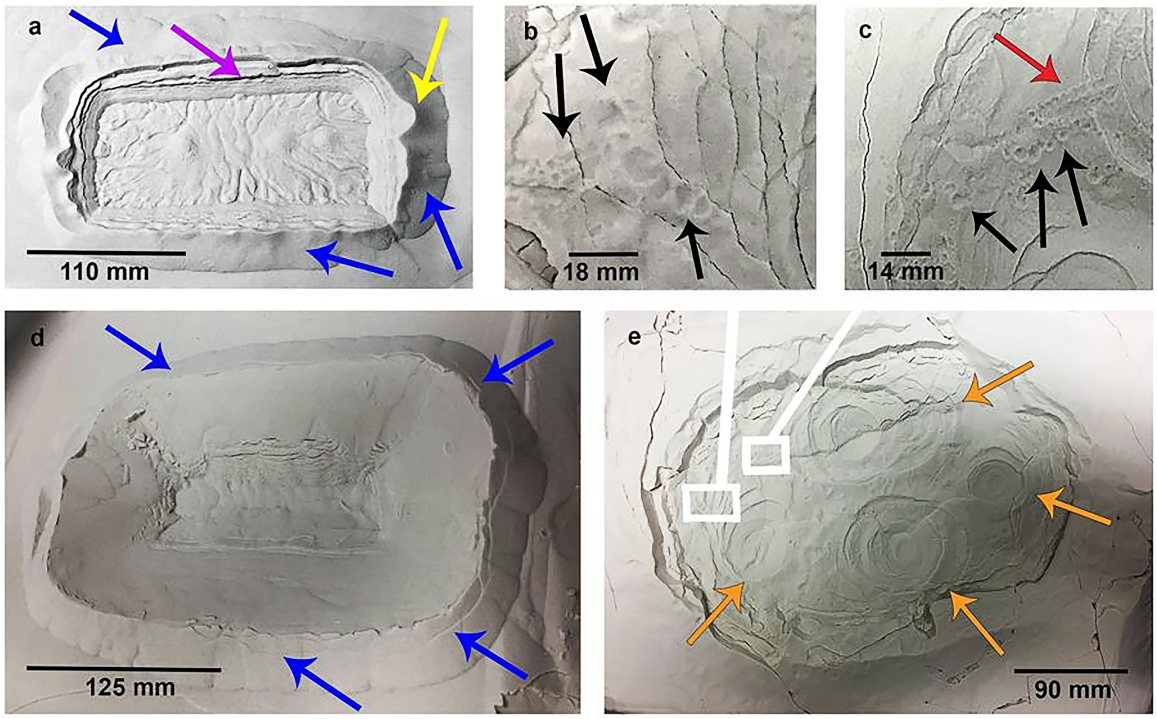

[h!]

FIGURE 3.3: Primary pits and detached impact pits formed during our experiments by the interaction between sublimating CO_2 ice and granular substrate. (a,b) Primary pits formed by block placement on beds of 45–90μm. Levées are denoted by blue arrows. Yellow arrow in (a) points to a preserved vent aperture. Purple arrow indicates a zone of slumping in (a). (c, d) Detached impact pits (black arrows) formed by return of granular clusters to a 4–45 μm bed surface as a sliding block burrowed beneath the bed and exhibited jet activity from the subsurface. Red arrow indicates linear strings of impact pits. These impact pits were ubiquitous over the primary pit surface (seen in e). (e) Wider view of the system formed when a block was slid onto a bed of 4–45 μm grains. Orange arrows identify collapsed pit morphologies which signify locations where jets emanated from the subsurface. White boxes show locations of (c) and (d), respectively.

of levées, from which jets of gas were observed to expel granular material to the main granular sheet (Supplementary Video 3.1). Some of these vent apertures were preserved after the sublimation process, while others were destroyed by gravitational collapse. After the initial rapid sublimation stage, sediment transport ceased and the block sublimated slowly for $\sim$ 7–11 hours. It is thought that at this stage, the temperature difference between the block and the granular substrate decreased below the Leidenfrost point, thus ending the levitation and sediment transport phase.

When a block was slid onto the bed surface, a greater range of dynamic responses was observed (Supplementary Video 3.3). In these cases, particularly in the 4–45 μm and

45–90 μm grain cases, sublimation dynamics mobilised grains on top of the block. This increased thermal contact between the substrate and the surface area of the block and subjected more grains to the Leidenfrost Effect and the force of rapid sublimation. Pits were generally deeper in these instances, compared to when a block was placed on a bed of the same grain size range (Table 3.1).

Levées that formed during each experiment increased in maximum height with decreasing grain size (Table 3.1). This is expected, since decreasing grain size increases grain mobility as the Shields parameter (a non-dimensional number used to calculate the initiation of motion of sediment in a fluid flow (Shields, 1936)), increases. Levée morphologies were comparable to those encircling the terminal pits of linear gullies on Mars. These were raised, positive relief features which surrounded the pit in each case. The relationship between levées and terrestrial debris flows combined with sinuosity has previously been invoked to support a debris flow genesis for gullies (including linear gullies) on Mars (Mangold et al., 2010). Our experiments highlight the equifinality of the granular response to the movement of dry and wet fluids. Levées formed without the need for downslope block movement and granular material was transported to the side under the influence of pressurised gas alone. This is consistent with the sliding CO_2 hypothesis which suggests that stationary blocks at linear gully termini are capable of excavating and transporting sediment to form pits and surrounding levées.

3.3.2 Furrow Formation via CO_2 Sublimation

Our laboratory experiments are the first that show that features similar to the sand furrows on Mars can form by sublimating CO_2. The furrows form under the CO_2 block and closely resemble Martian furrows — they are negative relief features similar in pattern and planform though on a smaller scale. The furrows observed displayed a range of patterns (linear, sinuous, dendritic and curvilinear). Martian furrows have been spatially correlated with dark fans, where vents in the ice are posited to form.

These fans are thought to be composed of sand transported from beneath the ice by the cryoventing mechanism (Bourke, 2013). Furrow networks observed in the laboratory terminated at vents that developed at the boundary between the ice block and the pit walls (Figure 3.4 a). When a block was placed on the bed surface and carefully lifted as observed in Supplementary Video 3.2, it was discovered that furrow mouths were located at regions where vents formed. Jets at vent locations were observed to transport grains from beneath the block. From these observations, we deduce that it is possible for furrows to be formed by pressurised gas that escapes through vents.

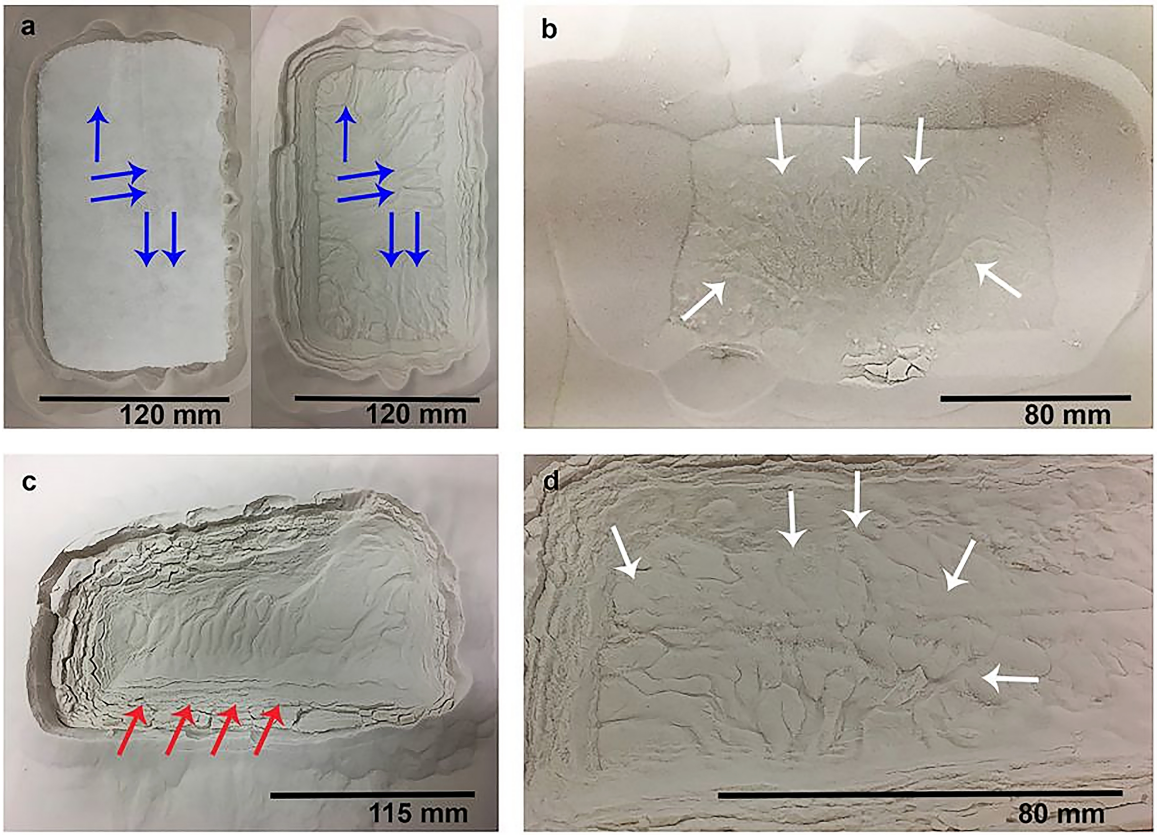

FIGURE 3.4: Furrow patterns and networks observed in the laboratory. (a) Before (left panel) and after (right panel) sublimation for experiment on a bed of 45–90 μm grains. Left panel: sublimating block. Arrows point to vents where gas escapes from beneath the block. Right panel: primary pit formed on the same bed by the block shown in left panel, containing linear and sinuous furrows. The direction of gas flow is marked by the convergence of furrows towards vent locations (blue). (b) Dendritic network of furrows (white arrows), formed in <1 minute when a block was placed on a bed of 75–150 μm grains. This block was lifted and then removed to demonstrate that dendritic patterns can rapidly form. (c) Primary pit containing linear and sinuous furrows extending across a pit floor on a bed of 4–45 μm grains. Vent apertures were not preserved, however by observation it was noted that vents operated on each side of the block. (d) Close-up of dendritic furrow network (white arrows) on a bed of 45–90 μm grains.

Furrow abundance increased with decreasing grain size (Figure 3.5 c). Considering also the general increase in pit depth (Figure 3.5 b) and maximum levée height with decreasing grain size (Table 3.1), we report a feedback between grain size and feature formation via CO_2 sublimation. When grain size distributions on Martian dunes are better constrained, this observation might shed light on why furrows are restricted to certain locations in the southern hemisphere (Nash and Bourke, 2015). However, we report that furrow pattern and network type are independent from grain size. Using the furrow pattern and furrow network classification derived from a survey of Martian dunes (Bourke, 2013), we classified the different network types formed by CO_2 sublimation according to planform. The following classes were delineated: linear (straight negative relief lines in the substrate), curvilinear (curved negative relief lines in the substrate showing one inflection point), sinuous (highly curved negative relief lines in the substrate displaying more than one inflection point) and dendritic (branching negative relief features in the substrate) (Bourke, 2013).

On Mars, the specific location and patterns of furrows on dunes changed between Mars years following emplacement and sublimation of the seasonal CO_2 ice deposit. We can report a similar outcome for our experiments where furrow location and pattern changes for similar grain sizes between experiments. In some cases, a variety of networks and patterns developed on beds of the same grain size range. We identified dendritic and curvilinear furrow networks on the 45–90 μm bed pit floor (Figure 3.4 d) while only linear and sinuous patterns resulted from a second experiment of block placement on a 4–45 μm bed (Figure 3.4 c).

Dendritic networks were observed in certain experiments across all grain sizes and these developed almost instantaneously as observed in Supplementary Video 3.2, rather than via a network growth over time. However, furrows detected in our experiments formed via the contact between a $\sim$ -80 CO_2 ice block and substrate which was roughly at room temperature and our incident ice was on a much smaller scale to that which seasonally covers Martian dunes. Our initial conditions were very different to

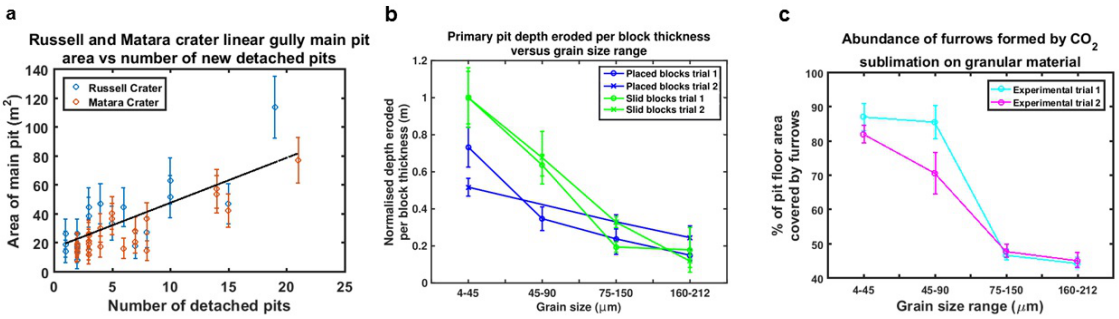

FIGURE 3.5: Observational and experimental trends of furrow and pit abundance and morphometry. (a) Martian detached pit abundance versus area of terminal pits in Russell and Matara Crater. Plot indicates an increase in the number of new detached pits each spring with increasing linear gully terminal pit area in Russell and Matara Crater. Error bars were calculated by taking 2 x the pixel width for each site and propagating the error on πr^2 for each terminal pit area). The R^2 value for the linear fit is 0.72 and the p value is < 0.01. (b) **Laboratory primary pit depth eroded per block thickness.** Plot indicating that pits observed in the laboratory were generally deeper on beds of the finest grain sizes. The CO_2 block placed on a bed of 45-90 grains in experiment 2 partially burrowed and therefore is not included here. Error bars denote vertical error (z error) on each DEM. This was calculated by taking 10 vertical sections of a ruler where available, or known measurement in the scene of the DEM, averaging them and differencing this value from the actual measurement. (c) **Furrow abundance observed in the laboratory versus grain size plot.** Plot shows furrow abundance observed in the laboratory decreased with increasing grain size. Error bars were calculated by defining horizontal uncertainty as better than 1 mm, defining furrows as negative relief erosional lines in the substrate, defining the pit floor as the section at 1 pixel resolution where the inner slope of the surrounding levée ended and relatively flat surface beneath where the block was began, and allowing for error in digitisation decisions when marking the pit floor and furrow outlines in ArcGIS. Considering these factors, uncertainty on measurements was estimated to be 10 orthophoto pixels in each case and their volumes were propagated within the furrow percentage expression to obtain an estimate of uncertainty on furrow abundance.

the gradual basal heating of the CO_2 ice sheet and consequent ice rupture proposed in the cryoventing model. However, we have demonstrated that dendritic patterns can form in a single cryoventing event, as was proposed for Mars (Bourke, 2013).

Dendritic patterns tended to form when there were few vents, and when vents were furthest apart. We note also that when vents were located directly across from one another at each side of the block, linear and sinuous furrows formed instead. This is consistent with the observation that cryoventing efficacy on Mars is constrained by vent spacing (Bourke, 2013). We interpret this laboratory observation as an indication that cryoventing is likely to be limited by a pressure gradient. High pressure gas at

the centre of the ice/substrate interface will be attracted towards an area of low pressure — such as that provided by a vent. If there is a roughly equal pressure gradient between the block centre and two lateral vents opposite one another, gas will escape at a similar rate towards either side and this will be reflected in the presence of linear or sinuous patterns that extend and connect across the base of the pit floor. We propose that Martian furrow formation and network type may be influenced by a pressure gradient, supplied either by inhomogeneous ice thickness on dune slopes and/or stress locations such as dune brinks. Further work may clarify the extent to which ice thickness and surface topography influence pressure gradients at furrow and dendritic trough locations on Mars.

3.3.3 Impact and Collapsed Pit Formation

In addition to primary pit formation, the cases where a block was slid onto grains of 4–45 μm and 45–90 μm revealed two additional pit types (Figure 3.3 c–e). These instances involved very different fluid dynamics to those observed in all other cases. Grain mobilisation induced by increased thermal contact between ice surface area and the warmer granular material, enabled the block to move downward, and the bed appeared fluidised (Supplementary Video 3.3). This process lasted ∼1 minute in each case before the block was observed to submerge fully within the granular bed. CO_2 gas jets escaped from the subsurface (Supplementary Video 3.3), excavating the material in the space surrounding their path and providing room for adjacent material to sink, forming collapsed pits (Figure 3.3 e). These endogenic pits were characterised by concentric tensional fissures and did not have raised rims.

Finally, a third pit type was observed to form via the return of jetted sediment to the steady bed surface. These impact pits (Figure 3.3 c,e) were smaller in diameter than the primary pit and varied little in size (up to 6 mm in diameter, to below our measurement accuracy). Some occurred in strings and all possessed raised rims, suggesting

surface material was ejected in their formation. Following the cessation of sublimation, impact pits were ubiquitous across the primary pit, levées and surrounding bed surface.

3.3.4 Laboratory DEM Uncertainty Estimates

There are several factors which contribute to uncertainties in our DEM measurements. Firstly there are errors due to imprecision in construction and measurement of our scale objects (calibration targets). The construction of the objects was much more accurate than the measurement of their locations which we estimate as better than $\pm 1\,mm$. Additionally, changes in relative humidity in the laboratory environment, though small, may have caused the wooden triangle to expand and contract slightly during imaging and external vibrational disturbances cannot be entirely accounted for. We evaluated these errors in the SfM model using a bootstrap approach. We randomly perturbed the measurements of the calibration targets by $\pm 1\,mm$ and then re–ran the SfM software. As one would expect, if enough images are used and the targets well located, the outputs of the SfM varied by no more than $\pm 1\,mm$ in each direction. Although care was taken to sample the flat bed far enough away from the pit site for grain transport to affect the initial surface measurement when measuring pit depths, sediment transport during venting may have introduced a small uncertainty due to potential vertical accretion of $\sim$ 2 grains in each case where a block was placed onto the surface and in the cases where the block was slid onto the $75-150\,\mu\,m$ and $160-212\,\mu\,m$ grains. An upper estimate of 10 grains may have accreted onto the flat surface when a block was slid onto $4-45\,\mu\,m$ and $45-90\,\mu\,m$ granular bed. However, in all cases these fall within the error estimated for our measurements.

Despite efforts to ensure optimum quality when photographing the region of interest, external factors such as the response of the high albedo grains to lighting differences and reflection from the container in some cases, may have led to noise affecting

our measurements, particularly in the flat regions used to measure pit depth. We estimated the contribution of noise to our uncertainties in each case by drawing 5 topographic profiles of $\sim 10\,cm$ very closely together across a flat region of interest. We detrended and averaged this data and estimated noise by calculating the standard deviation in each case. The uncertainty provided by noise is included in Table 3.1. Additionally, despite zooming to one pixel to take our vertical and horizontal measurements, operator error may have occurred. Having tested our approach by making repeat measurements, we estimate the contribution of this error to be ± 1 pixel in each case. For a pilot run of the first trial of experiments, we included an additional scale which was established by placing a plastic ruler with millimetre graduations on the inner wall of the container which was visible in multiple overlapping images. This scale was established by placing a marker at the lower edge of the marking specifying 0 cm and another at the lower edge of the marking which denoted 30 cm on the ruler and then specifying a scale bar between them of 30 cm. However with this approach, resolution and reprojection error did not differ significantly from models developed having used only the coded markers. Additionally, difficulty in placing the points accurately could have introduced auxiliary errors, whereas 12–bit coded markers can be decoded precisely by Agisoft Photoscan. Therefore, we consider automatic coded target detection as more precise than manual marker placement.

For the first run of experiments the ruler was reconstructed within the scene of each 3D model but we did not use it for scale bar development. However, the ruler was later used to estimate the vertical uncertainties in the model. For this, a known vertical section of the ruler of 1.3 cm was measured within the model ten times along its length in order to sample any vertical distortions or variations which may have affected our measurements of the nearby pit. For each of these measurements, we zoomed into one pixel and used the Interpolate Line tool in ArcGIS to calculate the vertical distance between the tip of the ruler and a dark strip at its centre which we knew measured 1.3 cm. For the second run of experiments, the ruler was not

available within the reconstructed scene. Instead a known distance of 3.3 cm from the top of the container to a horizontal indentation which ran around the inner wall of the container, was measured 10 times along its length within the model in the same manner as for the ruler. The standard deviation of the values from the actual value were the greatest errors involved in our measurements and we have used these as an approximation of z error within our models. These data are included in Table 3.1.

3.3.5 Pit Measurements in Proctor, Russell and Matara Craters

For morphometric measurements, we surveyed 60 primary terminal pits on Russell Crater mega-dune and 135 primary terminal pits at 13 sites in Proctor Crater. This preliminary study was carried out purely to demonstrate an initial trend that may help us to assess our laboratory data in the context of Martian dunes and is not intended as an exhaustive survey of Martian linear gully pits.

All terminal pits were characterised by a roughly circular depression surrounded by circular levées, were shallow ($<$ 1m–2.5 m) and varied greatly in diameter, from $<$1 m to as much as 19 m. Pits were generally wider than their accompanying channels. This is consistent with our laboratory observations that pits were wider in diameter than the sublimating blocks which formed them. We propose that blocks translating down-slope do so quite rapidly and so the width of the channel carved corresponds with block width, while the stationary block may sublimate at the terminus, eroding and transporting material for longer at the site.

In Proctor Crater, the average primary terminal pit width was 3.2 $\pm$ 0.5 m and the majority of pits (83.7% of those sampled) were less than 4 m in diameter, with the minimum pit diameter being 1.4 m. The remaining 16.3% of pits were between 4 m and 8 m in diameter (maximum 7.4 m in diameter). Only 16 terminal pits were deeper than the vertical uncertainty of 1.08 m on the Proctor Crater DTM used. The aspect ratios of terminal pits ranged between 0.8 and 1.7.

The Russell Crater terminal pits are larger. Only 11.7% of terminal pits sampled were 4 m or less in diameter, while 46.7% of terminal pits were between 4 and 8 m in diameter and 41.6% were between 8 m and 19 m in diameter. The minimum primary terminal pit width on Russell Crater mega-dune was 2.7 m and the maximum primary terminal pit width was 18.6 m. Only 3 primary terminal pits were deeper than the upper limit vertical uncertainty of 1.7 m on the Russell Crater DTM, and for these we determined an aspect ratio range between 3.6 and 8.3. Detached pits on Russell Crater Mega-dune of average diameter 2.5 m were found predominantly in the vicinity of the largest primary terminal pits. Other large primary terminal pits were not accompanied by detached pits. However, these particular linear gullies indicated higher probability of block energy loss such as high sinuosity and lateral small channels. These activities may have slowed blocks down or broken them up before reaching the termini.

We observed a trend in Russell Crater and Matara Crater detached pit data (Figure 3.5 a), which suggests that the abundance of these multiple detached pits at linear gully termini increases with the surface area of the newest/widened terminal pit. Should terminal pits be formed via the sublimation of CO_2 ice blocks, the data suggest that a greater block size (and hence greater surface area exposed to sublimation) produces more detached pits. This is in agreement with our laboratory observations that "detached" impact pits formed on finer grain sizes when a greater amount of CO_2 ice surface area was undergoing the initial rapid sublimation dynamics of the Leidenfrost Effect, allowing it to burrow.

We hypothesise that the impact pits observed in the laboratory were formed through a clustering (Royer et al., 2009) instability in the granular jets 3.6. This lends credence to our hypothesis that the multiple detached pits surrounding many Martian linear gully terminal pits (Figure 3.2 a–d) may be formed by a similar mechanism involving granular jets. We reason that at linear gully termini, the sublimating CO_2 may become unstable as blocks reach a terminal velocity (and greater drag force) at the

lower dune slipface, which is reflected in the confinement of these detached pits to the lower ∼200 m of the channel vicinity (Figure 3.2 a–d). Granular clusters may become entrained within sublimating CO_2 gas jets as the block sublimates. We propose that these are splayed out radially from the terminal pit to form smaller, shallower detached pits upon return impact to the sandy surface, in a similar manner to the mechanism by which impact pits were observed to form in our laboratory experiments (Supplementary Video 3.4). However, our laboratory experiments required jetting of an endogenic origin which resulted in terraced collapsed pits seen in Figure 3.3 e. Similar morphologies have yet to be identified on Mars, but it is possible that inset pits seen inside terminal pits may denote locations where blocks have burrowed beneath the surface. Alternatively, inset pits could indicate new, inner paths of blocks within pre-existing channels. However, the ratio of collapsed to impact pits in our laboratory experiments ranged from 5.3–10 and the ratios of inset pits to smallest detached pits in Russell Crater ranged from 4.3–8.1 and so certainly for the smaller detached pits in this setting, our proposed process is plausible. A detailed numerical mode of jetting activity under Martian conditions would allow us to understand the effect of scaling on the proposed process.

In one instance, a high albedo block was measured within a pit on Russell Crater mega-dune (Figure 3.2 a) during MY 30, which disappeared the following year and hence was likely to be CO_2 (Dundas et al., 2012). The pit was observed to widen by 2.1 m in MY 31 during the disappearance of the block. We measured the block in MY 30 to be 2.4 m wide, giving a pit to block widening factor of 0.9. This is consistent with the degree to which we observed pits to erode in the laboratory setting. The pit to block width ratio observed in our laboratory experiments ranged from 1.08 to 1.72. Considering a horizontal uncertainty in this HiRISE image of 0.25 cm/pixel, this observed pit widening by a high albedo block is consistent a CO_2 block hypothesis. Considering our scaling arguments, it is likely that the high albedo object was a CO_2 block which eroded its surroundings to widen a pre-existing pit.

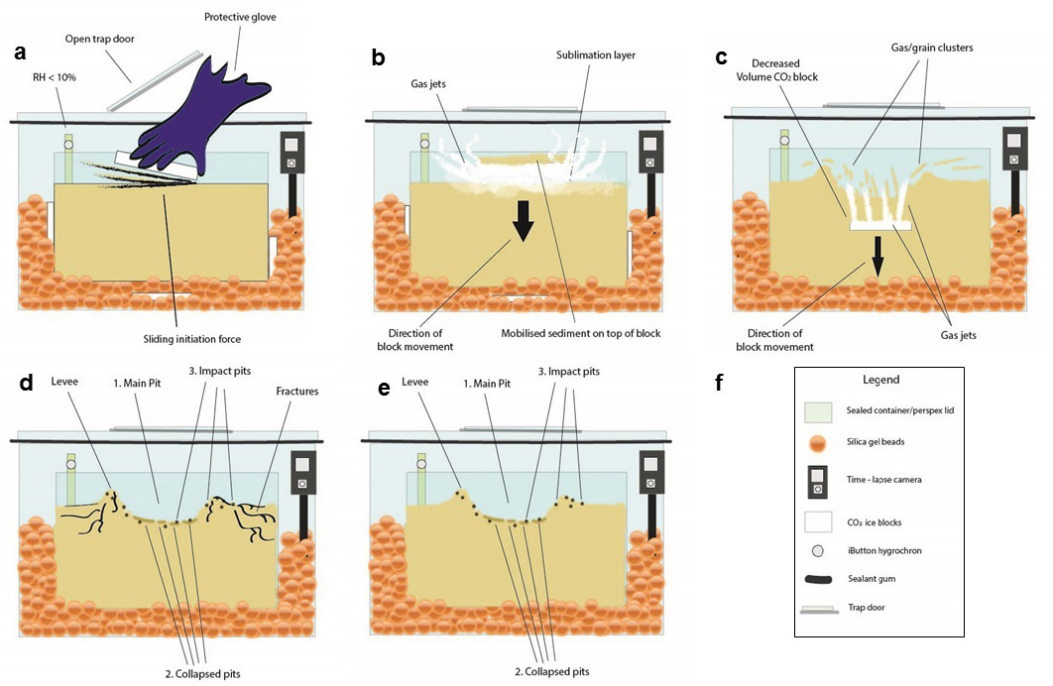

FIGURE 3.6: Conceptual model of three pit formation modes. (a) Block is slid onto grains (beige), increasing thermal contact. (b) Grains are mobilised on top of the block via escaping pressurised gas, increasing CO_2 ice exposure to the Leidenfrost Effect. (c) Block submerges; gas jets escape and surface material sinks forming collapsed pits. (d) Impact pits form by substrate return via fluid instability such as inelastic collapse of gas jets or granular clustering within jets; returned grains impact the surface forming shallow, rimmed impact pits. (e) 3 resultant pit morphologies; primary pit, collapsed pits, impact pits (within main pit and surroundings bed surface) and cracks. (f) Legend.

The wide variation in aspect ratio found at both locations is consistent with a dry ice block hypothesis. The blocks that naturally fall from over steepened cornices or steep alcove walls will have a range of sizes and will not be symmetric, thus they will form a wide variety of pit dimensions. Considering the average grain size range reported for the Bagnold dunes on Mars (200–300 μm) (Bridges et al., 2016), we used the values in Table 3.1 and our calculated scale factor of 0.61 (see Experimental Scaling) to estimate the block or slab sizes needed to form our range of pits. Using our upper grain size ranges of 75–150 μm and 160–212 μm, we estimate that the block or slab sizes needed to form the pits we have surveyed range from 1.2 m–6.5 m in Proctor Crater and 2.4 m–16.3 m in Russell Crater. High albedo blocks of dimensions between 1.6 and 6 m have been measured in our survey of Russell Crater, however larger blocks have yet to be identified.

The lower range of normalised pit to block width ratios is consistent with dimensions we have observed on Mars using HiRISE images in which high albedo blocks have been identified in linear gully channels in Matara Crater (Diniega et al., 2013) and in channels and pits in Russell Crater (Dundas et al., 2012). The ratio of channel width to block width in Matara Crater ranges from 1.9 to 1.1 and in Russell Crater, observed ratios were 1.7 to 2.0. Allowing for measurement uncertainty of one pixel width (0.25 m), these values fall within our estimated range of 1.08–1.72. Although these channels have clearly been eroded prior to the observations of these blocks within them, we can speculate that blocks of similar size to those observed eroded them. Should further data be collected on block sizes at these locations, our laboratory data can be drawn upon to assess whether pit dimensions in the locality are likely to be formed by these CO_2 ice blocks and perhaps, by how much pit dimensions might grow seasonally.

3.3.6 Mars DTM Accuracy

Per communications with S. Sutton in addition to Kirk et al., 2008 (Kirk et al., 2008), we provide calculations of the vertical and horizontal accuracy of the HiRISE DTMs used in our survey of Martian pits.

3.3.6.1 Horizontal Accuracy

Horizontal accuracy was determined by the post spacing found in the README file of each DTM. For DTEEC_003080_1325_004077 and DTEEC_007018_1255_007229 the horizontal accuracy was 1 m/post.

3.3.6.2 Vertical Accuracy

Vertical accuracy was determined using the following formula (Kirk et al., 2008):

$$EP = \frac{\Delta p \times IFOV}{parallax/height} \tag{3.1}$$

Where EP is the expected vertical precision, Δp is the sub–pixel matching quality taken as the total RMS found in the README file of each DTM, IFOV is the Instantaneous Field Of View of the image pixels in meters on the ground. This was determined using the non-map-projected pixel scale of the original data reported on the HiRISE image page under "Original image scale range". The average of the two halves was taken. Parallax/height was taken as the tangent of the convergence angle for each stereo pair (calculated below).

3.3.6.3 Convergence Angle

The convergence angle is the algebraic sum of the emission angles. If images are taken from opposite sides, emission angles are added. If taken from the same side, these are differenced.

Calculations of Vertical Precision for DTEEC_007018_1255_007229 (Russell Crater):

- Horizontal accuracy: 1 m/pixel
- $\Delta p = 0.372$
- PSP_007018_1255 IFOV = 0.254 m
- PSP_007229_1255 IFOV = 0.507 m

- PSP_007018_1255 longitude = 12.9677°
- PSP_007018_1255 sub–sc–lon = 13.3769°
- PSP_007018_1255 emission angle = 3.42699°
- PSP_007229_1255 longitude = 12.9056°
- PSP_007229_1255 sub–sc–lon = 12.2307°
- PSP_007229_1255 emission angle = 5.73872°
- Convergence angle= 3.4+5.7 = 9.1°
- $EP = \frac{(0.372 \times 0.507)}{Tan(9.1°)} = 1.2m$

For the calculations of uncertainty on terminal pit area expressed as error bars in Figure 3.5 a, we simply propagated horizontal uncertainty as follows:

$$\sigma A = \sqrt{\Sigma(2\,\pi\,r_i)^2 \times \delta_H^2} \tag{3.2}$$

where σA is the uncertainty on the area of each pit, r_i is the radius of the primary terminal pit (or additional radii of secondary and tertiary terminal pits) and δ_H is the horizontal uncertainty on the DTM in each case.

Calculations of Vertical Precision for DTEEC_003800_1325_004077_1325 (Proctor Crater):

- Horizontal accuracy = 1 m/pixel
- $\Delta\, p$ = unknown (use 0.2 as an estimate)
- PSP_003800_1325 IFOV = 0.253 m
- PSP_004077_1325 IFOV = 0.282 m

- PSP_003800_1325 longitude = 30.6667°
- PSP_003800_1325 sub-sc-lon = 30.1359°
- PSP_003800_1325 emission angle = 5.30512°
- PSP_004077_1325 longitude = 30.6691°
- PSP_004077_1325 sub-sc-lon = 27.664°
- PSP_004077_1325 emission angle = 27.7249°
- Convergence angle = 27.7249-5.30512 = 22.419°
- $EP = \frac{(0.2 \times 0.282)}{Tan(22.419°)} = 0.15\,m$

Since we used an estimate of 0.2 for $\Delta\, p$, the estimate of vertical precision is possibly on the low side. We thus take the estimated vertical precision for this DTM to be better than 50 cm.

3.3.7 Scaling Discussion

A complete discussion of the scaling is beyond the scope of this chapter and requires a detailed mathematical model. Such an analysis for the levitation of blocks has been presented previously (Diniega et al., 2013). For the geomorphological effects we build on this work and apply dimensional analysis. The key observation is that behaviour is extremely sensitive to grain size. On Earth and even on Mars, grains with radius r $< 1\,mm$ are roughly in the Stokes regime and have fall velocity

$$u_f = \frac{2}{9}\,\frac{\rho_s}{\nu}\,g\,r^2 \tag{3.3}$$

where ρ_s is the density of the particles, ν the dynamic viscosity of the atmosphere and g gravity. ρ_s and ν are roughly the same on Earth and Mars despite the huge

difference in atmospheric density. To compensate for the difference in gravity the particles need only be reduced in size by the ratio $\sqrt{\frac{g_T}{g_M}} = \sqrt{\frac{9.8}{3.7}} = 0.61$. The thermal response is given by

$$\frac{(T - T_s)I}{\sqrt{t}} \tag{3.4}$$

where T is the initial temperature of the sand, T_s is the sublimation temperature, t is time and I is the thermal inertia. On Mars $I \approx 120\, J\, m^{-2}\, K^{-1}\, s^{-1/2}$ whereas for the glass spheres on Earth $I \approx 420\, J\, m^{-2}\, K^{-1}\, s^{-1/2}$. There is a difference in composition of the granular material used in these experiments and aeolian sand on Mars. Data on chemical composition of grains on Martian sand dunes does not yet appear to be well-constrained. However, preliminary data of grains on the Bagnold dunes (Bridges et al., 2016) reports that grains are mostly dark grey and sometimes show multicoloured patches suggestive of multiple mineralogies. Some are brick-red/brown and may be pieces of local vein fill minerals. Others are green, brown (suggested to be olivine), colourless, and translucent spheres (Bridges et al., 2016). The grains used in our experiments were soda lime glass beads containing $< 75\%\, SiO_2$ and traces of Na_2O, CaO, MgO and free iron. Other environmental differences include Martian atmospheric surface density which is $\sim 0.020 kg\, m^{-3}$ whereas Earth's is $1.2 kg\, m^{-3}$. Differences in temperatures and atmospheric pressure as well as other differences in sediment properties can be found in (Supplementary Table 3.2). There is also a difference in the sublimation temperatures with $T_s = 147$K on Mars and 195K on Earth. Gully activity in the southern hemisphere is thought to have occurred when dune surface temperatures ranged from 190 K to 260 K (Dundas et al., 2012). The temperature of the granular material used in the experiments was 295K, but was not precisely controlled and may have been as much as 20K warmer or colder, ranging from 293 K to 313 K. For our qualitative results the temperature difference was therefore roughly equivalent. The significant difference in thermal inertia simply means that there will have been a significant heat flux for a $\frac{I_T}{I_M} \approx 12$ times longer time. The most significant difference in relation to morphology is the size of the block. On Mars, blocks will be of the order of 1m whereas blocks used in our experiments were

Variable	Mars	Earth	Units	Description
		Ambient Conditions		
T_o	260	300	K	Surface temperature
p_o	510	1.0110^5	Pa	Atmospheric pressure
g	3.7	9.81	$m\,s^{-2}$	Gravity
		Sand		
κ	0.013	0.26	$W\,m^{-1}\,K^{-1}$	Thermal conductivity
c	680	830	$J\,kg^{-11}\,K^{-1}$	Heat capacity
k	10^{-9}	10^{-11}	m^2	Permeability
ρ_s	1600	1540	$kg\,m^{-3}$	Density
$I_s = \sqrt{\kappa\,c\,\rho_s}$	119	576	$J\,m^{-2}\,K^{-1}s^{-1/2}$	Thermal inertia
		Glass Spheres		
κ		0.15	$W\,m^{-1}\,K^{-1}$	Thermal conductivity
c		800	$J\,kg^{-1}\,K^{-1}$	Heat capacity
k		310^{-11}	m^2	Permeability
ρ_s		1500	$kg\,m^{-3}$	Density
$I_s = \sqrt{\kappa\,c\,\rho_s}$		424	$Jm^{-2}K^{-1}s^{-1/2}$	Thermal inertia
		CO_2		
T_s	147	195	K	Ice block temperature
e	5.7110^5	5.7110^5	$J\,kg^{-1}$	Enthalpy of sublimation
ν_a		1.8110^{-5}	$Pa\,s$	Air dynamic viscosity
ν_c	1.3210^{-5}	1.3710^{-5}	$Pa\,s$	CO_2 dynamic viscosity
ρ_g	0.010	1.87	$kg\,m^{-3}$	gas density
ρ_c	1562	1562	$kg\,m^{-3}$	Solid density

TABLE 3.2: Relevant physical quantities for Martian Basaltic sand under Martian conditions. $T_o = 260\,K$ and $p_o = 510\,Pa$, dry Navajo Sand under Earth conditions ($T_o = 293\,K$ and $p_o = 101\,kPa$) and glass spheres under Earth conditions. Quantities for CO_2 are also specified for Martian and Earth conditions.

Trial	Granular surface temperature (K)
4–45 $\mu\,m$ placed	299
45–90 $\mu\,m$ placed	293
75–150 $\mu\,m$ placed	301
160–212 $\mu\,m$ placed	298
4–45 $\mu\,m$ slid	308
45–90 $\mu\,m$ slid	298
75–150 $\mu\,m$ slid	294
160–212 $\mu\,m$ slid	303

TABLE 3.3: Granular bed surface temperatures for repeat experiments (trial 2).

of the order of 0.1m. A detailed model of grain movement is necessary to account for this, but we have shown that the other differences should not be significant if the grain size is reduced to balance gravity.

Trial	DEM resolution (cm/pix)	Orthophoto resolution (cm/pix)	Target rms reprojection error (pix)	Ruler rms reprojection error (pix)
4-45 μm placed	0.043	0.011	0.299	0.372
45-90 μm placed	0.051	0.013	0.230	0.411
75-150 μm placed	0.051	0.011	0.183	0.264
160-212 μm placed	0.064	0.016	0.444	0.228
4-45 μm slid	0.037	0.009	0.253	0.385
45-90 μm slid	0.039	0.010	1.906	1.352
75-150 μm slid	0.042	0.011	0.084	0.064
160-212 μm slid	0.053	0.013	0.236	0.229

TABLE 3.4: Model parameters when a ruler was used as an additional reference scale. Because manually placing markers was deemed a less accurate approach, the auxiliary scale was not used for the models reported in this manuscript.

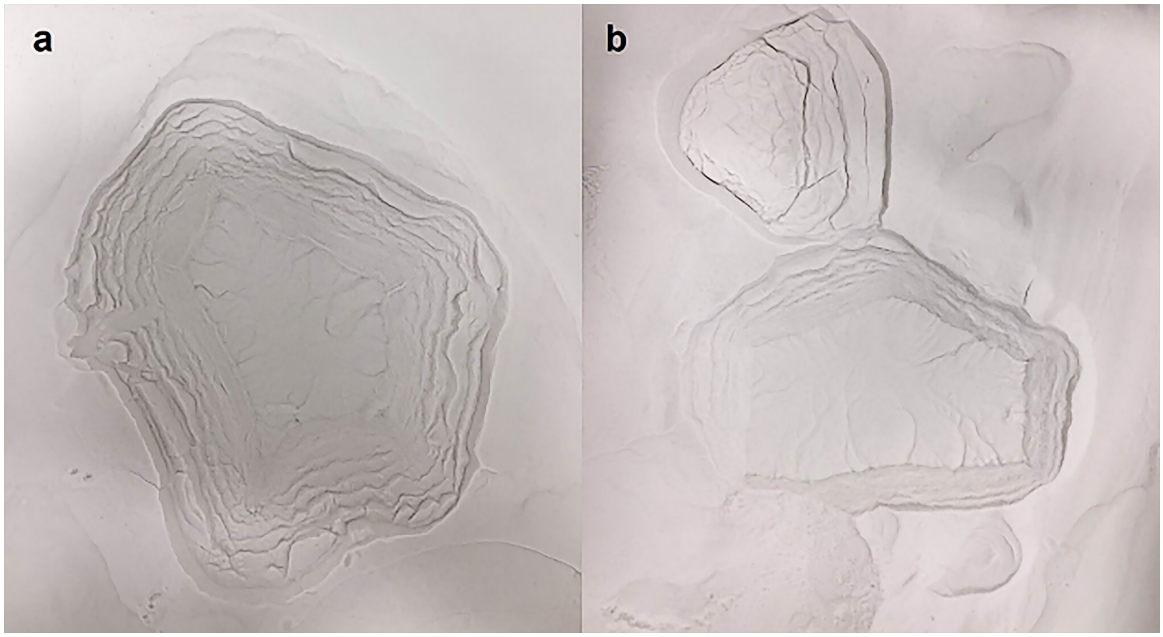

FIGURE 3.7: Circular primary pits observed in the laboratory. Images showing that circular pits formed when rounded block fragments were placed or slid onto a bed of 4–45 μm grains. (a) shows a pit formed by block fragment placement and (b) shows a pit formed when a slid fragment burrowed (top), juxtaposed with a pit (containing furrows) formed when a block fragment was placed (bottom).

3.4 Conclusion

Our experiments suggest that furrows and pits can be formed by the sublimation of CO_2 ice blocks. The differences in temperature, atmospheric density and pressure, and gravity can be accounted for in a scaling analysis by using different sized grains, but the difference in scale cannot easily be dealt with, thus though our evidence is suggestive it is not conclusive. The CO_2 block hypothesis (Diniega et al., 2013) is the only current hypothesis that can explain present-day linear gully pit formation. We have shown that stationary sublimating CO_2 ice blocks in contact with porous, mobile material are capable of transporting sediment to form primary pits and surrounding levées. Our scaling arguments and morphological observations suggest that primary pits may be analogous with Martian primary terminal pits in Russell, Matara and Proctor Craters. In particular, our observation of a high albedo block within a terminal pit and subsequent widening consistent with the ratios predicted from our laboratory data, suggest that linear gully pits may be formed and widened by CO_2 blocks.

Additionally, we have observed that collapsed pits and detached impact pits; two ancillary pit types, can form by sublimating CO_2 ice blocks and subsurface jetting. We have presented a new hypothesis for detached pit formation at linear gully termini. This hypothesis is consistent with the observed relationship between terminal pit area and number of associated new detached pits forming seasonally in Russell and Matara Crater and is supported by the laboratory observation that jetting activity can result in impact pits. Further work is required to appropriately address size scaling, and a detailed numerical model may give further insight.

Cryoventing is the only hypothesis that has been offered for sand furrows on Mars, but prior to this study there has been no physical evidence that a pressurised gas layer at a CO_2 ice and sandy interface can form the complex patterns similar to those observed on Martian dunes. Our results suggest that sublimating CO_2 generates gas flows sufficiently powerful to mobilise grains on top of the incident ice and add to the

granular sheet via venting — a process which is hypothesised to form the dark fans accompanying sand furrows (Bourke, 2013). We have shown for the first time, that a range of furrow morphologies can form by escaping pressurised gas at the interface between a CO_2 ice overburden, and that furrow pattern type is independent from the grain size distribution (within our grain size range) of the material into which it is eroded. The data suggest that cryoventing efficacy and furrow pattern type are limited by a pressure gradient provided by vent spacing. Additional data is required to assess the role of ice thickness and vent geometry in furrow formation.

Our study has delivered for the first time, physical evidence that (1) linear gully pits and (2) furrows; both active features observed to fade, extend and form in the contemporary Martian climate, may be forming via the action of sublimating CO_2 ice.

3.5 Supplementary Videos

- Video 3.1: Vents adding to sheet

  Video highlighting the mechanisms by which gas venting added to the granular sheet and transported sediment on top of a block which was placed on a bed of $4 - 45\,\mu m$ grains.

FIGURE 3.8: QR code to Video 3.1. Written link: https://youtu.be/ngzGpTBjbmM

- Video 3.2: Furrows forming at vent locations

  Video showing that dendritic furrow network mouths correspond with vent locations. This particular Video shows a block being placed and removed on a bed of $75 - 150\,\mu m$ grains.

FIGURE 3.9: QR code to Video 3.2. Written link: https://youtu.be/aNrDLsg3ms4

- Video 3.3: Burrowing CO_2 block

  Video showing the submersion of a CO2 ice block beneath a bed of $4 - 45\,\mu m$ glass spheres. Note gas jet activity and consequent grain transport.

FIGURE 3.10: QR code to Video 3.3. Written link: https://youtu.be/zyxIUM0sUNk

- Video 3.4: Impact pits forming

  Video showing the formation of detached and linear impact pits by granular clustering within gas jets when a block was slid onto a bed of $4 - 45\,\mu m$ grains.

FIGURE 3.11: QR code to Video 3.4. Written link: https://youtu.be/J$_C$$Njyzxg$$OY$

Chapter 4

The Formation of Araneiforms by Carbon Dioxide Venting and Vigorous Sublimation Dynamics Under Martian Atmospheric Pressure

4.1 Abstract

The local redistribution of granular material by sublimation of the southern seasonal CO_2 ice deposit is one of the most active surface processes on Mars today. This unique geomorphic mechanism is hypothesised to be the cause of the dendritic, branching, "spider"-like araneiform terrain and associated fans and spots - features which are native to Mars and have no Earth analogues. However, there is a paucity of empirical data to test the validity of this hypothesis. Additionally, it is unclear whether the organised radial patterns of araneiforms began as radial and then grew, or developed via a gradual connection of troughs towards their centres over time. Here we present the results of a suite of laboratory experiments undertaken to investigate if the interaction between a sublimating CO_2 ice overburden containing central vents and a porous, mobile regolith will mobilise grains from beneath the ice in the form of a plume to generate araneiform patterns. We quantify the branching and area of the dendritic features that form. We provide the first observations of plume activity via CO_2 sublimation and consequent erosion to form araneiform features. Based on calculations of the mass flux sublimation rate of CO_2 ice blocks buried under sediment and consequent volume transport, we show that CO_2 sublimation can be a highly efficient agent of sediment transport under present day Martian atmospheric pressure.

4.2 Introduction

The Martian surface is host to a variety of features which have no Earth analogs and are all active in some capacity today. These include the ephemeral sand furrows (Bourke and Cranford, 2011) which seasonally scour the surface of Martian dunes, only to be later erased by aeolian activity; the enduring and growing dendritic troughs of the southern mid-to-high latitudes (Portyankina et al., 2017b); and the 'spider-like' araneiform terrain of the south polar cryptic region (Kieffer et al., 2006; Piqueux et al., 2003) from which seasonal fans and spots frequently emanate (Thomas et al.,

2010). All of these active geomorphological features exhibit dendritic patterns. These patterns are fractal, resemble tree branches and are found on Earth in systems which are engendered by physical gradients, such as river systems, fork lightning strikes and even nerve endings in the human brain.

On Mars, dendritic patterns are emblematic of exotic geomorphological processes. These processes are driven by a cycle which does not occur on Earth; namely the seasonal phase change of carbon dioxide between solid and gas. The Martian atmosphere comprises over 95% CO_2 (Nier and McElroy, 1977), at least a quarter of which freezes each year (Leighton and Murray, 1966). As winter comes and temperatures decrease, a dry ice layer is deposited on the Martian surface (Leighton and Murray, 1966) ranging in thicknesses of nearly a metre at the poles, to a few millimetres further towards the equator (Aharonson et al., 2004; Smith et al., 2001). The average atmospheric pressure on Mars is very low at 6 mbar, below the triple point of CO_2 and so as this ice heats in spring, it sublimates; that is, it directly converts from solid to gas. The basal sublimation of the seasonal cap is now recognised as a cardinal geomorphological agent responsible for reworking the surface of Mars today (Kieffer et al., 2006), in particular forming araneiforms, which are unlike any surface feature seen on Earth.

Araneiforms (Figure 4.1), frequently dubbed "spiders", are characterised by one or more relatively central depressions from which radial tortuous troughs appear to emanate (Piqueux et al., 2003). These negative topography radial troughs become shallower further away from the central depression and have dendritic and tortuous network patterns. In spring, Araneiforms are frequently accompanied by relatively low albedo fans and spots (Figure 4.1 c-d) (Kieffer et al., 2006; Malin and Edgett, 2001; Piqueux et al., 2003) which appear on top of the CO_2 ice layer that covers them in spring. Araneiforms are observed mainly on the Cryptic Terrain of the South Polar

Layered Deposits (SPLD) Piqueux et al. (2003) and upon neighbouring crater ejecta blankets (Hansen et al., 2017; Schwamb et al., 2018). They usually occur in groups, sometimes packed densely enough to overlap (Piqueux et al., 2003) and are generally found on low surface slopes (Hansen et al., 2010). While the central depression of a single araneiform is typically $\sim$ 50 m across, the entire feature including its troughs spans from tens of metres to up to 1 km across (Hansen et al., 2010; Piqueux et al., 2003). A survey of araneiforms at the Inca City and Manhattan regions of the SPLD allowed a sub-classification of these features according to morphometry (Hansen et al., 2010). This classification identified araneiforms based on whether their patterns were radial or not, on the scale of channels relative to the central depression and on the tortuosity of the channels. "Fat spiders" (Figure 4.1 e-f) consist of wide central depressions with respect to radial troughs (Hansen et al., 2010) and are generally smaller. These spiders measure $\sim$ 50 m across with 30-40 m of that measuring across their centres. "Thin spiders" (Figure 4.1 g-h) have large, rough centres with long, thin troughs radiating outwards and generally cover more area ($\sim$ 100 m across). "Lace terrain" describes dense networks of channels similar in size where a singular radial spider morphology cannot be distinguished (Hansen et al., 2010) and "star-burst" araneiforms (Figure 4.1 a-b) are highly dendritic with thousands of branches, and can extend up to 1 km in diameter. These are all distinct types which are each located in different regions (Hao et al., 2019).

The propensity to form araneiforms has been attributed to the erodability of the surface material of the SPLD which is estimated to contain silt-sized particles 50-200 μ m in diameter (Paige and Keegan, 1994; Paige et al., 1994). The discovery that the fans and spots were appearing in a 'Cryptic Terrain', or region which remains at the same brightness temperature as CO_2 ice (Kieffer et al., 2006) in spring despite a decreasing albedo, led Kieffer to propose that the seasonal fans and spots were not exposed terrain as previously thought (Kossacki and Leliwa-Kopystynski, 2004), but

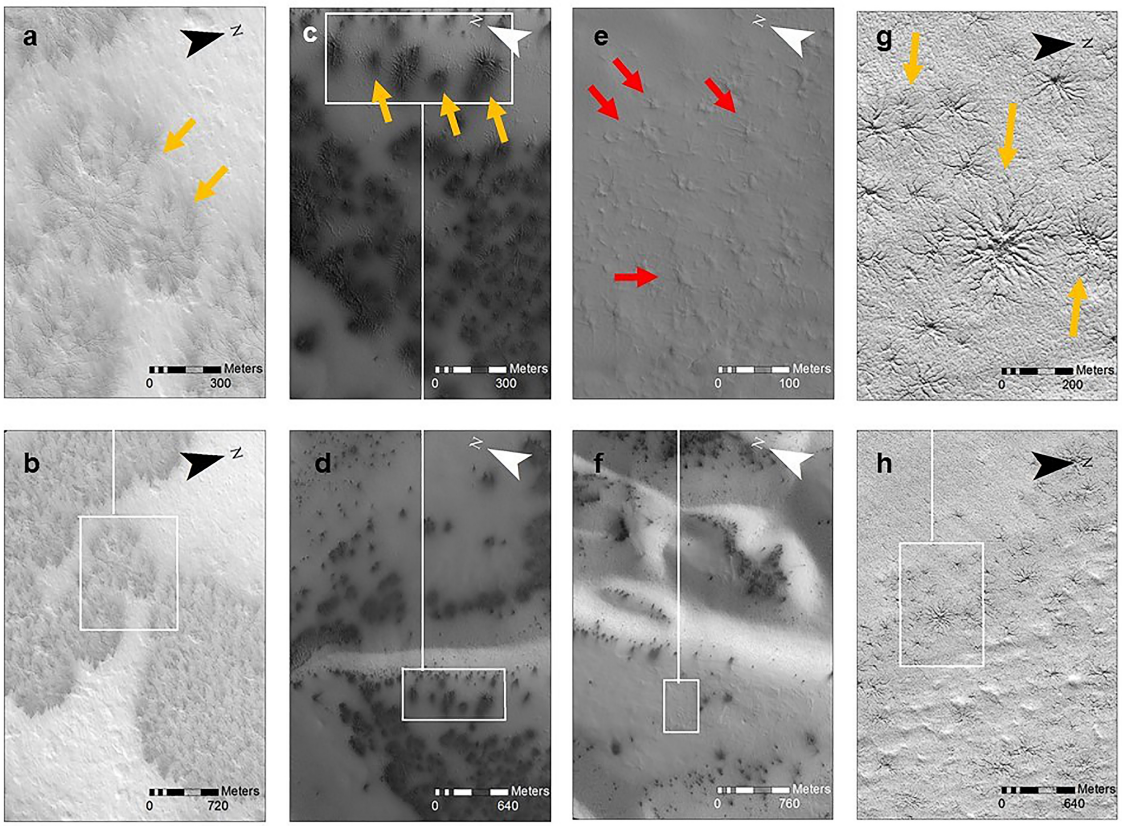

FIGURE 4.1: **Zoomed and corresponding context images of a variety of araneiform morphologies** (a,b) HiRISE image *ESP*_011486_0980 shows 'Starburst araneiforms' which are huge features. Central lat=−81.8 °, Central lon=76.17 °, L_s = 187.3 °. (c,d) HiRISE image *ESP*_011491_0985 shows seasonal dark albedo fans and spots. Central lat=−81.2 °, Central lon=296.04 °, L_s = 187.5 °. (e,f) shows 'fat spiders' in HiRISE image *ESP*_014282_0930. (g,h) shows close ups of 'classic' spiders in the same image as (e,f) only a different location within the site. Central lat=−87.02 °, Central lon=86.57 °, L_s = 320.5 °. HiRISE image credit: NASA/JPL/University of Arizona

in fact excavated sub-ice material transported on top of the ice by confined gas beneath the seasonal CO_2 layer. Invoking the "Solid State Greenhouse Effect" (Matson and Brown, 1989), whereby broad spectrum radiation infiltrates translucent ice to reach the subsurface, the model asserts that in spring, solar radiation penetrates the seasonal translucent slab ice and heats the regolith beneath it. Thermal radiation cannot escape through the ice overburden because it is opaque at thermal infrared wavelengths and so the ice will sublimate from the base. As pressure increases, at some point the ice will rupture and form a vent. Gas will escape through this vent, drawing with it unconsolidated fines from beneath the ice in the form of a plume, and depositing the material as relatively low albedo fans and spots at the surface. A combined effort by (Piqueux et al., 2003) who identified and described spiders,

and (Kieffer et al., 2006), who developed a formation hypothesis, linked araneiform formation with the seasonal appearance of fans and spots. Their dendritic negative topography patterns are thought to be eroded by pressurised escaping CO_2 gas (Kieffer et al., 2006; Piqueux et al., 2003). That the seasonal CO_2 deposit anneals annually into translucent slab ice has been confirmed by Mars Express Omega observations (Langevin et al., 2007) and it has been calculated that 70% of incident solar radiation will reach the regolith beneath the ice overburden (Kieffer, 2007). However, although laboratory experiments have generated araneiform patterns on thin films of sand using a Hele-Shaw cell (de Villiers et al., 2012), particles entrained in jets under Martian conditions have been successfully modelled (Thomas et al., 2011) and dust ejecta have been observed from within irradiated CO_2 ice (Kaufmann and Hagermann, 2017), a CO_2 venting process has never been observed to form araneiforms.

Many other open questions remain surrounding araneiforms and their proposed formation mechanism. Firstly, the seasonal appearance of fans and spots is to date the only notable activity associated with araneiforms. Additionally, despite observational campaigns (Hansen et al., 2010), a plume in action has not yet been observed. While the troughs are thought to marginally widen and deepen annually (Hansen et al., 2017), the Mars Reconnaissance Orbiter High Resolution Imaging Experiment (HiRISE) which has a resolution of 50 cm (McEwen et al., 2007), has not been able to detect changes in the araneiforms (Portyankina et al., 2017b) over the last 7 years of monitoring. Moreover, the radially organised patterns which characterise many araneiforms have not yet been observed to *form* in the present day. This either means that araneiforms are growing at a very slow rate and this change has simply not been observed yet, or present day atmospheric conditions and/or sediment consolidation are not conducive to erosion of the substrate.

However, due to the volume of material (on the order of $10^3 m^3$) (Hansen et al., 2010) that would need to be eroded in one process and hence the requirement of

an extremely high energy budget, it is assumed that these patterns require multiple erosional events to form. On this premise, estimates have been made to date the age of araneiforms to $1 \times 10^3 - 1 \times 10^4$ Mars years (MY) (Piqueux and Christensen, 2008; Portyankina et al., 2017b). The most recent effort at dating araneiforms was based on the idea that dendritic trough growth might represent the initial stages of araneiform development. Dendritic troughs are a recently identified class of negative topography, dendritic feature exclusive to the Martian southern hemisphere and are generally found on dune boundaries (Portyankina et al., 2017b). They endure seasonally and have been observed to extend and merge over the last 5 MY (Portyankina et al., 2017b). However, why gradually connecting dendritic troughs would eventually organise in the very distinct radial patterns of most araneiforms is unclear. It is possible that araneiforms did develop over time via a connection of tributaries as a central depression may continually provide a point of weakness for the ice to rupture (Hao et al., 2019). However, this does not explain why new troughs have not yet been observed to form within an existing radial araneiform in the present day. Whether the araneiforms of the SPLD were formed through connecting tributary systems over many years, or whether their radial patterns are relic features formed in different climatic period(s), remains uncertain. Moreover, though our prior experiments indicated that grain size and vent separation can influence cryoventing and subsequent patterns (Mc Keown et al., 2017) and observations of clustering araneiform sub-types on Mars have suggested grain size and sediment consolidation may play a role in morphology type (Hao et al., 2019), it is not clear what governs the differing araneiform morphologies, their varying levels of branching or the extent of the areas they cover.

Empirical observations are imperative to answering these open questions surrounding araneiforms. However the current empirical framework of sublimating CO_2 under Martian atmospheric conditions is thin, with few authors having tested the efficacy of this remote process as an agent of geomorphological change (Kaufmann and Hagermann, 2017; Mc Keown et al., 2017; Sylvest et al., 2016; Sylvest et al., 2018). Our

previous Earth based experiments indicated that dendritic morphologies formed when vents were located at a distance from each other; hence there was a larger difference between the pressure at the centre of a CO_2 ice block and a vent at its edge (Mc Keown et al., 2017). We hypothesise that just as furrow formation is governed by the direction and strength of a pressure gradient, araneiform formation will be too. Assuming ice thickness to be relatively uniform over a considerable distance, if a vent forms on shallow or flat terrain, gas will flow towards the vent from all directions as the pressure gradient from all directions towards the low pressure region at the vent will be similar. If this is the case, the troughs which make up the radial structure of an araneiform may all have been eroded in one or few event(s). If formed in this way, the smaller the vent is, the higher the pressure gradient and the more branched the pattern is likely to be. In addition, coarser grains will be mobilised less readily because they are heavier and will yield less detailed patterns.

4.3 Methods

In order to test the hypothesis that radial dendritic araneiform morphologies can form via basal sublimation of CO_2 and consequent plumes, and to answer some of the open ended questions surrounding the physical constraints on araneiform formation, experiments involving the placement of CO_2 blocks containing central vents on granular surfaces were performed under Martian pressure. We herein refer to this type of experiment as phase 1. As in our previous Earth - based experiments which explored furrow formation (Mc Keown et al., 2017), the basal heating of CO_2 ice was modelled by exploiting an effect similar to the *Leidenfrost Effect* (Leidenfrost, 1966), as in the work of Diniega et al., 2013 (Diniega et al., 2013). This is an effect which occurs when a substance (in our case solid CO_2), in contact with a surface far hotter than its boiling or sublimation point, will generate a cushion of high pressure vapour. The gas pressure of this vapour layer exceeds the pressure exerted by the weight of the CO_2 ice, allowing it to levitate. The stage at which solar irradiation heats the substrate

beneath seasonal ice on Mars enough that it will cause the ice to sublimate from its base can hence be approximated, albeit on a much smaller scale and with different levels of energy.

In order to study the influence of grain size and vent diameter as well as vent separation on feature morphometry, the area araneiforms cover and the level of branching, Digital Elevation Models (DEMs) of the surface features were generated by Structure from Motion (SfM) (Westoby et al., 2012). Feature dimensions were measured in ArcMap 10.4 and these data were analysed using Matlab R2018a.

The efficacy of CO_2 sublimation as an agent of sediment transport under Martian pressure was constrained by calculating mass flux rate of sublimating CO_2 and estimating sediment displacement per volume of subsurface CO_2. We herein refer to experiments of this nature as phase 2.

4.3.1 Experimental Setup

The Mars Simulation Chamber (Figure 4.2 a) at the Open University is capable of recreating atmospheric parameters characteristic of the Martian environment. The chamber measures 0.9 m in diameter and 1.8 m in length and can depress internal pressure to $<$ 6 mbar in less than 5 minutes. A glass aquarium was deployed on a flat track within the chamber and two Logitech webcams were positioned at both a nadir and side view of the tank. In each experimental trial, the tank was filled up to a height of $\sim 25\,cm$ with Guyson Honite glass spheres of distinct grain size ranges. These were chosen due to their unimodal nature which is helpful when developing numerical models. For phase 1 experiments, grain size ranges chosen were $160-212\,\mu\,m$, $150-250\,\mu\,m$, $250-425\,\mu\,m$ and $425-600\,\mu\,m$. For phase 2 experiments, the smaller

two grain size ranges were used. The smaller grain sizes were used to explore the maximum efficacy of CO_2 sublimation for dust sized particulate matter. A thermocouple was placed within the bed while one was placed outside of it in each case in order to monitor temperature. However this was only indicative of temperature away from the block in real time. Utilising data from extra pilot experiments we performed of thermal gradient measurements beneath the block, we report that initial bed temperature beneath the block was between 16-18 degrees C and temperature decreased exponentially over time to 0 degrees C in just under an hour. Pressure within the chamber was monitored carefully in real time with a pressure gauge.

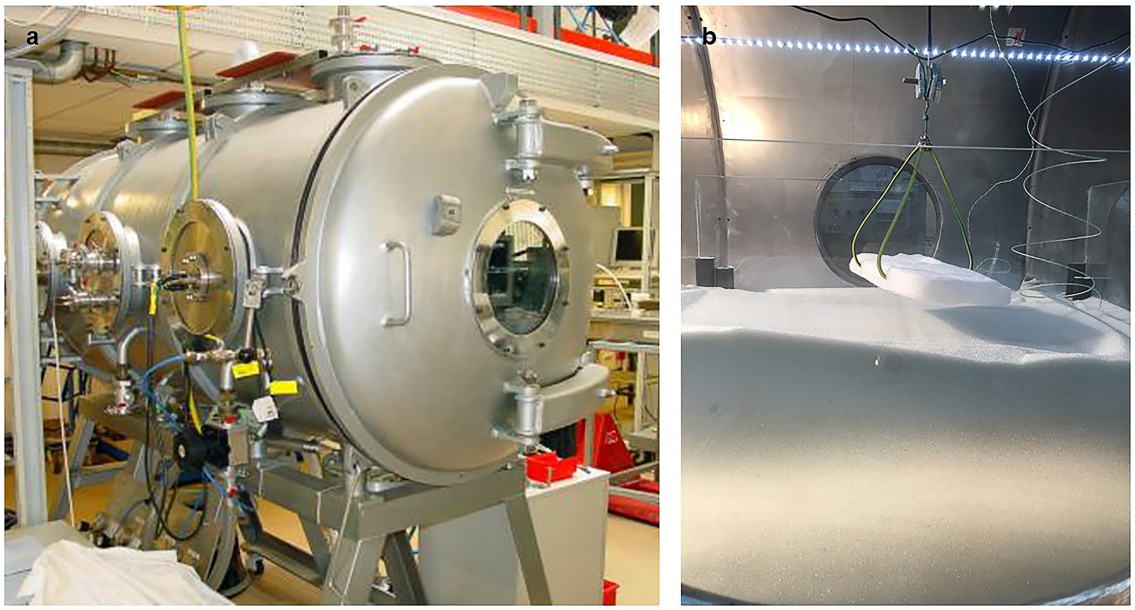

FIGURE 4.2: **Experimental setup** (a) shows the Mars Simulation Chamber which is capable of simulating Martian atmospheric parameters. The chamber measures 0.9 m in diameter. Image credit: The Open University. (b) shows a CO_2 block suspended above a granular bed with a claw which is slotted into holes drilled into its sides.

In order to establish scale in the DEMs, coded targets were printed and attached to plastic poles so that they could be seen at different heights above the sand bed. This was to avoid wide uncertainties in calculation of the z–plane in the 3D model. Their positions in x, y and z were measured with a metal ruler and to improve accuracy, photographs were taken of their positions relative to the mm markings on the ruler. The photos were zoomed so that sub - mm position accuracy could be achieved. A

pyramid-shaped claw attached to a pulley was developed and attached to an external mechanical feed-through (Figure 4.2 b). The pulley was given enough slack so that the claw would just touch the bed surface upon lowering and would be well above the bed when retracted. This was to allow control over timing of block contact with the bed surface and also to ensure the block could be held in place so it would not burrow and erase surface microtopography.

4.3.2 Experimental Protocol

For each experiment, the glass spheres were levelled using a spirit level and smoothed with a metal ruler. Each block used measured roughly $\sim 20\,cm \times 10\,cm \times 2\,cm$. Two holes were drilled on one of the longest sides of a CO_2 ice block and one was drilled on the opposite side so that the claw could be slotted into the block. These cavities were drilled only $\sim 2\,cm$ into the $10\,cm$ width of the block. The holes were drilled close to the bottom of the block so that the claw would not pass through the block fully as the ice sublimated and hence detach the block prematurely while the experiment was taking place. For phase 1 experiments, holes were created at the centres of the blocks by drilling through fully with different sized drillbits. To investigate the effect of vent dimension and spacing on araneiform morphometry, three scenarios were explored: a central hole initially measuring 5 mm in diameter, a central hole initially measuring 3 mm in diameter and two holes along the long axis of the block and at the centre of the short axis, initially measuring 3 mm in diameter and 60 mm apart. In phase 2 experiments, only holes at the sides of the block were generated in order to insert the claw. All experiments were performed in duplicate.

In each case, the block was weighed using a digital scales and its dimensions were measured with a metal ruler. The time of measurement was noted. The claw was slotted into the block and the block was suspended from the pulley above the bed surface

(Figure 4.2 b). The chamber was sealed, depressurised and when ambient pressure reached 6 mbar, the block was gently lowered onto the surface using the pulley. The time between block measurement and contact with the granular surface exceeded no more than $\sim$ 5 minutes for each experiment. Our measured rates of CO_2 sublimation under Mars and Earth pressures (Chapter 3) were averaged to account for the amount of CO_2 that was likely to have sublimated during chamber depressurisation. This was subtracted from the measured mass in each case to estimate block mass upon surface contact. The chamber pressure was monitored so that it did not drastically deviate from average Martian atmospheric surface pressure. The chamber is difficult to maintain at an exact low pressure for these types of experiments however because the pumping rate needs to match volatile evolution in order to remain constant and so this fluctuated, but did not deviate by more than 3 mbar in any case. In phase 1 experiments, the block was lowered so that it was sitting on the bed surface, but also held in place by tension in the pulley. The block was allowed to sublimate for $\sim$ 5 minutes and was then raised very carefully above the bed surface. This was to avoid the block detaching and burrowing, hence erasing surface topography generated by the venting process, and also to avoid spilling granular material from the top of the block on to the surface feature generated.

For phase 2 experiments, the block was lowered and the pulley was left slack to allow the block to detach from the claw as it sublimated and burrow within the granular bed. Once detached, the claw was raised while burrowing continued. Once sublimation had ceased (i.e. the bed was observed to be still and no granular ejecta were observed), the chamber was repressurised and the bed surface was imaged at many overlapping positions to collect data for DEM production.

4.3.3 Digital Elevation Model Development

Both the araneiform features and volume change resulting from burrowing were modelled in three dimensions by SfM using Agisoft Photoscan. SfM is a technique for reconstructing three dimensional structures from a series of two dimensional images. Agisoft Photoscan is commercially available software which can photogrammetrically process digital images to create a 3D reference frame. Each feature produced was imaged at many overlapping positions. For ground control, coded markers were placed within the scene. Agisoft Photoscan detects the centre of coded markers enabling the production of highly accurate DEMs and the accurate measurement of features in the scene. Agisoft recommend that three or more scale bars are optimal. Therefore, a local coordinate system composed of seven coded markers at known distances and heights apart from one another, was used to establish scale. Black and white circular 12-bit coded markers 30 mm in diameter were printed on paper and fixed upon plastic poles which were stuck securely to the container floor with silicone. The (x, y, z) coordinates of the marker centres were carefully measured with a metal ruler and photographs of their positions were taken. The photographs were zoomed and accurate positions were noted. These were later entered in Agisoft Photoscan to develop scale bars for reference within the models. Their coordinates (in metres) were: (0.016, 0.014, 0.2745), (0.0455, 0.013, 0.2595), (0.343, 0.013, 0.2585), (0.3685, 0.0145, 0.2775), (0.3695, 0.5465, 0.258), (0.3685, 0.5710, 0.2725), (0.0135, 0.5425, 0.26), (0.013, 0.5705, 0.298) and these have accuracy $< 1mm$. The targets were close enough to the bed centre so that they could be seen in multiple overlapping images. Constancy of target position was assured by the aquarium containing sediment which was heavy enough that it was extremely difficult to move within the chamber.

The images were captured with an iPhone 6s 12 megapixel camera. Images were taken at a maximum distance of $< 1\,m$ from the bed surface and minimum distance of $\sim 0.1\,m$ at a variety of angles with respect to the image subject in each case.

Camera positions were not recorded, as Agisoft Photoscan can compute accurate estimates and 'Location Services' were disabled in order not to interfere with position interpolation in the model. The focal length on the camera and aperture were fixed at 4.15 mm and f2.2 respectively and otherwise, the camera was not calibrated. Between 30 and 70 images were captured for each experiment depending on the level of detail to be recorded. The images were then aligned and referenced in Agisoft Photoscan, to build a point cloud, mesh and (after extraneous dense cloud data were removed), generate a DEM and corresponding orthophoto of each feature. The dimensions of each feature were then measured in ArcMap 10.4, using the DEM and orthophoto. These measurements, along with DEM and orthophoto resolution can be found in Table 4.1

The depth, width and area of araneiform features and their morphological components produced on each bed surface were recorded using polygonal mapping in ArcMap 10.4. Width was calculated using the 'Measure' tool and taking the average of 5 cross-sections across a similar region. Depth was calculated using the 'Interpolate Line' tool, identifying the difference between the highest and lowest point on each side of the resultant plot and averaging these, then taking an average of 5 of these cross-sections across a similar region. Area rather than volume was measured as most of the araneiforms were sub–DEM resolution in depth and approximating would introduce considerable error. The area of the flat pit floor in each case was determined by zooming in to optimal pixel resolution on the orthophoto overlain above the DEM and using the free-hand polygon tool to mark the line where the inner slope of levées ended and the flat pit floor began. The pit floor is defined as the reasonably flat area directly below where the incident block was for which the perimeter is identified as the line between where the inner levee slope ended at 1 pixel resolution. Levées are defined as the positive relief material surrounding the pit which was excavated and pushed to the sides of the block during sublimation. The area of the space between araneiform networks was determined by zooming in to optimal pixel resolution and

mapping the outer edge of each araneiform leg which was identified as where a region of negative topography ended and positive relief began. This total area was differenced from the total pit floor area to get the area covered by araneiform patterns. This was then expressed as a percentage of pit floor area.

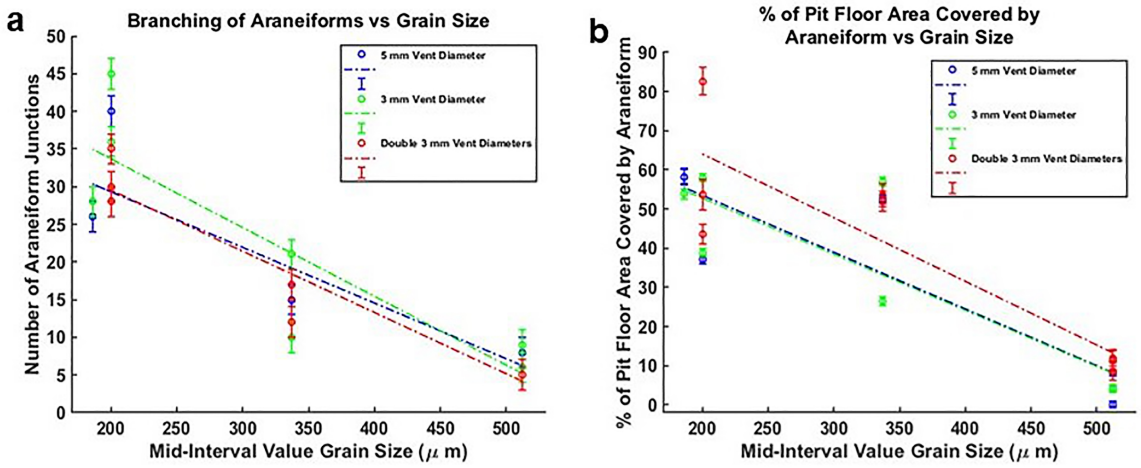

FIGURE 4.3: **Araneiform morphometry.** (a) shows a decrease in the level of branching with grain size. Level of branching has greater variance for finer grain sizes while for coarser grains of 450-600 μm, is more consistent. The R^2 value for double araneiforms is 0.94, for single araneiforms generated using a 3 mm vent is 0.76 and for single araneiforms generated with a 5 mm vent is 0.82. The p values for all are < 0.05. (b) shows a decrease in area covered by araneiforms with grain size. The R^2 value for double araneiforms is 0.8, for single araneiforms generated using a 3 mm vent is 0.74 and for single araneiforms generated with a 5 mm vent is 0.82. The p values for all are < 0.05

The error bars seen in Figure 4.3 were calculated considering the factors that contributed to measurement uncertainty. Firstly there are errors due to imprecision in construction and measurement of our calibration targets. The construction of the objects was much more accurate than the measurement of their locations which we estimate as better than 1 mm. Additionally, some of the targets were covered with sediment during the sublimation process making it difficult to pinpoint their exact centres. Additionally, despite zooming to one pixel to take our vertical and horizontal measurements, operator error may have occurred. Having tested our approach by making repeat measurements, we estimate the contribution of this error to be ± 3 pixels in each case, or ± 9 pixels for each dimension squared. In considering all of

these errors, an estimate of 10 pixel widths was used to cover uncertainty when calculating the area covered by araneiforms. This was propagated in the formula for percentage area using standard error propagation.

The level of branching of araneiforms was determined by counting the number of 'junctions' on each araneiform. A junction is defined as where one branch meets another. Any araneiforms which were partially covered by sediment which fell from the suspended block after sublimation were not analysed in this way and were not included on the plots in Figure 4.3 for consistency. An uncertainty of 2 branches was used in each case as though care was taken, operator error may have mistaken image artefacts for very small branches.

For phase 2 experiments, sediment volume displacement was estimated. Differencing before and after DEMs was not possible due to the high albedo of the granular surface which is difficult to capture as a 3D model when flat. Additionally, due to bright regions on the relatively gentle slopes left after the block had burrowed, DEMs contained holes in some places. Thus, generating a planar surface in ArcMap 10.4 under which to interpolate volume would reduce the accuracy of our volume calculations.

Instead, because the surface was smoothed and levelled prior to each experiment, the initial height of the levelled glass spheres in the container was noted. The initial volume was calculated as width x length x height of the bed in each case. In all cases, dips in the bed were visible in the relevant DEM. Regions of similar depth were identified and the average depth for each region was noted by interpolating a line across the dip and subtracting the average maximum depth from the original height of the unperturbed bed. A polygon tool was then used to mark the outer edges of these individual regions and the area they covered was calculated. These areas were then multiplied by average depth and summed together in order to get an estimate of

the volume displaced during the burrowing process. In cases where the moving block had increased the sediment height in locations, the difference between the original bed height and new height were multiplied by area. This method, while approximate, avoided incorporating bright regions with holes into volume calculations which could introduce order of magnitude uncertainties into our volume estimates.

Images of the resultant bed surface were taken immediately after sublimation for photogrammetry. Sublimation, or mass flux rate was calculated by measuring the mass of the CO_2 block before and after sublimation and burrowing. Activity due to burrowing was taken as complete once no movement was observed within the bed. If any ice remained, by this point, the bed had cooled sufficiently to allow for very slow ice sublimation. If any CO_2 ice remained within the bed post - burrowing, this ice was removed and weighed. Sublimation time was taken as the time between block contact with the surface and the time activity was observed to cease. This time was recorded via webcam. Mass flux rate could then be found by dividing mass difference by sublimation time.

4.4 Results and Discussion

4.4.1 Phase 1: Araneiform Formation

Features analagous in morphology (though orders of magnitude lesser in scale) to araneiforms formed following each experimental trial (Figures 4.4, 4.5, 4.6) . On Mars, Araneiforms are between $\sim$ $10\,m$ and $1\,km$ in total extent while our experimental chamber and ice supply limited physical modelling of araneiforms to the cm scale and so numerical modelling will be required to extrapolate the processes observed in the laboratory to the Martian scale. Excluding the vast difference in scale

however and considering morphology only, we used the classification for araneiforms provided by Hansen (Hansen et al., 2010) to identify the features and to subclassify them. Each feature had negative topography, had a central depression and troughs which were dendritic and tortuous, especially for finer grain sizes. Troughs decreased in depth with distance from the central depression, similar to the Martian forms. In the majority of cases the troughs were radially organised, barring the two instances where the block slipped slightly upon lifting and the resultant forms appeared to interlink and overlap in a more disorganised 'lace' morphology with no distinct centre. The latter were not used for analysis. All radial dendritic patterns formed in one instance and did not require multiple events of trough connection towards a common centre, as was proposed. As the block was uniform in thickness in each case, it is thought that gas flowed from the middle section of the block and out through the central vent from a region of high pressure, to a region of low pressure.

4.4.1.1 Plume Observations

Plumes of CO_2 ejecta entraining sediment were observed in each case (Video 4.1). These are the first observations of plumes depositing material on top of ice and consequently eroding radial araneiform structures. These types of plumes driven by momentum but denser than the ambient fluid are known in the fluid dynamic community as fountains. Unlike on Mars where winds are thought to frequently redistribute the jetted subsurface material in fan shapes away from the centre of the araneiform, the material carried within the plume either fell down onto the surrounding bed or directly back down through the vent. The latter process formed a central raised spot within the central depression. Plume height was simply observed and not measured because in some cases, the plume height was limited by the height of the chamber but differences according to (i) vent diameter and (ii) grain size, could be qualitatively observed. Vent diameter affected plume height significantly, with ejecta from plumes

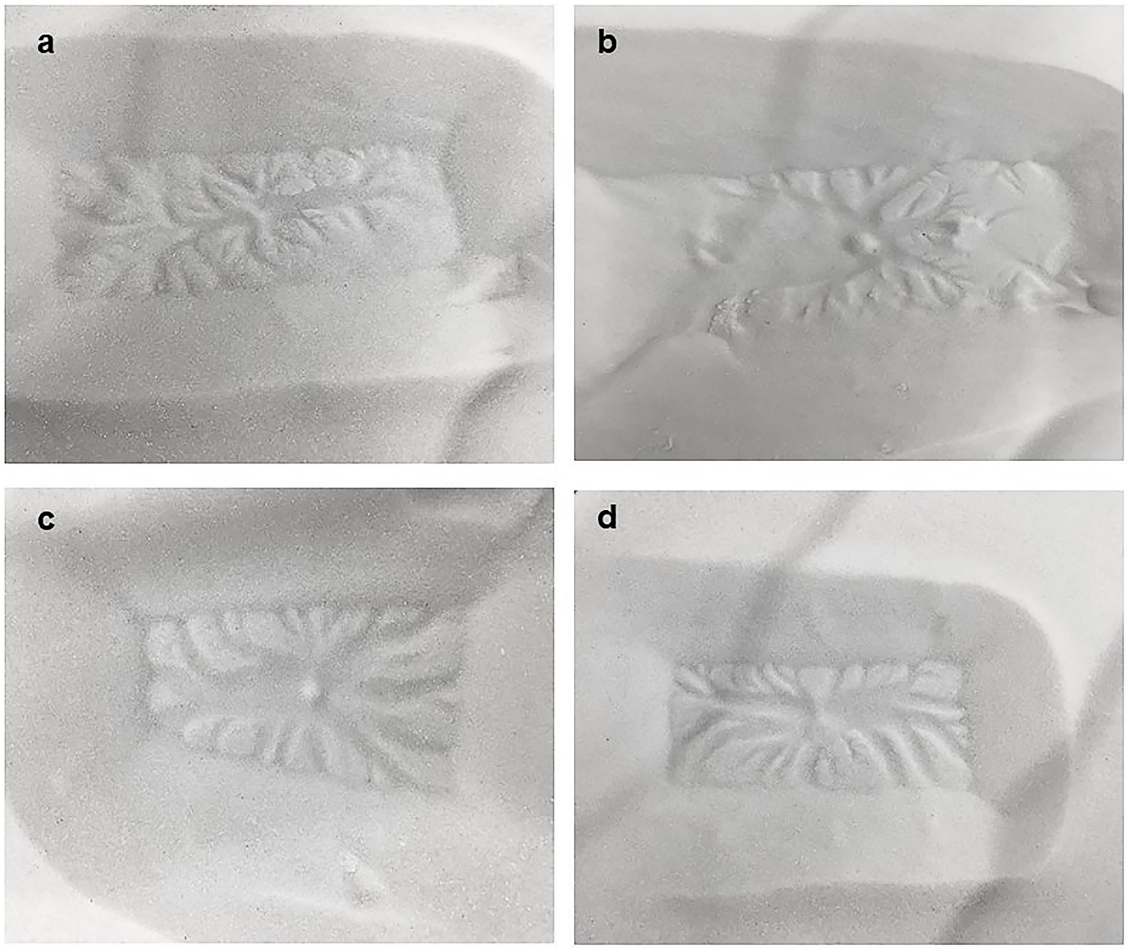

FIGURE 4.4: **Level of branching and vent diameter.** (a) shows an araneiform formed with a 3 mm vent on 250-425 μm grains. (b) shows an araneiform formed with a 3 mm vent on 160-212 μm grains. (c) shows an araneiform formed with a 5 mm vent on 160-212 μm grains. (d) shows an araneiform formed with a 5 mm vent on 250-425 μm grains. Level of branching increases (i) when smaller central vents were used and (ii) with smaller grain sizes.

emanating from 3 mm diameter vents reaching the chamber ceiling ($\sim$ 0.6 m above the bed surface) in many cases at high velocity relative to plumes from 5 mm vents, while 5 mm vent plumes were more diffuse, with grains only reaching the top of the claw ($\sim$ 0.15 m above the bed surface). We attribute this difference to the higher gradient in pressure sub-slab to the top of the central hole, since if the same volume flow rate is forced through a smaller vent the pressure will increase. For laminar flow this increase will be inversely proportional to the area squared. At higher velocities where the flow becomes turbulent it will increase as the power of -3/2 of the area. Grain size also affected plume height and the distribution of plume material to the

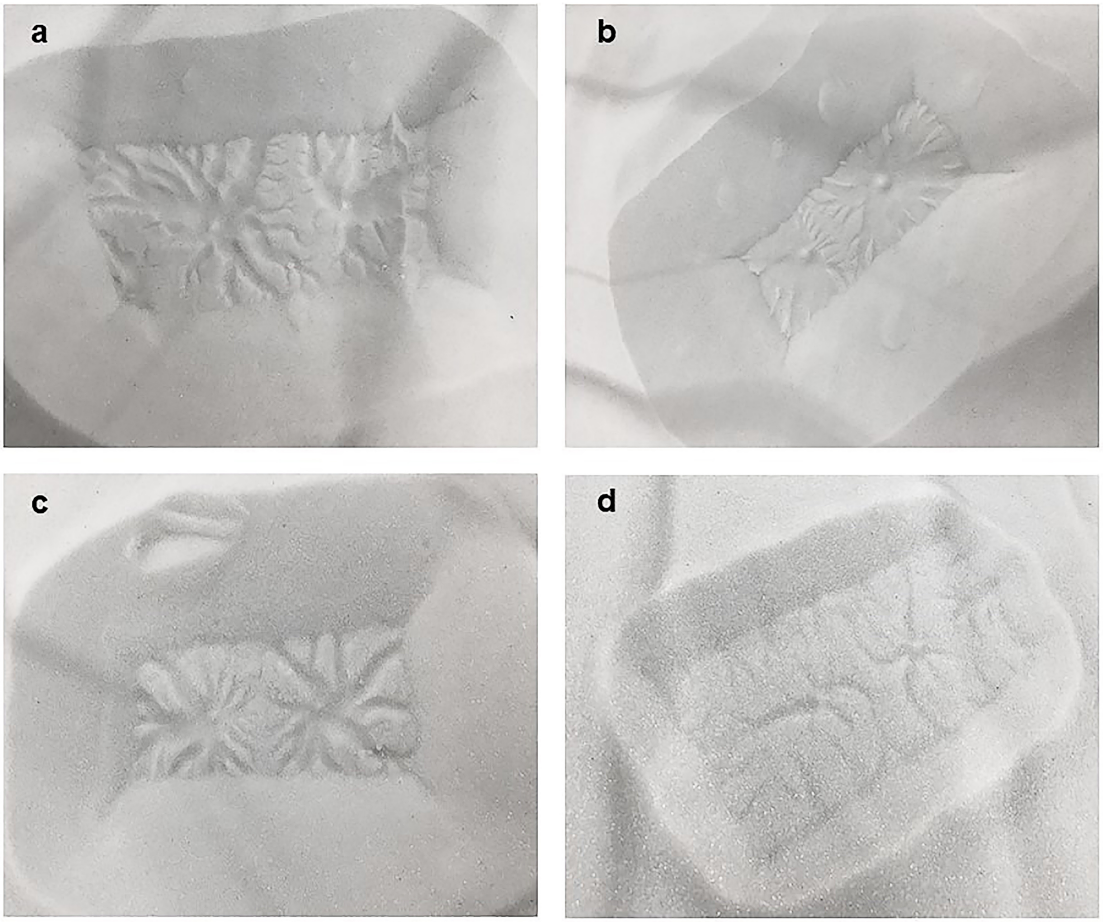

FIGURE 4.5: **Double araneiforms.** Double araneiforms formed on beds of grain sizes ranging from 150 to 600 μm when two 3 mm vents were created at the centre of short diameter of the incident block, 6 cm apart. (a) shows double araneiforms on 150-250 μm grains. (b) shows double araneiforms on 150-250 μm grains. (c) shows double araneiforms on 250-425 μm grains. (d) shows double araneiforms on 450-600 μm grains. Sublimation was highly vigorous for the 160-212 μm experiments, particularly with two central vents. This caused rapid sediment transport back on top of the block and pit and hence surface features were concealed by this burying effect.

surrounding area in each case. For coarser grains, plumes were again lower relative to those seen for vents of the same dimensions for finer grains.

4.4.1.2 The Effect of Grain Size on Araneiform Morphometry

The effect of grain size on the level of branching of the araneiforms is seen in Figure 4.3 a. Points where fallen sediment covers part of the araneiform are not included.

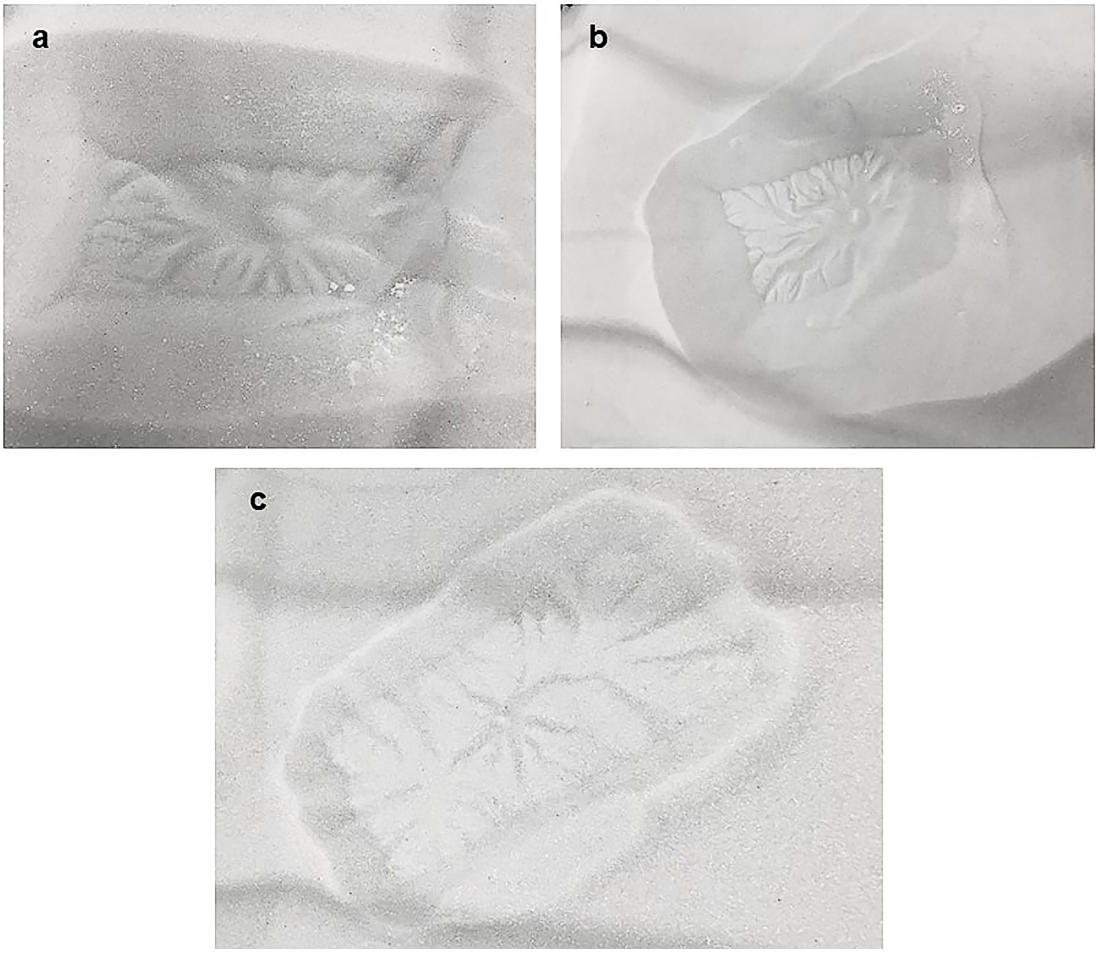

FIGURE 4.6: **Area covered by araneiform with grain size.** (a) shows araneiform formed with a 5 mm vent on 160-212 μm grains. (b) shows araneiform formed with a 5 mm vent on 150-250 μm grains. (c) shows araneiform formed with a 5 mm vent on 425-600 μm grains. The area the araneiforms cover increases with smaller grain sizes.

The level of branching of araneiforms decreases with increasing grain size. In addition, araneiform legs were observed to be more sinuous for finer grain sizes. Outlying points for our finest grain size of 160-212 μm are probably due to erasure of part of the eroded pit surface by infalling sediment from levées and from grains from the top of the lifted ice block. As in Table 4.1, the difference between the widest and thinnest leg of the araneiform became less with increasing grain size also. This initially suggests that subsurface streams of gas are more uniform for coarser grain sizes, but is more likely due to thinner streams having less erosional capability on coarser grains which are more difficult to mobilise and hence not leaving an imprint on the surface. Most notable is the sharp contrast in morphometry between all other grain sizes and our coarsest grain sizes of $425 - 600\,\mu m$ which show very low levels of branching.

This dependence on mean grain size may help to explain the distinction between the location of furrows and dendritic troughs and the dendritic araneiform terrain. Furrows can have a range of morphologies including linear and sinuous, are very shallow (Bourke, 2013) and are only found on dune slopes and sandy patches in interdune regions. An upper limit of the grain size distribution on Martian dunes was recently provided by the Curiosity rover expedition to the Bagnold dune field on Mars from $< 150\,\mu m - 1\,mm$ (Bridges et al., 2016). Dendritic troughs are found on interdune material which is believed to be finer and less consolidated, while fines in the SPLD are thought to range from 50-200 μm (Paige et al., 1994) and hence are more mobile.

The effect of grain size on the area covered by araneiforms is seen in Figure 4.3 a and Figure 4.6. Finer grains are more mobile and hence the imprint of many CO_2 subsurface gas conduits are visible on the resultant araneiform (Figure 4.6 b). There appears to be a cut off point at $425 - 600\,\mu m$ where while the radial patterns are detectable, these are shallow and have very low levels of branching (Figure 4.6 c). Araneiform development will of course vary with the vast scale differences between the laboratory setting and the SPLD on Mars and with other external factors such as ice grain size and thickness. However, while vent separation was kept relatively consistent between different grain size trials, we report that the aerial coverage of radial troughs is dependent on grain size.

4.4.1.3 The Effect of Vent Diameter on Araneiform Morphometry

The effect of vent diameter on the level of branching and feature morphometry is subtle for our range of grain sizes. We attribute this to not having wide enough blocks to explore a wide enough range of trough extents. However, in the cases where 5 mm vents were used, troughs reach the edge of where the block was placed and the central depressions are noticeably wide in comparison to the length of araneiform legs

(Figure 4.4). Additionally, the level of branching for the finest three grain size ranges was generally higher when a smaller 3 mm vent was used.

Because vents were acting at both the sides of the block and at the location of the central hole, in all cases, short, linear or sinuous furrows also formed at the sides of the block as in (Mc Keown et al., 2017). This was expected as vents would form at regions where there was a slight gap between the block and the granular surface. In many cases, the araneiform legs stopped at the location where the edge of the block was, suggesting that in these instances, legs would extend further had there been more distance to the next vent. Double araneiforms formed when 3 mm vents were acting 60 mm apart (Figure 4.5). However, no conclusion can be drawn on the influence of vent separation on araneiform morphometry as our CO_2 samples were so small. Vent separation in our cases ranged only from 50-105 mm. A deeper insight to the effect of vent separation on araneiform morphologies could be achieved with a higher pressure gradient using a wider slab of CO_2.

Our initial results indicate that there may be a feedback between vent diameter and araneiform morphometry. If formed in one venting episode, 'fat spiders' may have formed by wider vents or close vent separation, whereas the more dendritic 'thin spiders' with small central depressions could have formed by the action of small vents or wide vent spacing. Additionally, given the sharp difference in morphometry with grain size and the fact that the distinct Martian araneiform morphologies tend to cluster in separate regions, it is possible that different levels of regolith consolidation or grain size may influence the different morphologies.

4.4.2 Phase 2: CO_2 Sublimation Efficacy

When a CO_2 block was allowed to sublimate on beds of $160-212\,\mu\,m$ and $150-250\,\mu\,m$, a unique vigorous rapid sublimation process was observed (Video 4.2). In each experiment, the block spun and was highly mobile within the container via sublimating gas exerting pressure on surrounding grains. In each case, the mobility of the block was limited by the floor or walls of the container and it is thought that the block would have continued on its course if not obstructed. Rapid sublimation continued until the temperature of the granular bed reached $\sim\ -30^{\circ}\,C$. Sediment was transported as high as the chamber roof ($\sim\ 0.6m$ above the bed surface) and so we report a lower limit of how high sediment can be transported via this process.

An average mass flux sublimation rate of sublimating CO_2 under Martian atmospheric pressure was calculated to be 22.6 $\frac{g}{min}$. This is over 16 times the rate at which CO_2 ice blocks sublimated on beds of $160-212\mu\,m$ grains under Earth conditions (Mc Keown et al., 2017), indicating that the low pressure on Mars alone can influence sublimation efficacy by an order of magnitude. In each case, sediment was transported out from the container to the surroundings of the chamber. As outlined in *Methods*, the percentage volume of material transported out of the container was calculated in each case. This ranged from 6% to 16% of material ejected from the confinement of the container resulting in $\sim\ 8\,\%-27\,\%$ of material excavated by CO_2 sublimation per kg of CO_2.

Extrapolating these values to the amount of CO_2 required to mobilise a 1000 m^3 volume araneiform on Mars is not informative as the situation involved in the subsurface heating of regolith beneath an ice overburden is vastly different to a buried CO_2 ice block. The former is a gradual process and not all faces of the CO_2 layer would be exposed to warm regolith. Additionally, the scaling differences in sediment ejecta distances are significant. The extreme difference in ice mass and thickness

will introduce factors which affect sublimation efficacy, as well as differences due to lower gravity on Mars. A detailed numerical model will be required to exploit the data reported here in order to further understand the vast scale of the araneiforms of the SPLD on Mars and it is questionable with such a high requirement of sublimation energy, that such vast volumes of material could have been ejected in a single, or few event(s). However, we have provided a first step in empirically investigating the efficiency of sublimating CO_2 ice as an agent of the transport of granular material. Both the qualitative (observational) and quantitative data may be drawn upon in order to test, refine and develop models of CO_2 sublimation under Martian conditions.

Nonetheless, we have shown that radial araneiform *patterns* in the laboratory can form in one venting event. From our observations that on the lab scale at least, araneiforms can begin as one radial structure, we suggest that it may be possible for Martian araneiforms to begin their lifetime as a radial pattern which eventually grew by successive events, perhaps in a climate more conducive to more energetic sublimation with more intense insolation/higher temperatures (Figure 4.7 a-d) during the planets changes in obliquity, or when regolith was less consolidated. If the radial patterns of Martian araneiforms did indeed form in a past climate, our observations suggest that it is more likely that a smaller scale radial pattern was carved and troughs eventually widened, lengthened and deepened over time to form the giant structures visible on Mars today (Figure 4.7 g, h). If this was the case, it is possible that the existing topography provided by the araneiforms causes points of weakness (Figure 4.7 d) whereby overlying ice is more likely to crack seasonally, yet the underlying material may be too consolidated to be eroded further today or present day climate conditions are not conducive to the energy required to erode coarser or more consolidated granular material. It is plausible that the dark fans and spots which appear annually in similar locations are therefore recycled dust which deposits in summer and settles into the negative topography of the araneiforms. Only 7 MY have been monitored by HiRISE and limited temporal studies have been conducted

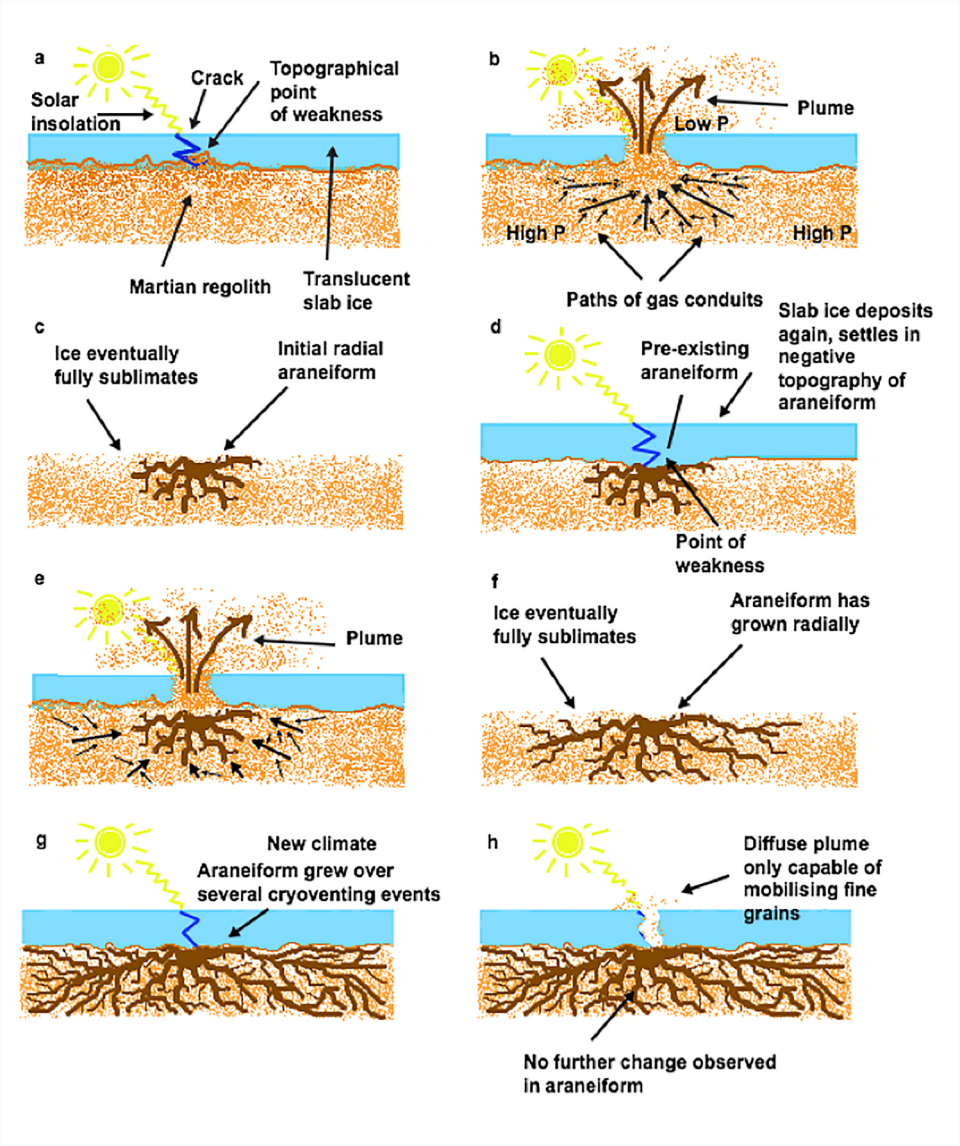

FIGURE 4.7: **Araneiform development hypothesis suggesting araneiforms formed in a paleoclimate** and their activity today is not growing existing radial araneiforms. (a-c) show initial araneiform development as suggested by Kieffer and Piqueux (Kieffer et al., 2006; Piqueux et al., 2003). (d-f) However we suggest that a radial structure develops initially and grows during this paleoclimate which is conducive to more energetic cryoventing. (g-h) show the present day Martian climate where fans and spots still reappear, however we suggest the coarser grains are not eroded and fans and spots are recycled dust transported by a much more diffuse plume than in b and e.

(Portyankina et al., 2017b). The upcoming extended Planet Four: Terrains (Hansen et al., 2017; Portyankina et al., 2017b; Schwamb et al., 2018) campaign, along with extensive numerical modelling and comparison predicted past climatic conditions from Global Climate Models is an opportunity for further insights on whether this is the case or whether the araneiform troughs grow over time.

4.5 Conclusion

We have reported the first physical observations of (i) araneiform formation and (ii) plume activity and have reconciled feature with process on the laboratory scale. We show that sublimation efficacy of CO_2 increases by a factor of 16 under Martian pressure. We find that the area covered by araneiforms on the laboratory scale decreases with increasing grain size suggesting that regions of different regolith grain size on Mars might constrain the varied araneiform morphometries. We report that the level of branching of araneiforms increases with (i) decreasing grain size and (ii) smaller vents, lending further credence to the proposal that this is a pressure gradient limited process. We find that wider centres result from wider vents and that shorter, more consistent width legs are formed on coarser grain sizes, suggesting that perhaps the 'fat' spider morphologies are constrained by wider vents or coarser grained material and that classic, 'thin' spiders may have formed via the action of smaller vents or on more mobile material. We show that radial dendritic araneiform patterns can form in one venting process and at this scale do not require multiple events causing dendritic structures to connect at a central point. From this, we offer an alternative hypothesis that radial araneiform patterns developed in one or few instances in a past climate and that perhaps trough dimensions grew over multiple MY. We suggest rigorous temporal surveys of araneiforms over multiple MY will shed light on whether dust ejecta originate from the troughs or are merely seasonal dust deposits which are recycled annually in this unique geomorphic process which is unlike any on Earth.

4.6 Supplementary Videos

- **Video 4.1:** Video showing a plume of CO_2 gas and sediment ejecta emanating from a central 5 mm vent on a bed of $150 - 250\,\mu m$ grains.
- **Video 4.2:** Video showing a violent, rapid sublimation process when a CO_2 block was placed on a bed of $150 - 250\,\mu m$ grains.

Block area (cm^2)	**Block mass (g)**	**Vent diameter (mm)**	**Grain size (μm)**	**Width centre (cm)**	**Pit floor area (cm^2)**	**Araneiform area (cm^2)**	**% Area**	**Widest trough (cm)**	**Thinnest trough (cm)**	**DEM resolution (mm/pix)**	**Orthophoto resolution (mm/pix)**	**RMS Model uncertainty (m)**	**Number of junctions**
241.5	820	5	425-600	2.69	176.07	14.37	8.16	0.7	0.5	0.619	0.155	0.01	8
234	760	double	425-600	1.36	78.4	9.07	11.57	0.74	0.46	0.76	0.19	0.002	5
234	760	double	425-600	1.82	71.38	8.04	11.26	0.72	0.42	0.76	0.19	0.002	5
230	750	3	425-600	1.33	162.23	7.08	4.36	0.8	0.39	0.533	0.133	0.002	9
224.3	750	double	425-600	1.23	69.46	5.96	8.58	0.91	0.45	0.636	0.159	0.003	5
224.3	750	double	425-600	1.13	81.23	9.63	11.86	1.17	0.48	0.636	0.159	0.0034	5
209	550	5	425-600	1.13	182.3	19.66	0.11	0.91	0.33	0.524	0.131	0.0037	6
207	710	3	425-600	1.42	168	6.64	3.95	0.64	0.264	0.621	0.115	0.0022	6
214.5	690	5	250-425	5.3	118.7	62.36	52.54	1.02	0.3	0.707	0.117	0.0044	15
240	850	3	250-425	7.4	109.1	28.8	26.4	0.54	0.14	0.497	0.122	0.0042	21
240	830	3	250-425	4.7	134	76.55	57.13	1.77	0.475	0.533	0.133	0.008	10
246	830	double	250-425	2.9	39.84	21.3	53.46	1.1	0.467	0.414	0.104	0.0058	12
246	830	double	250-425	2.92	46.55	24.2	51.99	1.07	0.55	0.414	0.104	0.0058	17
203.5	620	5	160-212	6.44	80.4	46.87	58.3	2.04	0.378	0.477	0.119	0.0021	26
203.5	615	5	160-212	7.2	80.4	46.87	58.3	0.95	0.32	0.614	0.154	0.002	28
203.5	600	3	160-212	5.87	100.28	54	53.85	0.91	0.284	0.489	0.112	0.0023	28
224.3	680	5	150-250	4.3	124.42	46.14	37.08	1.44	0.24	0.444	0.111	0.0099	40
240	745	5	150-250	2.93	47	5.1	10.85	0.82	0.12	1.4	0.138	0.0159	28
246	830	double	150-250	4.7	49.37	40.81	82.66	1.38	0.263	0.524	0.131	0.0044	28
246	830	double	150-250	4.4	31.05	23.5	75.68	2.02	0.136	0.524	0.131	0.0045	17
224.3	670	double	150-250	4.1	45.52	24.4	53.6	1.27	0.367	0.629	0.157	0.0022	35
224.3	670	double	150-250	3.67	66.21	28.87	43.6	1.1	0.387	0.629	0.157	0.0022	30
224.3	790	3	150-250	4.32	127.15	49.46	38.9	1.58	0.575	0.46	0.115	0.0025	36
224.3	750	3	150-250	6.1	120.22	69.66	57.94	1.3	0.3	0.403	0.101	0.0068	45

TABLE 4.1: Summary of measured and controlled parameters

FIGURE 4.8: QR code to Video 4.1. Written link: https://youtu.be/DY0iowq568o

FIGURE 4.9: QR code to Video 4.2. Written link: https://youtu.be/0zKsIx5W84c

Chapter 5

Morphometric Trends and Implications for the Formation of Araneiforms

Abstract

Araneiforms are an exotic class of feature exclusive to the Martian south polar terrain. The dilation and recession of the seasonal ice deposit has long been understood to be responsible for their gradual formation. However, radial araneiforms have not been observed to form or extend in the present day. Here we present an alternative hypothesis that the radial araneiforms of the South Polar Layered Deposits and surrounding regions were formed in a relic climatic period on Mars and that the observed contemporary fan and spot activity is due to recycling of seasonal dust deposits which accumulate in their negative topography. We present the results of a survey designed to investigate the environmental factors which may influence araneiform morphometry and find that present–day ice thickness distribution does not appear to control morphometry. However, we find that pressure gradient controls the level of branching of these dendritic features in the form of (i) inferred vent spacing and (ii) inferred vent width. From this survey, we develop a more extended classification of araneiforms than previously offered, based on their measured morphometries.

5.1 Introduction

The volatile constituents and surrounding terrain of the south pole on Mars preserve an inventory of clues to the planets rich climatic history and have been studied for decades (Hess et al., 1979; Leighton and Murray, 1966). The Martian south pole is veneered by a residual cap of CO_2 ice (Leighton and Murray, 1966) known as the South Polar Residual Cap (SPRC) which survives the southern summer (Kieffer, 1979; Paige et al., 1990) and is located between -84° to -89° latitude and 220° and 50° longitude. Its surface is landscaped by quasi–circular flat bottomed pits known colloquially as "swiss–cheese terrain", scarps, mesas and troughs (Malin et al., 2001; Thomas et al., 2016). The inhomogeneous erosion of the different "units" of the SPRC concurrent with ongoing deposition has archived climate change on Mars over the last

century (Byrne and Ingersoll, 2003; Thomas et al., 2005) and is thus a useful resource in understanding the historic response of the Martian surface to changes in orbital obliquity. The SPRC is superposed on and surrounded by a perennial water ice cap (Bibring et al., 2004; Byrne and Ingersoll, 2003; Titus et al., 2003) that contains distinct bands of water ice and admixed dust (Zuber et al., 2007) which is up to 3 km in thickness Smith et al. (1999). Beneath this lie vast quantities of sequestered CO_2 ice reservoirs which measure 9,500 to 12,500 cubic kilometres in volume Phillips et al. (2011). Cumatively, these regions are known as the South Polar Layered Deposits (SPLD) and are understood to have formed during distinct periods of Mars's orbital obliquity (Montmessin et al., 2007).

Supplementary to these, a present–day seasonal CO_2 ice layer deposits annually on the surface in winter in the form of ice and snow Leighton and Murray (1966); Smith et al. (2001). This tapers in thickness from 1-2 m at the poles, to several millimetres further towards the equator (Aharonson et al., 2004; Smith et al., 2001). The sublimation of the seasonal CO_2 ice deposit back into the Martian atmosphere in spring is recognised as a cardinal agent of contemporary surface change on Mars (Mangold, 2011).

A prime example of surface modification on present–day Mars via the putative role of seasonal carbon dioxide sublimation are the fans and spots that reappear annually within the icy regions of the higher southern latitudes. Their discovery was a major paradigm shift in our understanding of geomorphic processes on present–day Mars (Kieffer et al., 2006; Malin and Edgett, 2001). Having measured the brightness temperature of these features which were originally proposed to be bare, defrosted ground (Kossacki and Leliwa-Kopystynski, 2004), Kieffer discovered that the recurring low albedo fans and spots remained just below the brightness temperature of CO_2 ice and hence must be composed of a very thin layer of material on top of a sheet of

CO_2 ice (Kieffer et al., 2006). The co-location of fans and spots with the location of radial dendritic and tortuous negative topography features known as "araneiforms" (Piqueux et al., 2003), led Kieffer and Piqueux to develop a theoretical framework for the contemporaneous formation of araneiforms and dark spots. A geomorphic process in which "cold jets" are responsible for the erosion of the araneiforms and deposition of the spots was proposed. It was suggested that the seasonal ice slab on Mars is large–grained and translucent and thus can be penetrated by broad spectrum solar radiation (Kieffer et al., 2006). Radiation will heat the particulate regolith beneath the ice but refracted rays will be trapped, thus inducing basal sublimation of the ice overburden in what is known as the *Solid State Greenhouse Effect* (Matson and Brown, 1989). Eventually cryostatic pressure will be exceeded by basal gas pressure and the ice will rupture. Points of weakness will be exploited to allow subsurface high velocity gas streams to rush towards the vent, eroding and depositing dark, dusty material in its wake.

Araneiforms were posited to mark the imprint of the path of this gas and spots were proposed to be composed of the transported material. The more oblate fans were explained by the transport of this mobile material by katabatic winds. However, a major gap in the generally–accepted model for araneiform formation is the fact that the distinct *radial* araneiform morphologies have not been observed to form or change in the present day, while spots and fans appear at or surround their locations annually.

Due to the radial tortuous nature of some morphologies, araneiforms are often colllo-quially referred to as "spiders". The broader term, "araneiform", meaning "spider–like" has recently been adopted for all dendritic morphologies in the south polar region in order to avoid confusion with the terrestrial bioform and also to include features which do not have a distinct radial form, but resemble araneiforms in their tortuos-ity and branched nature (Hansen et al., 2010). In addition, similar though smaller

scale members of the Martian dendrite family such as sand furrows on northern hemisphere dunes (Bourke, 2013; Bourke and Cranford, 2011) and dendritic troughs in the southern mid–latitudes (Portyankina et al., 2017b) have been observed to form today on sandy substrates. These have been speculated to represent early stages of araneiform development (Portyankina et al., 2017b) as they resemble single branches of araneiforms. However, there are still unresolved issues regarding the spatial concentration of dendritic troughs to dune regions (Portyankina et al., 2017b), their absence (to date) in the more southern regions where radial araneiforms are present and the absence of any currently forming radial araneiforms. In addition, the evolution of dendritic troughs to the radial patterns are not well understood.

This chapter focuses on radial araneiforms. There are sub-categories of araneiform morphologies (Figure 5.1): 1. Thin or "classic" araneiforms comprise of narrow central depressions relative to their full extent (Hansen et al., 2010). Troughs are generally thin and typically are more branched than their "fat" counterparts. 2. Fat araneiforms comprise of relatively wide central depressions with respect to their full extent. Troughs are generally wider than those belonging to thin araneiforms and no more than $\sim$ 20 troughs emanate from their centres. 3. Starburst araneiforms are the largest noted araneiforms and are highly dendritic. They can have over 1000 branches. 4. Eponymous "baby" araneiforms have not been explicitly classified, but are generally among the smallest known spiders detected on Mars. Though the features have been classified (Hansen et al., 2010) and extensively mapped (Piqueux et al., 2003; Schwamb et al., 2018), there is a dearth of information derived from orbital data on what may control this diverse array of morphologies.

Our previous laboratory experiments under Martian pressure (Mc Keown et al., submitted) (Chapter 4) were designed to further understand the physical constraints on araneiform morphometry. Our results indicated that when our (small scale)

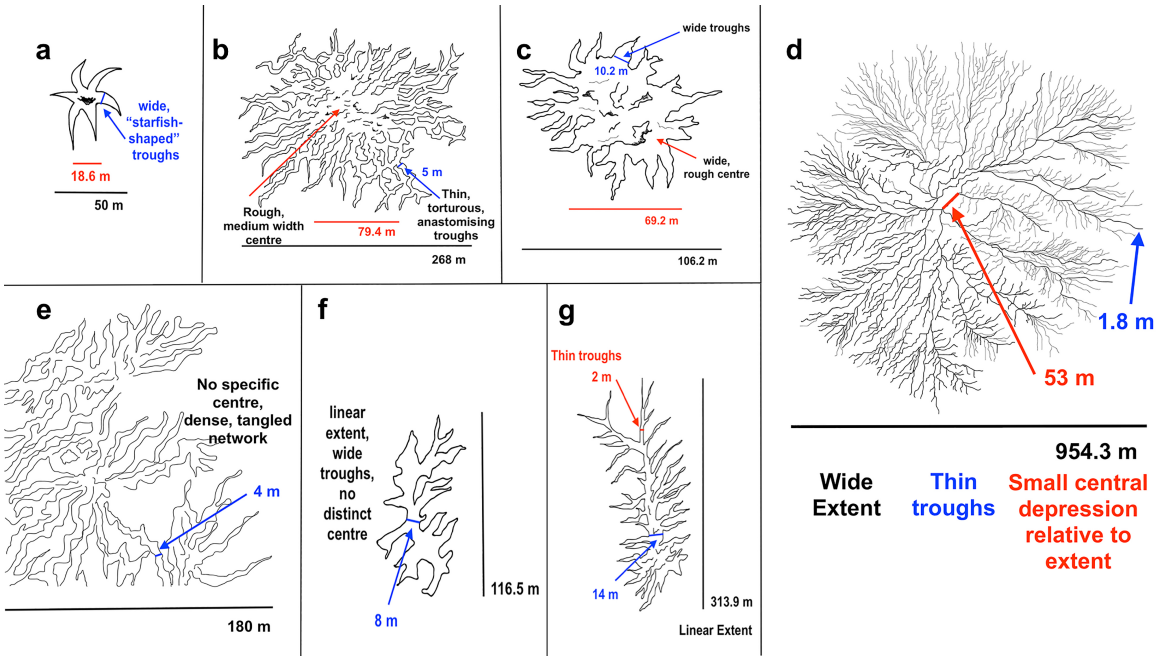

FIGURE 5.1: Araneiform Classification based on morphometry. (a) shows a baby araneiform. These are usually less than 50 m in full extent diameter and are "starfish" shaped. Their troughs (usually < 10) are "spiky" in form and are not tortuous. (b) shows a classic araneiform. These have rough centres with many tortuous, braided and anastomising troughs. (c) shows a fat araneiform. These are generally over 50 m in full extent diameter, have wide and short troughs and low full extent to centre ratios. (d) shows a starburst araneiform. These can span up to 1 km in diameter, have small central depressions and often have in excess of $\sim 10^3$ thin branches. (e) depicts lace terrain. This tangled araneiform type has no distinct centre and often covers multiple km of terrain. (f) shows rake araneiforms. These are linear, small in dimension, have no distinct central depression, but have wide troughs. (g) shows linear araneiforms which are long and linear in morphology and have thin tortuous troughs.

araneiforms formed in a short period during one or few instances of powerful sublimation, pressure gradient was a presiding constraint on araneiform morphometry. In particular, inferred pressure gradient influenced the level of branching of the araneiforms and trough and central depression dimension. The level of branching of araneiforms was higher with (i) smaller grain size and (ii) smaller vent diameter. Smaller vent diameter inferred a stronger pressure gradient because if the same volume flow rate is forced through a smaller gap the pressure will increase. For laminar flow this increase will be inversely proportional to the area squared. At higher velocities and turbulent flow, it will increase as the power of -3/2 of the area. In all cases radial araneiforms developed in one venting episode, without the requisite for multiple connections of

troughs over time. Here we hypothesise that araneiforms on Mars formed in a relic period of orbital obliquity whereby the paleoclimate was such that ice thickness, atmospheric conditions and sediment induration accommodated a pressure gradient for cryoventing, energetic enough to erode an initial araneiform pattern in few instances (by more rapid sublimation dynamics). As was suggested (Mc Keown et al., submitted), the seasonal fans and spots which appear annually on present–day Mars may simply be recycled dust brought to the surface of the ice and annealed back through seasonally to fall within pre–existing troughs as this cryoventing efficacy may not currently be strong enough to erode the substrate of the SPLD. If our laboratory observation–based hypothesis were of merit, environmental factors such as thicker ice, smaller central vents, and wider vent spacing would cause a higher pressure gradient and hence form araneiforms that are more dendritic in morphology. Thinner ice layers, wider central vents and closer vent spacing would result in less branched araneiforms. The objectives of this study were therefore to determine the relationship between the level of branching and:

1. inferred vent diameter
2. inferred vent spacing
3. present day ice thickness

5.2 Methods

In order to to investigate whether there is a feedback between (i) inferred vent diameter (ii) inferred vent spacing and the level of branching of araneiforms, HiRISE images ESP_049046_0985, PSP_004907_0945 and ESP_013833_0980 were selected for three sites at latitudes and longitudes -81.459° , 296.281° , -85.464° , 83.558° and -81.813° and 76.170° respectively (Figure 5.2). The first site is known informally as

Inca City, the second, as Oswego and the third is unnamed. These sites were selected firstly based on whether araneiforms had been observed in these locations previously (Hansen et al., 2010) and secondly if they contained a range of araneiform scales and morphologies. Collectively, the locations selected represent "thin", "fat", "classic" and "starburst" araneiforms. As araneiforms have not yet been observed to change in scale (Portyankina et al., 2017b) over the past several Mars years monitored by HiRISE, differences in MY between images are not considered significant. Hence, similar L_s in southern summer and similar emission angles as close as possible to nadir were favoured for consistency between images. This was to avoid lighting artefacts or disparities due to roll of the camera. L_s were 297.7° , 294.9° and 300.1° and emission angles were 1.4° , 0.6° and 9.5° respectively. The cartographic projection used was polar stereographic.

This research was conducted to test the hypothesis that araneiforms developed in a past climate through one or few instances of seasonal sublimation. Since observations of the original vents responsible for these features are unavailable, we assume based on their radial geometry and our laboratory observations of radial araneiforms developing from a central vent (Mc Keown et al., submitted), that these vents originated at araneiform centres. Apparent vent width was approximated to scale with araneiform central depression width, as was the case in our laboratory experiments (Mc Keown et al., submitted). Vents and subsequent spot and fan activity have been observed at different locations on araneiform troughs as well as at their centres in the past few MY (Hansen et al., 2010; Kieffer et al., 2006; Piqueux et al., 2003). However, as these have not been observed to alter araneiform morphometry, we focus on their centres as an approximation for the location of original vents which may have been responsible for their radial morphologies.

Since the centres of overlapping and conjoining araneiforms are difficult to identify

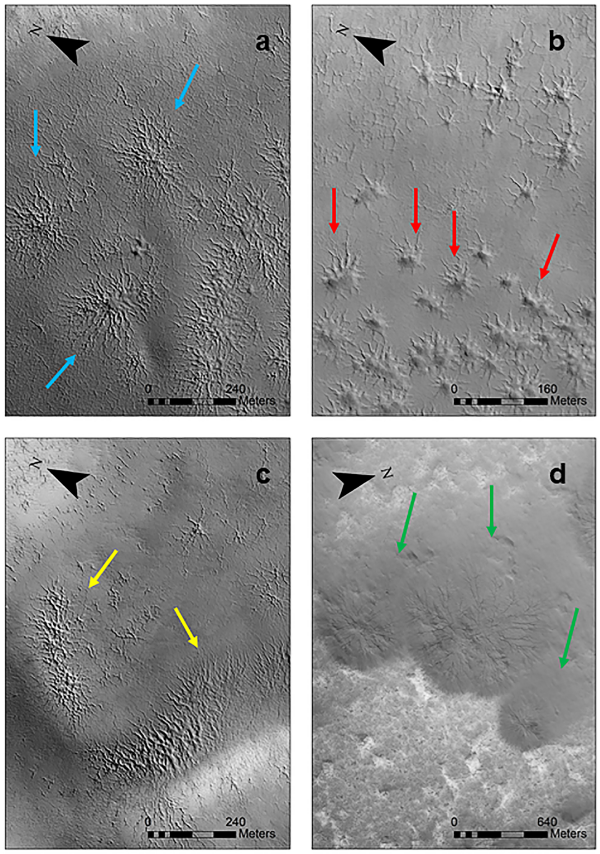

FIGURE 5.2: Examples of different araneiform morphologies. (a) blue arrows show classic araneiforms in Inca City, (b) red arrows show fat araneiforms in Inca City, (c) yellow arrows show lace terrain in Inca City and (d) green arrows show starburst araneiforms in an unnamed location. Inca City images are taken from HiRISE image ESP_049046_0985 and starburst araneiform image is taken from HiRISE image ESP_013147_0980. HiRISE image credit: NASA/JPL/University of Arizona

by eye, including these in our dataset would expose the data to wide uncertainty margins. Hence, only distinctly *radial* araneiforms which were isolated from adjacent araneiforms were surveyed. Additionally, araneiforms with no distinct centres for example lace terrain (e.g. Figure 5.2 c) or araneiforms along hill slopes, were not included to limit the amount of variables studied, as high slope angles would affect pressure gradient during araneiform formation. ArcMap 10.4 was used to collect morphometric data from imported HiRISE images. We measured the distance between the centres of individual araneiforms which we use as a proxy for vent spacing. The central diameter was estimated by measuring the distance between the mouth of a radial trough at one side of its central depression and the mouth of a radial trough on the opposite side. Because radial araneiform centres are rarely symmetrical and often

oblate, this was repeated 5 times for each feature. The point at which the 5 lines intersected was approximated to be the centre. The full extent of araneiforms was measured in a similar manner, drawing a polyline across its widest diameter, from the apex of a trough to the apex of a trough on the opposite side. This was repeated 5 times and an average was taken. In order to get the average distance from a singular araneiform to its adjacent araneiforms, a polyline was then drawn from each individual araneiform centre to five of the closest neigbouring araneiform centres. The mean of these 5 distances was taken.

The level of branching of each araneiform was determined as in our laboratory experiments (Mc Keown et al., submitted), by counting the number of "junctions" on their troughs. A junction is defined as where one branch meets another. These were counted from the circumference of each araneiform in towards its centre. In the case of highly dendritic, tortuous araneiforms, higher uncertainties in counting junctions by eye were considered as in Figure 5.4 and Figure 5.3. Uncertainties were approximated as 10% of the total number of junctions for each data point. Additionally, when superposed on patterned ground, if a perceived outer junction aligned with the general pattern of surrounding terrain it was not included. The plots in Figure 5.4 and Figure 5.3 were generated using Matlab 2018a.

The effect of ice thickness on araneiform morphology was qualitatively assessed by observing the different morphologies at a number of sites of decreasing latitude. In addition to the images mentioned above, HiRISE images ESP_047991_0980, ESP_048777_0990 and ESP_040664_1050 with central lat=-81.8°and lon=302.41°, lat=-80.71°and lon=75.87°, lat=-74.7°, lon=168.41°taken at L_s=246.3°, L_s=284.9°, L_s=317.5°respectively, were studied (Figure 5.5). Their respective emission angles were e=0.1°, 5.5°and 0.7°. Araneiform types were noted according to the classification in (Hansen et al., 2010)

and in some cases descriptions of morphologies were added where feature type was not precisely classified as in Figure 5.1.

5.3 Results and Discussion

One hundred and twelve araneiforms were surveyed. A distinct difference in morphometry between classes is reported with fat araneiforms having an average central depression of 44.1 m and full extent of 78.6 m giving an average extent to central depression ratio of 1.8. Classic or thin araneiforms had an average central depression of 100.6 m, average full extent of 229.5 m and centre to extent ratio of 2.3. Starburst araneiforms, while vastly greater in scale than all other araneiform types, had the most narrow central depressions with an average of 29.7 m. Their average full extent was 685.2 m giving an extent to central depression ratio of 23.1.

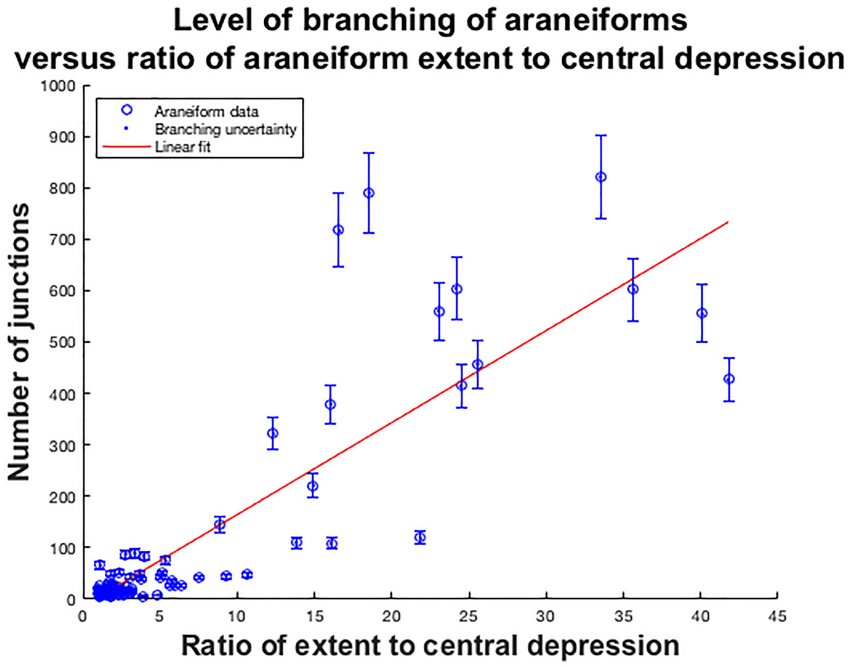

FIGURE 5.3: Level of branching of araneiforms versus ratio of araneiform extent to central depression diameter. p–value < 0.05, $R^2 = 0.73$.

In general, the level of branching was higher with a higher ratio of full extent to central depression diameter (Figure 5.3). This suggests that smaller vents produced

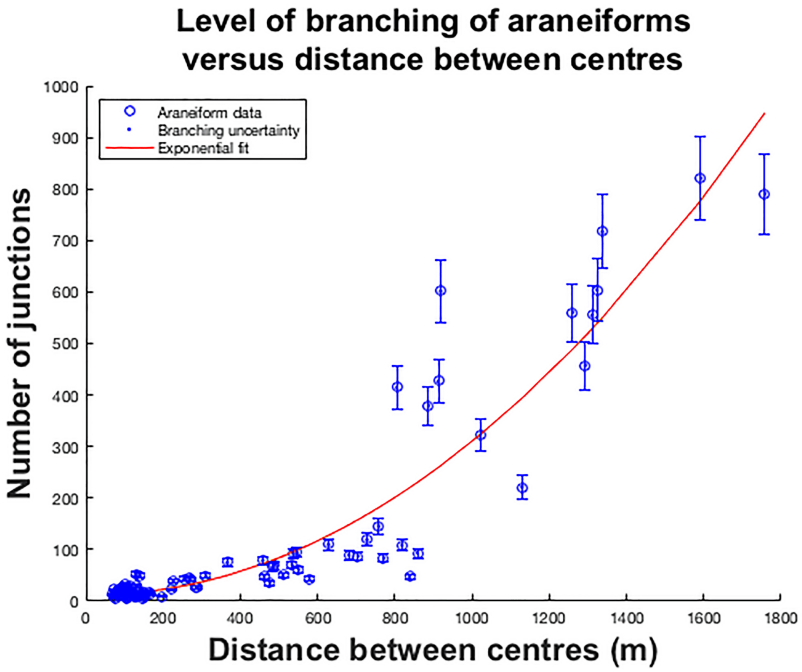

FIGURE 5.4: Level of branching of araneiforms versus distances between araneiform centres. p–value < 0.05, $R^2 = 0.74$.

more dendritic morphologies, as was the case in our lab experiments. We infer that smaller vents provided a higher pressure gradient between subsurface gas and the vent opening at the surface of the ice overburden. However we take caution with these data due to the fact that longer troughs are probabilistically more likely to contain more visible "junctions" and so araneiforms with wider extents cover more surface area.

A generally increasing trend of the level of branching of araneiforms with distances between centres was observed (Figure 5.4). This suggests that if ice thickness when the araneiforms formed was relatively uniform across the area of terrain covered by the araneiforms and if venting occurred relatively simultaneously as the ice cracked, that higher pressure gradient caused more dendritic morphologies, as was the case for our empirical results from our laboratory experiments (Mc Keown et al., submitted). "Fat" araneiforms were always spaced closer than classic or thin morphologies, suggesting their formation was due to a lower pressure gradient supply with vents acting in close proximity to one another. However, the data became more stochastic for larger araneiforms as some smaller araneiforms were interspersed throughout

their locations and this is reflected in the higher standard deviation within the upper right hand corner of Figure 5.4. The methodology of measuring distances between araneiform centres assumes original vents of all araneiforms were acting at once. This may not have been the case - however we can imagine that if one araneiform formed in a given MY, existing surrounding araneiforms may have provided locations of weakness in the ice more likely to crack at a similar time.

Current ice thickness does not appear to be a strong influential factor on morphometry. One would expect that at higher latitudes and higher inferred ice thickness, that higher pressure gradient would be supplied during seasonal venting and hence more dendritic morphologies would be observed. However, a diverse variety of araneiform morphologies were observed within the latitudinal transect studied (Figure 5.5), with no quantifiable relationship to latitude. Ice coverage and thickness with regard to small–scale features such as araneiforms is poorly constrained due to relatively low spatial resolution of CRISM and SHARAD which are optimised for broader and deeper observations of geographic distributions. Approximating ice tapering as linear with decreasing latitude has limitations and ice cover may not be entirely homogeneous. In addition, it is difficult to account for the possible effects of cold trapping in microclimates such as craters. The fact that "fat" araneiforms were observed in two regions outside the SPLD which are believed to be composed of more consolidated material, suggests that either (a) regolith consolidation and/or grain size distribution is a more influential factor in controlling araneiform morphology or (b) seasonal ice deposit thickness has been non-linear throughout the climatic episodes during which the putative relic araneiforms of the higher polar latitudes developed. The recent observations of dendritic troughs (Portyankina et al., 2017b) and further monitoring of their development with present–day thickness of the seasonal ice deposit might elucidate whether and to what extent ice thickness can play a role on araneiform morphology. In addition, laboratory experiments designed to investigate variation of araneiform morphometry with incident ice thickness will provide empirical data

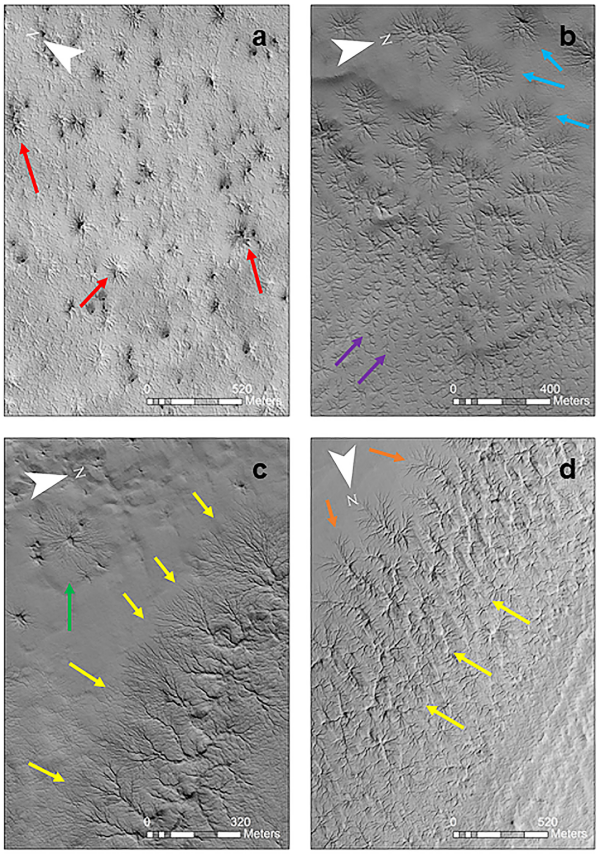

FIGURE 5.5: Examples of different araneiform morphologies with inferred ice thickness across a latitudinal transect between lat= -85°and -74.7°and lon=75.9°and 302.4°. (a) red arrows show fat araneiforms off the SPLD at lat=-81.92°., (b) purple arrows show "rake" and blue arrows show classic araneiforms at lat=-80.71°, (c) green arrow shows a starburst araneiform and yellow arrows indicate lace araneiforms at lat=-80.71°and (d) yellow arrows show lace and orange arrows show "linear" araneiforms at lat=-74.7°. As depicted in this frame of images, inferred seasonal ice thickness with latitude has no obvious influence on araneiform morphology type. The presence of fat araneiforms off the SPLD and in localised regions on lower elevations of Inca city suggests that regolith consolidation plays a more influential role on morphometry. Image (a) is from HiRISE image ESP_047991_0980 with central lat=-81.8°and lon=302.41°taken at L_s=246.3°with emission angle e=0.1°. Image (b,c) are from HiRISE image ESP_048777_0990 with central lat=-80.71°and lon=75.87°taken at L_s=284.9°with emission angle e=5.5°. Image (d) is from HiRISE image ESP_040664_1050 with central lat=-74.7°, lon=168.41°taken at L_s=317.5°at emission angle e=0.7°. HiRISE image credit: NASA/JPL/University of Arizona

which can be extrapolated to Martian scales with numerical modelling. Noting the discrepancy in scale between the araneiforms observed in the laboratory and those on Mars, we caution that our approach is incremental in terms of investigating whether these features could be remnants of a past climate on Mars and suggest that intensive numerical modelling of ice thickness and vent spacing would challenge and supplement

our alternative hypothesis adequately.

5.4 Conclusion

Our survey of araneiforms has revealed an apparent feedback between environmental factors and their distinct morphologies. The level of branching of araneiforms generally increases with (i) inferred vent separation (ii) inferred vent diameter. This suggests that araneiform formation on Mars is a pressure gradient–limited process and our observations on Mars are thus consistent with those from our laboratory experiments under Mars conditions, lending further credence to the well–accepted idea that their formation has been due to basal CO_2 sublimation. Further understanding of the grain size distribution in the southern polar latitudes and regolith consolidation may shed more light on why certain araneiform morphologies tend to congregate. Our qualitative survey of araneiform morphology with inferred ice thickness is inconclusive. There is no distinct evidence of araneiform morphology "tapering off" at lower latitudes, as classic araneiforms, fat araneiforms, and lace terrain are found at sites as high as -85°and as low as -74.7°. A further understanding of the role of ice thickness on araneiform morphology derived from future laboratory experiments and ongoing surveys of dendritic troughs (Portyankina et al., 2017b) may further explain (i) their different morphologies and (ii) why the distinct radial araneiforms are only found in the high southern latitudes.

Chapter 6

Conclusion and Future Work

The main research outcomes are discussed below with respect to the aims established in the introduction, while the significance of this thesis to the wider field of study and its implications for future work are also considered. The aims of the thesis were:

1. To determine if CO_2 block sublimation can form linear gully primary terminal pits, associated levées and detached pits.

2. To determine if pressurised escaping CO_2 gas can erode sand furrow morphologies.

3. To determine if pressurised escaping CO_2 is capable of forming radial araneiform morphologies.

1. Low–humidity experiments were performed on granular substrate under Earth conditions of sliding and hence partially buried CO_2 blocks. The response of a granular bed across a range of grain sizes was documented and the features produced were quantitatively measured. For the first time, pits and surrounding levées were observed to form via the action of stationary sublimating CO_2 blocks. Pits formed across discrete grain size ranges between 4–45 μm and 160–212 μm and were deeper for finer grain sizes. In addition, three pit morphologies were identified; primary, collapsed and impact pits. Primary pits were formed by the in–situ sublimation of CO_2 ice blocks on porous, mobile regolith and collapsed and impact pits were formed via subsurface jetting. From these observations, a hypothesis for detached pit formation at linear gully termini on Mars was developed involving granular clustering in unstable sublimation jets and impact upon return to the surface.

   A survey of linear gully pits in Russell, Proctor and Matara Crater was conducted in order to (a) characterise the different terminal pit morphologies (b) investigate if there is evidence of a relationship between the morphometries of

these terminal pits and the observed presence of detached pits and (c) to investigate the range of block sizes which may be reactivating and widening linear gully channels and pits seasonally and compare with the documented lab–generated granular bed response to given CO_2 block dimensions. Several pit morphologies were characterised including primary, secondary and tertiary main pits, inset pits and detached pits. An initial trend was observed whereby the number of observed new detached pits increased with main pit area. These data are interpreted to suggest that detached pit abundance scales with increased surface area of CO_2 blocks exposed to sublimation. Future work will extend this initial survey to more linear gully sites in order to more rigorously test the observations. High albedo objects interpreted to be blocks within linear gully channels and pits on Mars were measured and corresponding channel and pit widening was determined. Dimensions of pits formed in the laboratory were compared with the dimensions of the CO_2 blocks that formed them and pit width per unit length of CO_2 ice was recorded. The extent to which channels and pits widened annually closely corresponded with the morphometric change predicted from these measurements, strongly suggesting that sliding CO_2 block sublimation may be responsible for linear gully modification in the present–day.

Experiments were performed under Earth conditions and Martian atmospheric pressure in order to quantify gas pressure of a vapor layer and heat transfer between sublimating CO_2 ice blocks and granular beds of a range of grain sizes in order to (a) generate empirical data to feed into the semi–analytic model and (b) test the model output. Empirical data was successfully collected by L.E.M. and initial interpretation of the empirical data with regard to observations while conducting the experiments suggests that further modification of the numerical model is required to account for the more turbulent fluid regimes experienced under Martian pressure.

Some ideas for future work surrounding this vein of research are as follows:

(a) Future modelling work can more rigorously address scaling and assess whether blocks of CO_2 ice may have instigated channel formation, or whether they modify existing channels in the present–day. Additionally, future modelling work will consider non–Darcy regimes and implement these into the pre-existing numerical model (Diniega et al., 2013) to more accurately account for the vigorous rapid sublimation which may be more efficient at modifying the Martian surface in the present day than previously thought.

(b) In particular, modelling of fine sediment entrainment in granular jets and predictions of cluster viscosity/density will be important in validating the granular clustering hypothesis surrounding detached pits. Additionally, future long–term monitoring of linear gully detached pit formation in the present day and distance of impact pits compared with model output predictions may support or reject this hypothesis.

(c) Now that the physical properties of seasonal ice on Mars are becoming better understood (Chinnery et al., 2018; Portyankina, G. and Merrison, J. and Iversen, J.J. and Yoldi, Z. and Hansen, C.J. and Aye, K.-M. and Pommerol, A. and Thomas, N., 2019), a route for future work might be to test the alternative hypothesis surrounding detached pits (Diniega et al., 2013), that they may be caused by blocks breaking up at dune termini. First, linear dune gully sites could be surveyed in winter and distances between cracks could be measured in order to approximate block dimensions which form and widen linear gullies. Field tests similar to the ones conducted in Utah and Arizona by (Diniega et al., 2013) could then be re-performed; ice blocks tailored to the predicted ice grain size and proposed fracture density measurements at south polar dune regions could be specially made and mobilised down dune slopes of similar angles to those

detected for linear gullies on Mars (Pasquon et al., 2016). Average quantitative measurements of block breakage and fracture density upon breaking at dune termini could then be utilised to predict what the average level of block breakage at dune termini on Mars might be. Supplementary work would be to modify the pre-existing model of sublimating, levitating blocks on Martian dunes (Diniega et al., 2013) in order to extrapolate these measurements to those expected under Martian gravity and hence better constrain whether blocks of a given size range (inferred from channel width/interannual widening measurements (Mc Keown et al., 2017) might break sufficiently to form a measured amount of new detached pits.

(d) Change detection analysis of fresh detached pits could be performed. If available, consecutive HiRISE images of the same site could be studied to investigate whether any traces of block fragments "sliding" away from the main pit to form detached pits are visible. These may be in the form of faint micro-channels radiating away from the main pit towards detached pits. This work would however have to be carefully planned and timed as such faint markings on the Martian surface tend to be ephemeral, being easily erased by aeolian activity.

(e) Finally, further work can be done under Martian conditions at the Open University Mars Simulation Chamber to investigate the nature of the mysterious digitate RDFs surrounding some linear gullies (Pasquon et al., 2016) for which the origin is unknown. They could be darker sediment from within channels which is ejected laterally as blocks slide through them. The force of the block moving downwards, as well as sublimation ejecting sediment laterally, could displace material lateral to the channels. This thesis reports on vigorous sublimation dynamics when a block is in contact with sandy substrate at 6 mbar (Mc Keown et al., submitted); showing that even when a block is stationary, sediment can be excavated from deep

within the bed and ejected laterally. More focused experiments could be performed with the same setup but with different grain sizes and sediment consolidation, putting upper and lower limits on ejecta distances from the original placement of the block. Ejecta distance could then be fed into to the model for Mars (Diniega et al., 2013) and extrapolated to solve how far a given block size and grain size distribution might transport sediment laterally for Martian gravity. HiRISE images could then be surveyed to investigate fracture density in the locality of linear gully sites and investigate whether the dark extent of RDFs correspond to those predicted by the suggested laboratory experiments and modelling efforts.

2. The erosion patterns resulting from the interaction between a gently placed CO_2 block and granular substrate were measured and these were compared to a pre-existing Martian furrow network classification (Bourke, 2013). A proof of concept was delivered and sand furrows were observed to form by pressurised escaping CO_2 gas on granular substrate for the first time.

The potential physical factors which control furrow pattern type and furrow density when a CO_2 block is gently placed on granular substrate were identified. A close relationship between inferred pressure gradient and furrow morphology was observed, suggesting that ice thickness and grain size on Mars may influence furrow and dendritic trough morphologies.

Future work surrounding furrows could involve making incremental improvements to the experiments performed:

(a) An idea would be not to use the Leidenfrost Effect to engender sublimation and also to re-perform the experiments under Mars conditions. This would model cryoventing more accurately and simulate the more diffuse sublimation processes involved in furrow developent. Additionally, the ice would

crack to form a vent, as is proposed for Mars. CO_2 could be condensed on sandy substrate in the Mars Simulation Chamber and gradual sublimation could be induced by insolating the ice layer with an intensity similar to that expected on Martian dunes where furrows develop. Insolation intensity, sediment consolidation, ice thickness, grain size distribution and dust content within the ice could be varied in order to understand the role of these factors on furrow development efficacy and pattern type. This would allow a better understanding of the role of insolation receipt, ice thickness and sediment consolidation on furrow development.

(b) The same experiments could be performed in order to better understand the potential role of topography on preferential cracking of the ice. Stones could be placed on the sand bed and undulations in the surface could be created. The surface could be exposed to insolation at varying angles in order to see if negative or positive surface topography would induce preferential cracking. Furrows are often observed near boulders and Bourke's cryoventing hypothesis for furrows asserts that overlying ice may preferentially crack near these regions. Experiments of this nature would lend further proof of concept for the model.

(c) Further experiments could be performed using Mars simulant regolith to investigate cryoventing efficacy with a wider grain size distribution more relevant to that expected on Martian dune and interdune material.

All of the aforementioned improvements to experiments could be repeated for araneiforms also.

3. The erosion patterns resulting from the interaction between a gently placed CO_2 block containing a central vent and granular substrate under Martian atmospheric pressure were investigated. Radial araneiforms were observed to form for the first time in one cryoventing episode, indicating that at least on the laboratory scale, multiple events are not required and a connection of troughs is

not necessitated for araneiform development. Plume activity associated with the subsurface erosion and deposition of spot material was observed for the first time, providing a proof of concept of the long–accepted but never validated cardinal hypothesis governing small–scale features on Mars; Kieffer's hypothesis (Kieffer et al., 2006). The relationship between radial araneiform morphometry observed in the laboratory and (a) grain size and (b) vent diameter were investigated. A strong dependence on grain size was observed, with more dendritic morphologies produced for finer grain sizes, wider vent separation and smaller vent diameters implicating stronger pressure gradients.

Unusual vigorous rapid sublimation dynamics were observed when a CO_2 block was placed on grain sizes below 160–212 μm under Martian pressure, with a mass flux rate over 16 times higher than under Earth conditions suggesting that CO_2 sublimation is a highly dynamic and efficient agent of sediment transport under Martian average atmospheric pressure. This activity is interpreted as due to turbulent fluid dynamic regimes under minimal pressure. This observation has far–reaching implications for the Martian surface as well as other planetary surfaces. It suggests that the presence of dust or even fine particulate matter will greatly increase sublimation efficacy, which is in agreement with observations of increased seasonal cap retreat following global dust storms on Mars (Kieffer et al., 2000; Piqueux, S. and Kleinbahl, A. and Hayne, P.O. and Kass, D.M. and Schofield, J.T. and McCleese, D.J., 2015). Our results when applied in the wider context, suggest that even small quantities of CO_2 under low pressures can have significant geomorphic agency (e.g. small, stationary blocks forming pits and levées and ejecting sediment far beyond the block surrounds). This will be important when considering landforms on terrestrial planetary bodies such as Vesta or the Moon which have minimal to no atmospheres and hence limited atmospheric volatiles.

A survey of araneiforms in the southern high latitudes on Mars was conducted. (a) The existing morphometric classification of araneiform sub–types was extended and a more stringent classification necessitating a distinction of sub–morphologies was established. These data can be used in future campaigns in order to assess the role of environmental factors on araneiform formation. (b) An investigation was carried out to determine whether there is a relationship between araneiform spacing and their level of branching and (c) An investigation was carried out to determine whether there is a relationship between the ratio of araneiform full extent to central depression and the level of branching of araneiforms. Inferred initial close vent spacing had an intimate link with low branching levels and "fat" araneiforms which was in agreement with our experimental predictions. Inferred wider vent spacing was observed to be correlated with more dendritic features, again agreeing with the experimental predictions reported in this thesis. These data indicated that pressure gradient plays a strong role in araneiform morphology and that further diffusion limited aggregation modelling, which relies strongly on physical gradients, is a correct path to take in extrapolating our empirical observations to Martian scales.

Many open questions surrounding araneiforms still persist. There is no evidence to show that araneiforms have newly formed or grown in the last 6 Mars years of high resolution observations. This thesis presents a new hypothesis that the radial araneiforms of the SPLD and surrounds are not currently forming as previously thought (Hansen et al., 2010; Portyankina et al., 2017b) and that they may have formed in a paleoclimate whereby atmospheric conditions were conducive to sufficiently energetic cryoventing. The potential factors which may have caused araneiform activity to cease are unclear. We propose that they include climate change over the course of Mars's history or the influence of global dust storms rendering rapid and effective sublimation more likely. A solid understanding of the role of ice thickness, dust presence, light intensity and

atmospheric parameters can allow us to interpret why some dendritic features are active in the present day, while others remain dormant and therefore will act as a window to better understanding the role of climate change on Martian surface modification. This vein of research could in and of itself, constitute an entire postdoctoral research project. An outline of proposed methodologies and potential deliverables of this potential research project is detailed below. All ideas were conceived and are intended to be executed in the near future by L.E.M.

The proposed research will:

(a) Develop a numerical model that will accurately describe the influence of (i) predicted temperature and atmospheric pressure ranges derived from pre-existing Martian global climate models (GCMs) and hence predicted ice thickness, (ii) varied dust abundances within the ice and (iii) regolith induration on (a) venting efficacy and (b) erodibility per unit grain size. Based on the results of this model araneiform formation can then be attributed to certain climatic conditions and might hence give a better understanding of why they do not form in the present day despite ongoing fan and spot activity.

A semi-analytic numerical model describing fluid dynamics of pressurised gas beneath a CO_2 ice overburden under different climatic conditions derived from pre-existing GCMs will be delivered. Boundary conditions reflective of a static ice sheet in thermal contact with porous substrate will be included. Laboratory-derived measurements of the volume of particulate regolith of discrete grain sizes eroded per unit (a) ice thickness and (b) pressure and temperature will be implemented into the model, in order to predict the erosional efficacy of cryoventing under different climatic conditions. The model will be modified to explain dynamics induced by varying

abundances of dust within the ice to predict the influence of global dust storms on sublimation efficacy.

(b) Survey HiRISE images of araneiforms following the current Mars year (MY) global dust storm to assess whether a higher volume of dust will affect vent efficacy or alter araneiform morphometry. The influence of a global dust storm on araneiform morphometry has not yet been assessed but is expected to enhance sublimation activity due to increased snowfall and rapid sublimation dynamics when dust is present (Mc Keown et al., submitted).

A survey of HiRISE images of araneiforms between the last and current Mars year will be conducted. ArcGIS software will be used to detect any measurable change in trough dimensions relative to the higher presence and spatial coverage of dust. ISIS3 software will be used to correct stereo pair image distortions and SOCET SET will be invoked to build Digital Terrain Models of araneiforms before and after the dust storm. These DTMs can then be differenced in order to assess whether there is any measurable topographic change in araneiforms following spring cryoventing. Additionally, average fan/spots over a given surface area will be counted to assess whether cryoventing activity increases relative to the presence of dust in the ice (i) before and (ii) after the 2018 global dust storm.

(c) Perform quantitative laboratory experiments to condense CO_2 as in (Portyankina, G. and Merrison, J. and Iversen, J.J. and Yoldi, Z. and Hansen, C.J. and Aye, K.-M. and Pommerol, A. and Thomas, N., 2019; Sylvest et al., 2016) on beds of a wide range of grain sizes under controlled Martian pressure and temperature ranges to investigate the influence of (a) changes in climate conditions, (b) dust, (c) light intensity (d) ice thickness and (e) sediment consolidation on venting and araneiform morphometry.

i. A CO_2 layer will be condensed on granular substrate (i) with and (ii) without a thin layer of dust at the interface between the ice and the granular bed. The CO_2 will then be irradiated with light with an intensity similar to that expected in the Spring at the Martian south pole.

ii. Structure from Motion technology will be used to build Digital Elevation Models in order to calculate trough erosional depth/width/length per volume dust present. These predictions will then be extrapolated to Martian scales and compared with the findings of the HiRISE survey in order to investigate whether global dust storms may have had an influence on araneiform formation over the course of history.

iii. CO_2 ice of constant thickness will be irradiated with varying degrees of light intensity in order to obtain intensity per unit ice thickness needed to cause venting. These data can then be used to predict, using pre-existing climate models on Mars (and hence predicted light intensity with changing obliquity), when the maximum araneiform activity would have occurred based on assumed ice thickness.

iv. Water-saturated granular beds will be frozen and he experiments listed above will be performed in order to assess the role of sediment compaction/induration and presence of excess ice on araneiform formation.

In this thesis, a new hypothesis is proposed - that the radial patterns of araneiforms developed in one or few powerful venting episodes during a relic climatic period, when the efficacy of cryoventing was sufficient enough to erode and lift coarser grained or well consolidated substrate above the ice. The proposed research will investigate the constraints on cryoventing posed by environmental factors such as ice thickness, dust presence, insolation intensity and ambient pressure and temperature; all factors which alter with changing climate. These data will be compared with conditions predicted by pre-existing global climate models in order to attribute araneiform formation to a certain period during the course

of Mars's climatic history and to better understand why sand furrows and dendritic troughs develop in the present day, while radial araneiforms do not. As such, the future work arising from the findings of this thesis could be used as a new approach to understanding climate change on Mars and its effect on the Martian surface.

Sublimation is a recognised geomorphic process (Mangold, 2011) and yet the empirical framework of its interaction with planetary surfaces until now, has been thin. This thesis reports the first empirical observations of CO_2 sublimation dynamics in the context of small–scale Martian surface features. These were previously only framed in a theoretical context due to lack of available ground–truth data. Furrow, linear gully pit and araneiforms are all features which are not observed on Earth and therefore require a robust inventory of observational data to test conceptual models of their formation. This thesis represents a body of work which has advanced the field of Martian sublimation geomorphology and can be drawn upon to test, validate and improve our perception of land–forming processes on Mars and other planetary surfaces.

Appendix A

Supplementary Material: The HiRISE Instrument Onboard the Mars Reconnaissance Orbiter

A.1 Abstract

This appendix provides detailed information on the High Resolution Imaging Science Experiment (HiRISE) and Digital Terrain Model development by the HiRISE team.

A.2 HiRISE

The theory surrounding CO_2 sublimation processes on Mars evolved largely through a new age of high resolution topographic imaging of the small–scale Martian surface enabled by NASA's HiRISE instrument (McEwen et al., 2007) on board the Mars Reconnaissance Orbiter (Zurek and Smrekar, 2007). HiRISE is a visible and near–infrared wavelength camera that operates in high (25 cm/pixel) resolution allowing detailed views of the Martian surface and change detection analysis. As with many NASA missions, observational data collected by the HiRISE instrument is freely available to planetary science professionals and members of the general public online (https://hirise.lpl.arizona.edu/). From an altitude of 200–400 km above the Martian surface, 1–metre sized features can be resolved with HiRISE. This unprecedented resolution has provided a new window into the Martian surface and has allowed the planetary science community to monitor the evolution of the Martian landscape in the present–day.

A.2.1 Instrument Specs

The HiRISE instrument (Figure A.1) was launched on board the Mars Reconnaissance Orbiter on 12th August 2005 and entered a 255 x 320 km Mars orbit on 10th March 2006 (McEwen et al., 2007) with a periapse near the south pole. HiRISE consists of a telescope and Focal Plane Subsystem (FPS) and two remote electronics boxes; one for power supply and another for instrument controller electronics. The telescope is

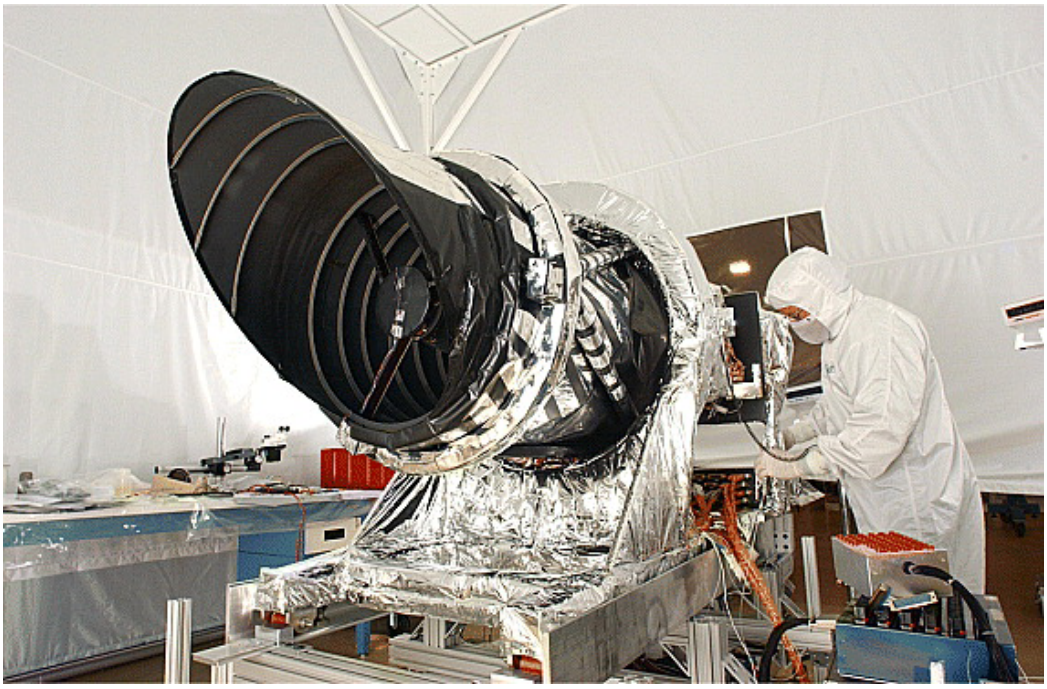

FIGURE A.1: The HiRISE instrument at Ball Aerospace and Technology Corporation in Boulder, Colorado. Source: A. McEwen (McEwen et al., 2007)

a 50 cm aperture, f/24 system (McEwen et al., 2007) and the focal plane contains 14 Charged Couple Device (CCD) detectors 2048 pixels wide and 128 pixels high that are operated in Time Delay Integration (TDI) mode. Time Delay Integration is used in order to gather enough image data to produce a high quality image. In TDI, each small patch of terrain is imaged up to 128 times. These signals are then summed in order to increase the Signal to Noise Ratio (SNR) of the resultant image (Bergstrom et al., 2004; Delemere et al., 2003; Dorn et al., 2004), which has been optimised to be 100:1.

HiRISE which has a ground track velocity of 3.2 km/s is a 'push–broom' imager. Push broom imaging is a type of remote–sensing imaging technique which operates along the track of the spacecraft. Advantages of this method include the acquisition of more light than other techniques because the instrument operates like a long–exposure camera, looking at a particular area for a longer time. In this configuration, detectors are organised in a linear array perpendicular to the flight direction and the spacecraft motion sweeps this array along the surface, imaging different areas of the surface as

the spacecraft flies forward. The field of view sets image swath width and the number of pixels sets pixel scale.

HiRISE images have a swath width of 6 km at 300 km altitude. The effective focal length defined as the distance from the primary plane of the lens to the focal point, when focusing light that is coming from infinity, is 12 m and the Instantaneous Field of View (IFOV) which is defined as the angle subtended by a single detector element on the axis of the instruments optical system, is $1\,\mu rad$. For regional context, the Mars Reconnaissance Orbiter Context Imager (CTX) supplements HiRISE images with a wider pixel scale, covering larger areas with lower resolution.

A.2.2 Digital Terrain Models

Stereo pairs allow a 3D view of the Martian surface terrain and are built by combining two images from left and right looking rolls of the spacecraft off nadir. One way to study geomorphology of the Martian surface in 3D is to use stereo pairs to develop Digital Terrain Models (DTMs), where the left looking image is displayed in red and the right looking image is displayed in green and/or blue. A DTM is a raster product of the ground surface in which a unique elevation value is assigned to each pixel. Corresponding metadata include map projection information so that each pixel can be related to latitude and longitude. This thesis utilises DTMs built and made available by the HiRISE team. A general timeline of HiRISE DTM development is as follows: firstly, corrections are made for any optical distortions intrinsic to the spacecraft such as "jitter" which occurs with small motions of the spacecraft around its normal pointing direction (Kirk et al., 2008). The next step is triangulation, where the stereo images are registered to each other and to the Mars Orbiter Laser Altimeter (MOLA) global elevation map (Kirk et al., 2008). Triangulation requires intense operator and computational time and so DTMs developed by the HiRISE team are

currently only available for 543 sites at the time of writing this thesis. After this stage, the DTM is generated and the terrain extraction output is assessed for any artefacts and edited where needed (Kirk et al., 2008). In general, terrain can be derived at a post spacing 4 times the pixel scale of each stereo pair. HiRISE images range from 0.25 - 0.5 m/pixel, so the post spacing is 1-2 m with vertical precision in the tens of centimetres. Precision in vertical measurements is improved when the difference in roll angle is greater, difference in incidence angle is lower to avoid disparity in shadows, and environmental conditions do not vary between the two images (i.e. they are taken a short time apart with similar lighting conditions to avoid shadow/frost artefacts).

Since DTMs are raster datasets, a useful product to combine with DTM analysis is its corresponding orthoimage which provides a solid visual effect for the user when analysing topographic variation. An orthoimage is an image which has been geometrically corrected so that the scale is uniform. The pixels have been projected so that the overall image is aerial. Accurate distances on the Martian surface can be measured because the topographic distortions originally used to create the associated DTM have been removed and the final product is map projected. In addition, HiRISE provide freely available map projected colour and black and white JPEG2000 images which are more abundant than orthoimages and thus can be useful for time–sensitive analysis of the Martian terrain.

Appendix B

Ongoing Research: A Quantitative Comparison Between Theory And Experiment for CO_2 Sublimation on a Granular Surface under Terrestrial and Martian Conditions

Abstract

The material presented in this appendix is ongoing research and thus is not presented as a research chapter, rather it is has been documented in Appendix B of this thesis. Future directions of this research and wider implications for the model in the context of understanding carbon dioxide sublimation on Mars are discussed further, in *Future Work*.

B.1 Introduction

Due to the remote nature of studying the inner planets, ground truth data for many Martian surface processes are not available. It is therefore necessary to use a combination of approaches to understand Martian surface processes. These include terrestrial field work, controlled laboratory experiments, multi–wavelength remote sensing and numerical modelling. The latter is an essential approach for the extrapolation of Earth analogue work to planets that have very different acceleration due to gravity, atmospheric circulation and orbital mechanics such as is found on Mars.

Numerical modelling is a widely applied technique used to solve complex mathematical equations that describe physical systems. Models make use of numerical time–integration procedures in order to predict the temporal evolution of the given system. Modelling has been of great benefit to our understanding of the present–day environment on Mars, as well as formulating predictions of past environments. For example modelling Mars' obliquity and eccentricity variations over geological timescales (Laskar et al., 2004; Ward, 1974; Ward et al., 1974) has allowed a greater understanding of global insolation and hence the history of Mars' waxing and waning CO_2 ice caps (Ward et al., 1974) and climate forcing of the polar layered deposits.

Numerical modelling has also emerged as a useful tool in understanding present–day surface processes on Mars. In particular, understanding surface processes initiated by sublimating carbon dioxide ice relies heavily on numerical modelling because as CO_2 is not naturally found in solid form on Earth, we have very little empirical data on how its phase changes interact with planetary surfaces. For example, modelling radiation absorption and scattering revealed insights to the waxing and waning nature of the enigmatic swiss cheese terrain (Thomas et al., 2000) of the south polar residual ice cap (Byrne and Ingersoll, 2003) on century timescales. Invoking a Computational Fluid Dynamics (CFD) code to model the dusty jets of the south polar cryptic region has allowed a prediction of fan and spot geometry as a function of slope and particle size (Thomas et al., 2011), modelling the irradiation of translucent slab ice has accurately attributed the timing of fan and spot activity to early spring (Portyankina et al., 2010) and applying a Diffusion Limited Aggregation code to fluid migration in porous material has predicted the dendritic patterns associated with araneiform terrain (Portyankina et al., 2017a).

Models of terrestrial processes benefit from the availability of empirical data which can be compared with the output of the model in order to test and refine it. However, testing models of Martian surface processes is not sufficiently rigorous by observation of surface changes alone and requires empirical data on the time evolution of physical variables under Martian conditions. An advent of laboratory modelling within Mars Chambers is building an inventory of parameters describing the behaviour of CO_2 ice under Martian pressure and temperature ranges (Chinnery et al., 2018; Kaufmann and Hagermann, 2017; Portyankina et al., 2018). This allows for validation and refinement of existing models and development of new ones, which aim to study active, seasonal processes on Mars.

B.1.1 The Sliding CO_2 Block Hypothesis

An example of a CO_2 related surface process which requires robust numerical modelling is the Sliding CO_2 block hypothesis for linear gully formation (Diniega et al., 2013). C. J. Hansen first proposed the hypothesis that linear gullies form when a block of CO_2 ice falls from a zone of high frost accumulation (i.e. from a dune brink) onto a relatively warm granular surface (i.e. the dune lee slope) and then sublimates sufficiently vigorously to levitate on a gas layer via the *Leidenfrost Effect* (Leidenfrost, 1966). The Leidenfrost Effect occurs when a substance comes in thermal contact with a surface that is at a much higher temperature than its boiling or sublimation point. The substance, in this case CO_2 ice, will then immediately be enveloped in a "vapor prison" if surrounded fully by the warmer material, as was seen in our first set of laboratory experiments (Mc Keown et al., 2017) (Chapter 3) where CO_2 blocks burrowed within granular material. If the material is sufficiently consolidated or of greater grain size however, only the bottom layer of the block will generate a vapor "cushion" whereby gas pressure is greater than the downward pressure exerted by the weight of the block and it will levitate. If the grains are sufficiently mobile, the sublimating gas will transport material from beneath the block to form levées and in turn excavate a shallow pit. On Mars, hybrid scenarios where blocks either partially burrow or glide upon a vapor layer and also translate downslope are proposed dependent on grain size and block dimensions (Diniega et al., 2013). The gaseous lubrication layer allows the blocks to move down even gentle slopes since solid friction is reduced significantly. Eventually the block will come to rest at the dune terminus and sublimate in situ to form a circular or quasi–circular pit. The hypothesis is supported by the observation of channel formation by sliding blocks on sand dunes on Earth (Diniega et al., 2013), that pits are generally slightly wider than their corresponding channels (Diniega et al., 2013; Mc Keown et al., 2017; Pasquon et al., 2016), that high albedo blocks have been detected within channels and pits (Diniega et al., 2013; Dundas et al., 2012) and that these have been measured to alter the dimension of pre–existing pits to an extent

expected by sublimating CO_2 (Mc Keown et al., 2017).

Results of stationary block sublimation experiments presented in Chapter 3 showed empirically that (i) circular pits and surrounding levées can form via this effect under Earth conditions and (ii) that annual changes in pit dimensions on Mars are consistent with erosional efficacy of CO_2 blocks measured in the laboratory. A mathematical model predicting the necessary physical parameters to sustain levitation and mobilisation was developed (Diniega et al., 2013). However, though this combined effort showed qualitatively that the Leidenfrost process can be highly effective for CO_2 blocks on Earth, there was no quantitative test of the model under either Earth or Martian conditions. This chapter describes the first quantitative experiments under Earth and Martian conditions to test a model of CO_2 block sublimation on granular substrate using a variety of grain sizes.

B.1.2 Mathematical Model of Block Motion

The mathematical model reported in (Diniega et al., 2013) describes the initiation of motion due to sublimation of a CO_2 ice block on a relatively warm substrate on Earth and Mars. The aims of the model were as follows:

1. To demonstrate that ice block sublimation will produce a layer of vapor whereby its gas pressure is sufficient to initiate and lubricate block transport downslope.

2. To estimate the timescales over which the sand would be warm enough to sustain levitation of the block and hence to estimate whether downslope transport is possible, or whether the sand would cool quickly enough to stop the motion of the block as it moves downslope.

A more detailed description and derivation of the following relationships can be found in (Diniega et al., 2013). However, a brief summary is as follows: Because the Martian

atmosphere is predominantly composed of gaseous CO_2, we can assume that the block is in equilibrium with the atmosphere. Thus, the initial temperature of the block can be taken as the sublimation temperature of CO_2 under Martian atmospheric pressure, denoted as T_s. The initial temperature of the sand is assumed to be uniform and is denoted by T_o (Diniega et al., 2013).

B.1.2.1 Vapor Pressure and Lift Force

In considering the first aim of the model, the criterion for levitation and rapid sublimation to occur is that the vapor pressure of the gas sublimating from the base of the block (assumed to be uniform over the surface area of the base of the block) will significantly exceed atmospheric pressure (Diniega et al., 2013). This is constrained by heat flux, which will reduce over time as the relatively cold CO_2 ice remains in thermal contact with the substrate. The flow rate of sublimating CO_2 is denoted by q and is approximated as perpendicular to the sandy surface. The gas flow velocity u_o is related to this by

$$u_o = \frac{q}{\rho_g} \tag{B.1}$$

where ρ_g is the density of CO_2 gas. The flow of gaseous CO_2 through the porous substrate can be described by *Darcy's Law* which is the principle that the mass flow rate between two points is directly proportional to the pressure drop between the points and the ability of the media through which it is flowing to obstruct the flow.

$$\nu\,\mathbf{u} = -\,k\,\Delta\,p \tag{B.2}$$

ν represents dynamic viscosity, $\mathbf{u}$ is the velocity of the CO_2 gas, k is the permeability of the sand, p is the gas pressure and the negative sign is reflective of the fact that fluids flow from areas of high pressure to low pressure. For a block somewhere between a rectangular shape with width 2R and length L such that R <<< L and disc shape

of radius R, pressure under the block and velocity components are as follows:

$$p = C_u \frac{u_o\,\nu}{k}\sqrt{R^2 - r^2}, \qquad u_r = C_u\,u_o\,\frac{r^2}{\sqrt{R^2 - r^2}}, \qquad u_z = u_o \tag{B.3}$$

Where C_u is a numerical factor which is = 1 in 2D and = $\frac{2}{\pi}$ in 3D. Since force is equal to pressure per unit area, integrating the above expression for pressure over the surface area of the block in contact with the substrate (A) gives us the lift force (F) required to levitate a block between the dimensions considered:

$$F = C_F\,A\,\frac{R\,u_o\,\nu}{k} \tag{B.4}$$

where C_F is a proportionality constant. In 2D A = 2RL and $C_F = \frac{\pi}{4}$ and in 3D, A = $\pi\,R^2$ and $C_F = \frac{4}{3\,\pi}$.

B.1.2.2 Thermal Gradient and Thermal Inertia

The heat transfer involved in this problem can be approximated by considering the one–dimensional heat equation:

$$\rho_s\,c\,\frac{\partial\,T}{\partial\,t} = \kappa\,\frac{\partial^2\,T}{\partial\,z^2}, \qquad T(t,0) = T_s, \qquad T(0,z) = T_o \tag{B.5}$$

where ρ_s is sand bulk density, c is its heat capacity, and κ is its thermal conductivity. Inputting our initial conditions and solving the PDE, we find that:

$$T = T_s + (T_o - T_s)\,erf\frac{z}{\sqrt{\frac{4\kappa\,t}{c\rho_s}}} \tag{B.6}$$

and the heat flux from the warm sand into the ice block is:

$$h(t) = \kappa\,\frac{\partial\,T}{\partial\,z}\Big|_{z=0} = (T_o - T_s)\sqrt{\frac{\kappa\,c\,\rho_s}{\pi\,t}} \tag{B.7}$$

where the top line of the square root denotes thermal inertia, or the degree of slowness with which the temperature of a body reaches that of its surroundings – in our case, the rate at which the temperature of the sand acclimates and reaches thermal equilibrium with the CO_2 block. It is assumed that all of the heat energy is used in sublimating the CO_2 and so we neglect the heating of the block and the sublimated gas.

While the model also considers the instigation of block translation downslope, because of the limited room and mobility under vacuum in the Mars chamber, our experiments consider only the sublimation and levitation of a *stationary* block. This is useful in predicting whether stationary CO_2 blocks which have come to rest at dune termini on Mars will excavate the pits exclusive to linear gullies.

Experiments using stationary block sublimation on granular substrate were performed in order to test the numerical model of CO_2 sublimation in the context of linear gully pit formation on Mars. The aim was to test if the model was robust under Earth and Mars conditions by examining whether the theoretical gas pressure and thermal gradient agreed with our experimental data.

Our experimental objectives were thus to (1) measure the gas pressure of the subliming vapor layer and its decline over time per given surface area of CO_2 in contact with the substrate under (i) Earth and (ii) Martian ambient pressure and compare this with model predictions of gas pressure for similar block dimensions and grain sizes and (2) measure the thermal gradient within the granular bed under (i) Earth and (ii) Martian ambient pressure and compare this with model predictions of thermal profiles for similar block dimensions and grain sizes.

B.2 Methods

B.2.1 Earth Experiments

In order to test the numerical model under Earth conditions and also to establish experimental protocol for our experiments under Mars conditions, the chamber described in Chapter 3 was deployed in the Civil Engineering laboratories at Trinity College, Dublin (Mc Keown et al., 2017). The previously established experimental protocol described in Chapter 3 was modified to accommodate measurements of temperature and pressure beneath a sublimating CO_2 ice block as follows:

A container was filled with 4–45 μm glass spheres and the bed was levelled using a metal ruler and spirit level. The height of the bed was marked on opposite sides of the container with a permanent marker at eye level to avoid parallax error. The finest glass spheres were chosen for this measurement for consistency as this would be the lowest height each of the beds would reach. We could therefore match all beds of the other grain sizes to this height, with some material left over. The container was then emptied, vacuumed and dusted. Five holes were drilled using a power drill in a straight vertical line either side of the experimental chamber 25 mm apart, beginning from where the height of the bed originally was. Taut non–conductive twine (synthetic fibre) was threaded through the 5 holes on each side and fastened beneath the container to ensure the twine did not sag and hence to ensure each taut section represented 25 mm intervals. Only insulating material was utilised in these experiments for accurate measurements of thermal gradient as heat transfer to conductive materials would affect measurements of the thermal gradient within the granular bed.

Plastic tubing was fed through the top hole and placed halfway across the first taut section of twine and positioned at the centre of the container with duct tape. This tubing was securely fastened to one port of a highly sensitive Validyne DP–15 (± 35 Pa)

differential pressure transducer and sealed with sealant gum. Differential pressure transducers measure gas pressure by calculating the difference between an input pressure and a reference pressure; in our case; ambient atmospheric pressure in the laboratory. This pressure is registered on an internal diaphragm and transmitted as a voltage signal which can then be calibrated. The pressure transducer effectively measures the lift force of the CO_2 block since this is the integrated differential pressure under the block. For such a sensitive pressure transducer the reference pressure was difficult to keep totally consistent due to movement within the laboratory or the vent system in the room. Four T–type thermocouples were secured to the bottom four sections of twine with duct tape and positioned vertically below the plastic tubing. The holes were then sealed with silicone and allowed to dry.

For each experimental trial performed in duplicate, the chamber was then filled with sieved and dried glass spheres of grain sizes either 4–45 $\mu\,m$, 45–90 $\mu\,m$, 75–150 $\mu\,m$ or 160–212 $\mu\,m$ and levelled using a metal ruler and spirit level. Glass spheres were employed due to their unimodal nature since the rough surface texture of natural grains is difficult to model numerically. Four different sizes were used as the theory predicts a very strong (quadratic) dependence of lift force on particle diameter. Care was taken to just slightly cover the plastic tubing connected to the pressure transducer with grains. The grains were mixed with a plastic stirrer to keep the initial temperature of the bed uniform. The lid on the chamber was secured with sealant gum. As in the experiments outlined in Chapter 3, the chamber was evacuated of moist air by placing CO_2 ice blocks upon the silica gel moat and allowing the blocks to sublimate until relative humidity was registered on the digital hygrometer as $< 10\,\%$. These were kept as far as possible from the instruments at the centre of the bed so that bed temperature remained homogeneous. However, conductivity was difficult to account for in the time during which humidity lowered, so the initial temperatures registered on the thermocouples may have differed by $\pm\,2\,^\circ$. All of the thermocouples and pressure transducer were connected to a National Instruments USB chassis. A

virtual instrument (VI) subroutine developed using LabView software to convert the analog output from the instruments to digital was activated to monitor pressure and temperature. The trap door was then quickly opened and a CO_2 ice block was placed on the granular surface directly above the sensors. Sufficient time was allowed for the block in each case to sublimate and data on pressure and temperature were acquired. These data were imported to a .csv file, read into Matlab and plotted over time.

B.2.2 Mars Experiments

In order to test the numerical model under Martian pressure, experiments were performed in the Mars Simulation Chamber at the Open University at a temperature of 293 K and a pressure of 600 Pa (6 mbar). Unlike in the Earth experiments, the chamber was not backfilled with pure CO_2 gas because the partial vacuum created had sufficiently few air molecules present and humidity was therefore negligible. A glass aquarium measuring $40 \times 40 \times 60\,cm$ was filled with Guyson Honite glass spheres of the same grain size ranges as the Earth experiments. A rake of four T–type thermocouples separated vertically by 25 mm was deployed at the centre of the aquarium and secured at the base with putty and silicone. In addition, two tubes were placed at two depths and were connected to two DP–15 ($\pm$35 Pa) differential pressure transducers. All hardware was connected to a National Instruments USB chassis which fed into a laptop with high RAM.

For each experimental trial, a block of CO_2 ice of approximately $400 \times 500 \times 200$ mm was drilled at its sides, weighed and measured and a claw was inserted into the holes. The claw was attached to a pulley which suspended the block above a granular bed as in our experiments described in Chapter 4 (Mc Keown et al., submitted). The aim of this was to keep the block out of thermal contact with the warm granular bed until the experiment began and until the ambient pressure reached 6 mbar. Once the desired pressure was achieved the block was lowered gently onto the surface, which

consisted of dried, sieved and levelled Guyson Honite Glass Spheres. A VI was created in LabView data acquisition software by J.N.M which converted the analog output from the hardware into digital. The data were saved to a laptop owned by J.N.M. J.N.M was then to use the laboratory pressure and temperature signals to read into a Matlab 2018a script where he was also to condition, plot the data and return to TCD for comparison and evaluation with the predicted output of the numerical model by L.E.M.

B.3 Results and Discussion:

B.3.1 Earth Experiments

For the Earth experiments, initial results indicate that gas pressure traces under Earth conditions were in strong agreement with the predicted theory for coarser grain sizes (Figure B.3). The pressure under the block for one experiment is shown in Figure B.3 compared to the model prediction. The data show that the simple model combining 1D heat transport and 3D Darcy flow captures the essential physics of the problem under Earth conditions. The laminar flow of gas from beneath a stationary CO_2 ice block in contact with porous substrate can be approximated by Darcy's Law and gas pressure decline scales as $\frac{1}{t^2}$ as predicted. Artefacts in the plots seen in Figure B.1 are attributed to the vent system in the laboratory. In addition, pressure needs to be carefully calibrated (i.e. the voltage signals need to be converted to units of pressure). J.N.M. has the calibration documents for the sensors used which he initially calibrated prior to the experiments and has not yet delivered it. However, initial results indicate a good agreement (Figure B.3).

B.3.2 Mars Experiments

The data for the experiments conducted in the Mars Chamber at the Open University have not yet been returned by Prof. McElwaine to TCD in a readable format. Therefore plots of the data are unavailable to report here.
The data processing, input to Matlab, conditioned, and plotted result have not yet been returned to TCD by Prof. McElwaine for comparison and evaluation. While this work is ongoing, what follows is a report of qualitative observations noted by the student during the experiments.

Initial assessment of the data by L.E.M. acquired from the Mars chamber suggest the numerical model accurately describes the thermal gradient and pressure decline once the block remains relatively stationary (i.e. on coarser, less mobile grains).

However, for the finer grain sizes used ($< 250\mu m$) gas flow under Mars conditions was much more rapid than anticipated and CO_2 mass flux was as much as 16 times higher than under ambient Earth pressure (see movie of vigorous sublimation, Chapter 4). This was calculated by L.E.M. by weighing the block pre and post sublimation, measuring time from initial placement until no motion within the granular bed on the video recording sublimation and dividing mass difference by time, as in Chapter 4. Once the block partially burrows and rapidly transports granular material in this way, the flow is estimated to enter a more turbulent non–Darcy regime whereby flow velocity and Reynolds number (describing the ratio of inertial forces to viscous forces in a fluid) increase significantly. Our data suggest that the presence of much finer grain sizes will alter the flow beneath sliding CO_2 ice blocks significantly, and non–Newtonian dynamics may need to be considered. Darcy's Law is only valid for slow, viscous flow with Reynold's numbers less than 1. The lack of mobility of the heavier coarser grains under Martian conditions allows for a smoother flow where viscous forces exceed inertial forces. In more turbulent flows, eddie currents and other flow

instabilities come into play which are more difficult to predict. The model will require refinement in the case of finer grain sizes–which may have important implications for the activity of linear gullies in the coming Mars spring due to increased dust deposition following the 2018 global dust storm. From our qualitative observations of enhanced erosion and material transport for finer grain sizes under Martian conditions, we expect that linear gully channels and pits will widen and deepen significantly in the next Martian spring and that increased pit formation will occur with increased dust deposition. These can be evaluated following appropriate data acquisition by the HiRISE camera in 2019–2020.

B.4 Conclusion

We have performed the first quantitative experiments to test a model of the interaction of a sublimating CO_2 ice block under Earth and Mars conditions. The data suggest that the model accurately predicts the thermal gradient and gas pressure decline for a CO_2 block on loose granular material under Earth conditions. This suggests that a sublimating CO_2 ice block will sublimate sufficiently vigorously and for a long enough time to erode loose dune material under Earth conditions. Since Martian pressure and gravity is much lower, we can expect that sublimation and levitation may be even more effective on Mars. However, further refinement of the numerical model is required to consider the transition to turbulent flow regimes under Martian pressure once a block partially burrows and vigorously sublimates. In addition to testing the numerical model of CO_2 block sublimation specific to linear gully formation, these data can be drawn upon to refine and test other models of CO_2 sublimation on Mars in order to further understand how this extant geomorphic agent modifies the Martian surface today.

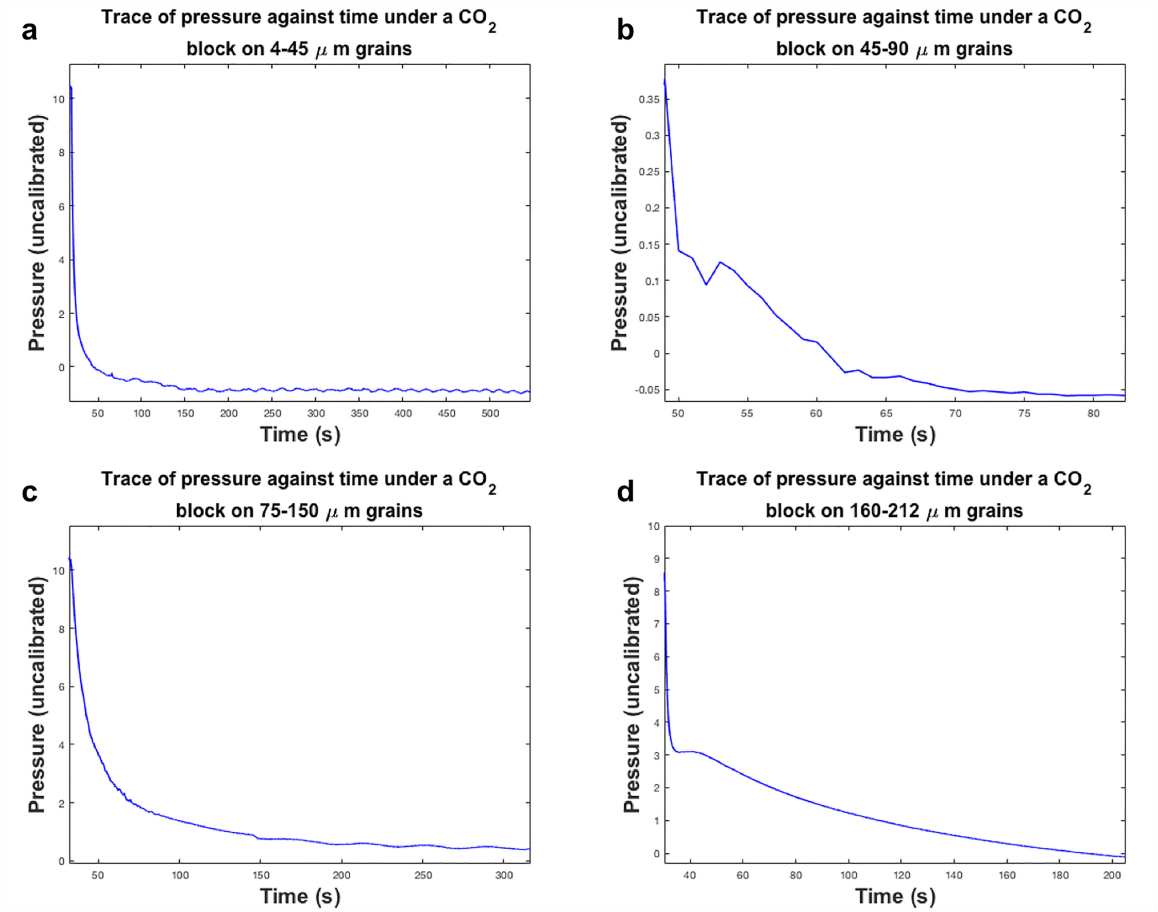

FIGURE B.1: Plots of pressure beneath CO_2 ice blocks on granular beds of discrete grain size ranges under Earth conditions

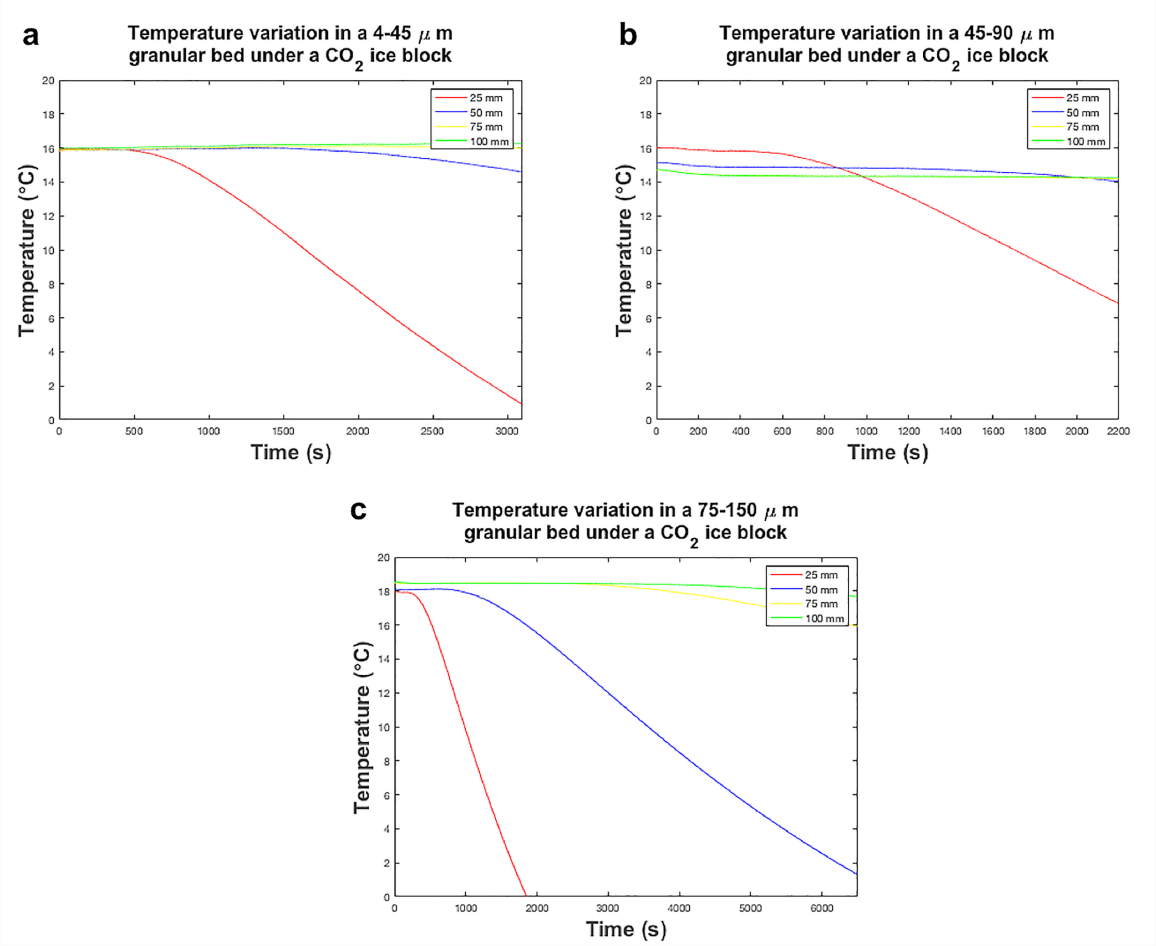

FIGURE B.2: Plots of temperature beneath CO_2 ice blocks on granular beds of discrete grain size ranges under Earth conditions

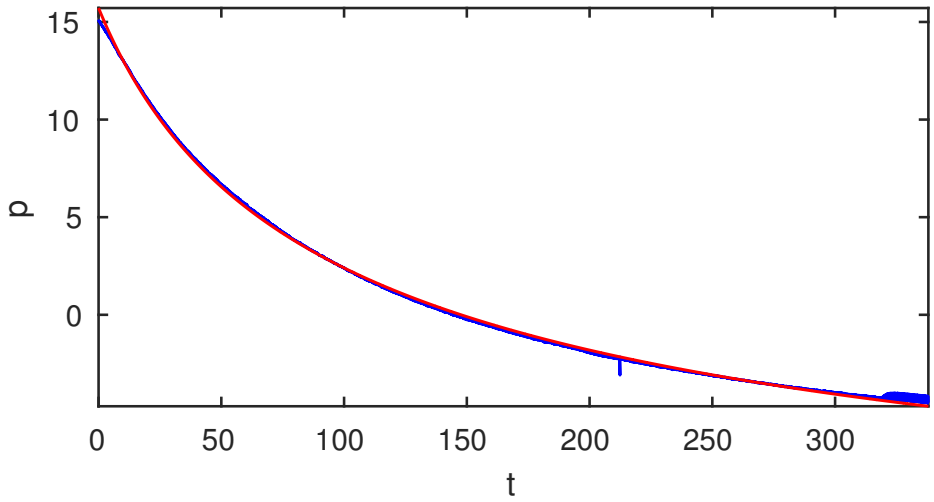

FIGURE B.3: Trace of pressure (Pa) against time (s) under a CO_2 block. Blue is experimental data, red is theoretical prediction. Data processed and plot produced by J.N.M. (Mc Keown et al., 2018)

Bibliography

M. H. Acuña, J. E. P. Connerney, F.N. Ness, R. P. Lin, D. Mitchell, C. W. Carlson, J. McFadden, K. A. Anderson, H. Rème, C. Mazelle, D. Vignes, P. Wasilewski, and P. Cloutier. Global distribution of crustal magnetization discovered by the mars global surveyor mag/er experiment. 284(5415):790–793, 1999.

O. Aharonson, M. T. Zuber, D. E. Smith, G. A. Neumann, W. C. Feldman, and T. H. Prettyman. Depth, distribution, and density of CO_2 deposition on Mars. *Journal of Geophysical Research (Planets)*, 109, 2004.

J.C. Andrews-Hanna, M.T. Zuber, and W. B. Banerdt. The Borealis basin and the origin of the martian crustal dichotomy. *Nature*, 453, 2008.

K.S. Auld and J.C. Dixon. A classification of martian gullies from hirise imagery. *Planetary and Space Science*, 131:88 – 101, 2016.

M. Balme, N. Mangold, D. Baratoux, F. Costard, M. Gosselin, P. Masson, P. Pinet, and G. Neukum. Orientation and distribution of recent gullies in the southern hemisphere of mars: Observations from high resolution stereo camera/mars express (hrsc/mex) and mars orbiter camera/mars global surveyor (moc/mgs) data. *Journal of Geophysical Research: Planets*, 111, 2006.

G.D. Bart. Comparison of small lunar landslides and martian gullies. *Icarus*, 187(2): 417 – 421, 2007.

P. Becerra, S. Byrne, and A. J. Brown. Transient bright "halos" on the South Polar Residual Cap of Mars: Implications for mass-balance. *Icarus*, 251:211–225, 2015.

P. Becerra, S. Byrne, M. M. Sori, S. Sutton, and K. E. Herkenhoff. Stratigraphy of the north polar layered deposits of Mars from high-resolution topography. *Journal of Geophysical Research (Planets)*, 121:1445–1471, 2016.

J.W. Bergstrom, W. A. Delamere, and A. McEwen. Mro high resolution imaging science experiment (hirise): Instrument test, calibration and operating constraints. In *International Astronautical Federation - 55th International Astronautical Congress 2004*, volume 9, pages 6210–6216, 2004.

A. Bhardwaj, L. Sam, J.F. Martín-Torres, M. Zorzano, and M.R. Fonseca. Martian slope streaks as plausible indicators of transient water activity. *Scientific Reports*, 7(1):7074, 2017.

J. Bibring, Y. Langevin, F. Poulet, A. Gendrin, B. Gondet, M. Berthé, A. Soufflot, P. Drossart, M. Combes, G. Bellucci, V. Moroz, N. Mangold, B. Schmitt, and the OMEGA team. Perennial water ice identified in the south polar cap of mars. *Nature*, 428, 2004.

M. Bourke and Z. McGaley-Towle. Why do sand furrow distributions vary in the North Polar latitudes on Mars? In *EGU General Assembly Conference Abstracts*, volume 16, page 13626, 2014a.

M. Bourke, J. Nield, S. Diniega, C. Hansen, and J. McElwaine. A field study of the geomorphic effects of sublimating CO_2 blocks on dune slopes at Coral Pink Dunes, Utah. In *EGU General Assembly Conference Abstracts*, volume 18, page 10450, 2016a.

M. C. Bourke. The formation of sand furrows by cryo-venting on Martian dunes. In *Lunar and Planetary Science Conference*, volume 44, page 2919, 2013.

M. C. Bourke and A. Cranford. Seasonal furrow formation on Mars polar dunes. In *Fifth International Conference on Mars Polar Science and Exploration*, volume 1623 of *LPI Contributions*, page 6059, 2011.

M. C. Bourke and Z. McGaley-Towle. Latitudinal variation in sand furrows in the north polar region of Mars. In *Lunar and Planetary Science Conference*, volume 45, page 2716, 2014b.

M. C. Bourke, J. M. Nield, S. Diniega, C. J. Hansen, J. N. McElwain, and T. N. Titus. The geomorphic effect of sublimating CO_2 blocks on dune lee slopes at Grand Falls, Arizona. In *Lunar and Planetary Science Conference*, volume 47, page 2407, 2016b.

G. W. Brass. Stability of brines on Mars. *Icarus*, 42:20–28, 1980.

N. T. Bridges, F. Ayoub, J-P. Avouac, S. Leprince, A. Lucas, and S. Mattson. Earth-like sand fluxes on mars. *Nature*, 485, 2012.

N. T. Bridges, B. L. Ehlmann, R. C. Ewing, C. E. Newman, R. Sullivan, P. G. Conrad, A. Cousin, K. S. Edgett, M. R. Fisk, A. A. Fraeman, J. R. Johnson, M. Lamb, M. Lapotre, S. Le Mouélic, G. M. Martinez, P.-Y. Meslin, P. Pinet, L. M. Thompson, J. Van Beek, A. R. Vasavada, and R. C. Wiens. Investigation of the Bagnold dunes by the Curiosity rover: Overview of initial results from the first study of an active dune field on another planet. In *Lunar and Planetary Science Conference*, volume 47, page 2298, 2016.

D.M. Burr, K.L. Tanaka, and K. Yoshikawa. Pingos on earth and mars. *Planetary and Space Science*, 57(5):541 – 555, 2009.

S. Byrne and A.P. Ingersoll. A sublimation model for martian south polar ice features. *Science*, 299(5609):1051–1053, 2003.

S. Byrne, P. O. Hayne, P. Becerra, and HiRISE Team. Evolution and Stability of the Residual CO_2 Ice Cap. In *Lunar and Planetary Science Conference*, volume 46 of *Lunar and Planetary Inst. Technical Report*, page 1657, 2015.

Y. Cedillo-Flores, A.H. Treiman, J Lasue, and S. Clifford. Co2 gas fluidization in the initiation and formation of martian polar gullies. *Geophysical Research Letters*, 38, 11 2011.

V.F. Chevrier and E.G. Rivera-Valentin. Formation of recurring slope lineae by liquid brines on present-day mars. *Geophysical Research Letters*, 39(21), 2012.

H. E. Chinnery, A. Hagermann, E. Kaufmann, and S. R. Lewis. The penetration of solar radiation into carbon dioxide ice. *Journal of Geophysical Research: Planets*, 123(4):864–871, 2018.

P. R. Christensen, J. L. Bandfield, J. F. Bell, N. Gorelick, V. E. Hamilton, A. Ivanov, B. M. Jakosky, H. H. Kieffer, M. D. Lane, M. C. Malin, T. McConnochie, A. S. McEwen, H. Y. McSween, G. L. Mehall, J. E. Moersch, K. H. Nealson, J. W. Rice, M. I. Richardson, S. W. Ruff, M. D. Smith, T. N. Titus, and M. B. Wyatt. Morphology and Composition of the Surface of Mars: Mars Odyssey THEMIS Results. *Science*, 300:2056–2061, 2003.

P.R. Christensen. Formation of recent martian gullies through melting of extensive water-rich snow deposits. *Nature*, 422, 2003.

S. J. Conway, T. N. Harrison, R. J. Soare, A. W. Britton, and L. J. Steele. New slope-normalized global gully density and orientation maps for mars. *Geological Society, London, Special Publications*, 467, 2017.

S.J. Conway and M.R. Balme. A novel topographic parameterization scheme indicates that martian gullies display the signature of liquid water. *Earth and Planetary Science Letters*, 454:36 – 45, 2016.

Conway, S.J. and Mangold, N. Evidence for Amazonian mid-latitude glaciation on Mars from impact crater asymmetry. *Icarus*, 225(1):413 – 423, 2013.

F. Costard, F. Forget, N. Mangold, and J. P. Peulvast. Formation of recent martian debris flows by melting of near-surface ground ice at high obliquity. 295(5552): 110–113, 2002.

G.E. Cushing, C.H. Okubo, and T.N. Titus. Atypical pit craters on mars: New insights from themis, ctx, and hirise observations. *Journal of Geophysical Research: Planets*, 120(6):1023–1043, 2015.

S. de Villiers, A. Nermoen, B. Jamtveit, J. Mathiesen, P. Meakin, and S. C. Werner. Formation of Martian araneiforms by gas-driven erosion of granular material. *Geophysical Research Letters*, 39, 2012.

A. Delemere, I. Becker, J. Bergstrom, J. Burkepile, J. Day, D. Dorn, D. Gallagher, C. Hamp, J. Lasco, B. Meiers, A. Sievers, S. Streetman, S. Tarr, M. Tommeraasen, and P. Volmer. MRO High Resolution Imaging Science Experiment (HIRISE): Instrument Development. In *Sixth International Conference on Mars*, 2003.

J.L. Dickson and J.W. Head. The formation and evolution of youthful gullies on mars: Gullies as the late-stage phase of mars's most recent ice age. *Icarus*, 204(1):63 – 86, 2009.

S. Diniega, S. Byrne, N. Bridges, C. Dundas, and A. McEwen. Seasonality of present-day Martian dune-gully activity. *Geology*, 2010.

S. Diniega, C. J. Hansen, J. N. McElwaine, C. H. Hugenholtz, C. M. Dundas, A. S. McEwen, and M. C. Bourke. A new dry hypothesis for the formation of Martian linear gullies. *Icarus*, 225:526–537, 2013.

D. A. Dorn, W. Meiers, J. Burkepile, E. D. Freymiller, A. W. Delamere, A. S. McEwen, P. Maggs, P. J. Pool, and I. Wallace. HiRISE focal plane for use on the Mars Reconnaissance Orbiter. In *Focal Plane Arrays for Space Telescopes*, volume 5167, pages 63–71, 2004.

C. M. Dundas, S. Diniega, C. J. Hansen, S. Byrne, and A. S. McEwen. Seasonal activity and morphological changes in Martian gullies. *Icarus*, 220:124–143, 2012.

C.M. Dundas, A.S. McEwen, S. Diniega, S. Byrne, and S. Martinez-Alonso. New and recent gully activity on mars as seen by hirise. *Geophysical Research Letters*, 37(7), 2012.

J. C. Ferris, J. M. Dohm, V. R. Baker, and T. Maddock. Dark slope streaks on mars: Are aqueous processes involved? *Geophysical Research Letters*, 29(10):128–1–128–4, 2002.

F. Forget, S. Byrne, J.W. Head, M.A. Mischna, and N. Schörghofer. *Recent Climate Variations*, pages 497–525. Cambridge Planetary Science. Cambridge University Press, 2017.

E.J. Gaidos. Cryovolcanism and the recent flow of liquid water on mars. *Icarus*, 153 (1):218 – 223, 2001.

M.S. Gilmore and E.L. Phillips. Role of aquicludes in formation of martian gullies. *Geology*, 30(12):1107, 2002.

J. Gómez-Elvira, C. Armiens, I. Carrasco, M. Genzer, F. Gómez, R. Haberle, V.E. Hamilton, A. Harri, O. Kahanpää, H.and Kemppinen, A. Lepinette, J. Martín Soler, J. Martín-Torres, J. Martínez-Frías, M. Mischna, L. Mora, S. Navarro, C. Newman, M.A. Pablo, V. Peinado, J. Polkko, S.C. R. Rafkin, M. Ramos, N.O. Rennó, M. Richardson, J.A. Rodríguez-Manfredi, J.J. Romeral Planelló, E. Sebastián, M. Torre Juárez, J. Torres, R. Urquí, A.R. Vasavada, J. Verdasca, and M. Zorzano. Curiosity's rover environmental monitoring station: Overview of the first 100 sols. *Journal of Geophysical Research: Planets*, 119(7):1680–1688, 2014.

R.M. Haberle, C.P. McKay, J. Schaeffer, N.A. Cabrol, E.A. Grin, A.P. Zent, and R. Quinn. On the possibility of liquid water on present-day mars. *Journal of Geophysical Research: Planets*, 106:23317–23326, 2001.

C. J. Hansen, N. Thomas, G. Portyankina, A. McEwen, T. Becker, S. Byrne, K. Herkenhoff, H. Kieffer, and M. Mellon. HiRISE observations of gas sublimation-driven activity in Mars' southern polar regions: I. Erosion of the surface. *Icarus*, 205:283–295, 2010.

C. J. Hansen, M. E. Schwamb, G. Portyankina, and K.-M. Aye. Planet Four: Terrains - Araneiform in the South Polar Region of Mars. In *Lunar and Planetary Science Conference*, volume 48 of *Lunar and Planetary Science Conference*, page 2812, 2017.

C.J. Hansen, M.C. Bourke, N.T. Bridges, S. Byrne, C. Colón, S. Diniega, C.M. Dundas, K. Herkenhoff, A. McEwen, M. Mellon, G. Portyankina, and N. Thomas. Seasonal erosion and restoration of mars' northern polar dunes. *Science*, 331 6017: 575–8, 2011.

J. Hao, G. G. Michael, S. Adeli, and R. Jaumann. Araneiform terrain formation in Angustus Labyrinthus, Mars. *Icarus*, 317:479–490, January 2019.

W.K. Hartmann, T. Thorsteinsson, and F. Sigurdsson. Martian hillside gullies and icelandic analogs. *Icarus*, 162(2):259 – 277, 2003.

P. O. Hayne, D. A. Paige, and N. G. Heavens. The role of snowfall in forming the seasonal ice caps of Mars: Models and constraints from the Mars Climate Sounder. *Icarus*, 231:122–130, 2014.

R. K. Hayward, K. F. Mullins, L. K. Fenton, T. M. Hare, T. N. Titus, M. C. Bourke, A. Colaprete, and P. R. Christensen. Mars Global Digital Dune Database and initial science results. *Journal of Geophysical Research (Planets)*, 2007.

J.W Head, J.F Mustard, M.A Kreslavsky, R.E Milliken, and D.R Marchant. Recent ice ages on Mars. *Nature*, 426(6968):797–802, 2003.

J.W. Head, D.R. Marchant, and M.A. Kreslavsky. Formation of gullies on mars: Link to recent climate history and insolation microenvironments implicate surface water flow origin. 105(36):13258–13263, 2008.

M. H. Hecht, S. P. Kounaves, R. C. Quinn, S. J. West, S. M. M. Young, D. W. Ming, D. C. Catling, B. C. Clark, W. V. Boynton, J. Hoffman, L. P. DeFlores, K. Gospodinova, J. Kapit, and P. H. Smith. Detection of perchlorate and the soluble chemistry of martian soil at the phoenix lander site. *Science*, 325(5936): 64–67, 2009.

J.L. Heldmann, O.B. Toon, W.H. Pollard, M.T. Mellon, J. Pitlick, C.P. McKay, and D.T. Andersen. Formation of martian gullies by the action of liquid water flowing

under current martian environmental conditions. *Journal of Geophysical Research: Planets*, 110, 2001.

J.L. Heldmann, E. Carlsson, H. Johansson, M.T. Mellon, and O.B. Toon. Observations of martian gullies and constraints on potential formation mechanisms: II. The northern hemisphere. *Icarus*, 188(2):324 – 344, 2007.

C. Herny, S.J. Conway, J. Raack, S. Carpy, T. Colleu-Banse, and M.R. Patel. Downslope sediment transport by boiling liquid water under mars-like conditions: experiments and potential implications for martian gullies. *Geological Society, London, Special Publications*, 467, 2018.

S.L. Hess, R.M. Henry, and J.E. Tillman. The seasonal variation of atmospheric pressure on mars as affected by the south polar cap. *Journal of Geophysical Research: Solid Earth*, 84:2923–2927, 1979.

N. Hoffman. Active polar gullies on mars and the role of carbon dioxide. *Astrobiology*, 2(3):313–323, 2002.

D.J. Hrubes. Mars atmosphere resource recovery system (marrs) final report. 2001.

C. H. Hugenholtz. Frosted granular flow: A new hypothesis for mass wasting in martian gullies. *Icarus*, 197:65–72, 2008.

A.P. Ingersoll. Mars: Occurrence of liquid water. *Science*, 168(3934):972–973, 1970.

T. Ishii and S. Sasaki. Formation of Recent Martian Gullies by Avalanches of CO_2 Frost. In *Lunar and Planetary Science Conference*, volume 35 of *Lunar and Planetary Inst. Technical Report*, 2004.

B.M. Jakosky, D. Brain, M. Chaffin, S. Curry, Deighan J., and et al. Loss of the martian atmosphere to space: Present-day loss rates determined from maven observations and integrated loss through time. *Icarus*, 315:146 – 157, 2018.

G. Jouannic, J. Gargani, S.J. Conway, F. Costard, M.R. Balme, M.R. Patel, M. Massé, C. Marmo, V. Jomelli, and G.G. Ori. Laboratory simulation of debris flows over

sand dunes: Insights into gully-formation (mars). *Geomorphology*, 231:101 – 115, 2015.

E. Kaufmann and A. Hagermann. Experimental investigation of insolation-driven dust ejection from Mars' CO_2 ice caps. *Icarus*, 282:118–126, 2017.

H. H. Kieffer, P. R. Christensen, and T. N. Titus. CO_2 jets formed by sublimation beneath translucent slab ice in Mars' seasonal south polar ice cap. *Nature*, 442: 793–796, 2006.

H.H. Kieffer. Mars south polar spring and summer temperatures: A residual co_2 frost. *Journal of Geophysical Research: Solid Earth*, 84:8263–8288, 1979.

H.H. Kieffer. Cold jets in the martian polar caps. *Journal of Geophysical Research: Planets*, 112, 2007.

H.H.. Kieffer, Stilman C.C. , T.Z. Martin, E.D. Miner, and F.D. Palluconi. Martian north pole summer temperatures: Dirty water ice. *Science*, 194(4271):1341–1344, 1976.

H.H. Kieffer, T.N. Titus, K.F. Mullins, and P.R. Christensen. Mars south polar spring and summer behavior observed by tes: Seasonal cap evolution controlled by frost grain size. *Journal of Geophysical Research: Planets*, 105:9653–9699, 2000.

R. L. Kirk, E. Howington-Kraus, M. R. Rosiek, J. A. Anderson, B. A. Archinal, K. J. Becker, D. A. Cook, D. M. Galuszka, P. E. Geissler, T. M. Hare, I. M. Holmberg, L. P. Keszthelyi, B. L. Redding, W. A. Delamere, D. Gallagher, J. D. Chapel, E. M. Eliason, R. King, and A. S. McEwen. Ultrahigh resolution topographic mapping of Mars with MRO HiRISE stereo images: Meter-scale slopes of candidate Phoenix landing sites. *Journal of Geophysical Research (Planets)*, 113:E00A24, 2008.

C.R Kochel and J. Trop. Earth analog for high-latitude landforms and recent flows on mars: Icy debris fans in the wrangell volcanic field, alaska. *Icarus*, 196:63–77, 2008.

K.J. Kossacki and J. Leliwa-Kopystynski. Non-uniform seasonal defrosting of subpolar dune field on Mars. *Icarus*, 168:201–204, 2004.

M.A. Kreslavsky and J.W. Head. Slope streaks on mars: A new 'wet' mechanism. *Icarus*, 201(2):517 – 527, 2009.

Y. Langevin, J.-P. Bibring, S. Murchie, M. Vincendon, F. Poulet, S. Douté, B. Gondet, H. Kieffer, and S. Le Mouélic. Evolution of the Seasonal Caps of Mars Observed by OMEGA on Mars Express. In *Seventh International Conference on Mars*, volume 1353, page 3246, 2007.

J. Laskar, A.C.M. Correia, M. Gastineau, F. Joutel, B. Levrard, and P. Robutel. Long term evolution and chaotic diffusion of the insolation quantities of mars. *Icarus*, 170(2):343 – 364, 2004.

Laskar, J. and Robutel, P. The chaotic obliquity of the planets. *Nature*, 361, 1993.

A. Lefort, P. S. Russell, N. Thomas, A. S. McEwen, C. M. Dundas, and R. L. Kirk. Observations of periglacial landforms in Utopia Planitia with the High Resolution Imaging Science Experiment (HiRISE). *Journal of Geophysical Research (Planets)*, 114, 2009.

J.G. Leidenfrost. On the fixation of water in diverse fire. *International Journal of Heat and Mass Transfer*, 9(11):1153 – 1166, 1966.

R. B. Leighton and B. C. Murray. Behavior of carbon dioxide and other volatiles on Mars. *Science*, 153:136–144, 1966.

M. C. Malin, M. H. Carr, G. E. Danielson, M. E. Davies, W. K. Hartmann, A. P. Ingersoll, P. B. James, H. Masursky, A. S. McEwen, L. A. Soderblom, P. Thomas, J. Veverka, M. A. Caplinger, M. A. Ravine, T. A. Soulanille, and J. L. Warren. Early views of the martian surface from the mars orbiter camera of mars global surveyor. *Science*, 279(5357):1681–1685, 1998.

M.C. Malin and K.S. Edgett. Mars Global Surveyor Mars Orbiter Camera: Interplanetary cruise through primary mission. *Journal of Geophysical Research: Planets*, 106(E10):23429–23570, 2001.

M.C. Malin, M.A. Caplinger, and S.D. Davis. Observational evidence for an active surface reservoir of solid carbon dioxide on mars. *Science*, 294(5549):2146–2148, 2001.

N. Mangold. Ice sublimation as a geomorphic process: A planetary perspective. *Geomorphology*, 126:1–17, 2011.

N. Mangold, F. Costard, F. Forget, and J.-P. Peulvast. Narrow gullies over high sand dunes on Mars: Evidence for flows triggered by liquid water near surface. In *Lunar and Planetary Science Conference*, volume 33, 2002a.

N. Mangold, F. Costard, F. Forget, and J.-P. Peulvast. Narrow Gullies over High Sand Dunes on Mars: Evidence for Flows Triggered by Liquid Water Near Surface. In *Lunar and Planetary Science Conference*, volume 33 of *Lunar and Planetary Science Conference*, 2002b.

N. Mangold, A. Mangeney, V. Migeon, V. Ansan, A. Lucas, D. Baratoux, and F. Bouchut. Sinuous gullies on Mars: Frequency, distribution, and implications for flow properties. *Journal of Geophysical Research (Planets)*, 115(14), 2010.

D.R. Marchant and J.W. Head. Antarctic dry valleys: Microclimate zonation, variable geomorphic processes, and implications for assessing climate change on mars. *Icarus*, 192(1):187 – 222, 2007.

F. J. Martín-Torres, M. Zorzano, P. Valentín-Serrano, A. Harri, M. Genzer, O. Kemppinen, E.G. Rivera-Valentin, I. Jun, J. Wray, M. Bo Madsen, W Goetz, A.S. McEwen, C. Hardgrove, N. Renno, V.F. Chevrier, M. Mischna, R. Navarro-González, J. Martínez-Frías, P. Conrad, T. McConnochie, C. Cockell, G. Berger, A. R. Vasavada, D. Sumner, and D. Vaniman. Transient liquid water and water activity at gale crater on mars. *Nature Geoscience*, 8, 2015.

M. Massé, S. J. Conway, J. Gargani, M. R. Patel, K. Pasquon, A. McEwen, S. Carpy, V. Chevrier, M. R. Balme, L. Ojha, M. Vincendon, F. Poulet, F. Costard, and G. Jouannic. Transport processes induced by metastable boiling water under martian surface conditions. *Nature Geoscience*, 9, 2016.

D.L. Matson and R.H. Brown. Solid-state greenhouse and their implications for icy satellites. *Icarus*, 77(1):67 – 81, 1989.

L. E. Mc Keown, M. C. Bourke, and J. N. McElwaine. Experiments on Sublimating Carbon Dioxide Ice and Implications for Contemporary Surface Processes on Mars. *Scientific Reports*, 7:14181, 2017.

L. E. Mc Keown, J. N. McElwaine, M. C. Bourke, M. E. Sylvest, and M. R. Patel. A Quantitative Comparison Between Theory and Experiment for CO_2 Sublimation on a Granular Surface Under Terrestrial and Martian Conditions and Morphological Results. In *Lunar and Planetary Science Conference*, volume 49, page 2374, 2018.

L.E. Mc Keown, M.C. Bourke, J.N. McElwaine, M.E. Sylvest, and M.R. Patel. The Formation of Araneiforms by Carbon Dioxide Venting and Vigorous Sublimation Dynamics Under Martian Conditions. *Scientific Reports*, submitted.

A. S. McEwen, E. M. Eliason, J. W. Bergstrom, N. T. Bridges, C. J. Hansen, W. A. Delamere, J. A. Grant, V. C. Gulick, K. E. Herkenhoff, L. Keszthelyi, R. L. Kirk, M. T. Mellon, S. W. Squyres, N. Thomas, and C. M. Weitz. Mars Reconnaissance Orbiter's High Resolution Imaging Science Experiment (HiRISE). *Journal of Geophysical Research (Planets)*, 112, 2007.

A.S. McEwen, C.M. Dundas, S.S. Mattson, A.D. Toigo, L. Ojha, J.J. Wray, M. Chojnacki, S. Byrne, S.L. Murchie, and N. Thomas. Recurring slope lineae in equatorial regions of mars. *Nature Geoscience*, 7, 2013.

M.T. Mellon and R.J. Phillips. Recent gullies on mars and the source of liquid water. *Journal of Geophysical Research: Planets*, 106(E10):23165–23179, 2001.

H. Miyamoto, J.M. Dohm, R.A. Beyer, and V.R. Baker. Fluid dynamical implications of anastomosing slope streaks on mars. *Journal of Geophysical Research: Planets*, 109, 2004.

F. Montmessin, R. M. Haberle, F. Forget, Y. Langevin, R. T. Clancy, and J.-P. Bibring. On the origin of perennial water ice at the south pole of mars: A precession-controlled mechanism? *Journal of Geophysical Research: Planets*, 112, 2007.

A. Morgenstern, E. Hauber, D. Reiss, S. van Gasselt, G. Grosse, and L. Schirrmeister. Deposition and degradation of a volatile-rich layer in Utopia Planitia and implications for climate history on Mars. *Journal of Geophysical Research (Planets)*, 112, 2007.

D.S. Musselwhite, T.D. Swindle, and J.I. Lunine. Liquid co_2 breakout and the formation of recent small gullies on mars. *Geophysical Research Letters*, 28(7):1283–1285, 2001.

C. Nash and M. Bourke. Southern hemisphere sand furrows: spatial patterning and implications for the cryo-venting process. In *EGU General Assembly Conference Abstracts*, volume 17, 2015.

A. O. Nier and M. B. McElroy. Composition and structure of Mars' upper atmosphere: Results from the neutral mass spectrometers on Viking 1 and 2. *Journal of Geophysical Research*, 82(28):4341–4349, 1977.

L. Ojha, M. Wilhelm, S.L. Murchie, A.S. McEwen, J.J. Wray, J. Hanley, M. Massé, and M. Chojnacki. Spectral evidence for hydrated salts in recurring slope lineae on mars. *Nature Geoscience*, 8, 2015.

D. A. Paige and K. D. Keegan. Thermal and albedo mapping of the polar regions of Mars using Viking thermal mapper observations: 2. South polar region. *Journal of Geophysical Research*, 99:25993–26013, 1994.

D. A. Paige, K. E. Herkenhoff, and B. C. Murray. Mariner 9 observations of the south polar cap of mars: Evidence for residual co_2 frost. *Journal of Geophysical Research: Solid Earth*, 95:1319–1335, 1990.

D. A. Paige, J. E. Bachman, and K. D. Keegan. Thermal and albedo mapping of the polar regions of Mars using Viking thermal mapper observations: 1. North polar region. *Journal of Geophysical Research*, 99:25959–25991, 1994.

K. Pasquon, J. Gargani, M. Massé, and S. J. Conway. Present-day formation and seasonal evolution of linear dune gullies on Mars. *Icarus*, 274:195–210, 2016.

K. Pasquon, J. Gargani, M. Nachon, S.J. Conway, M. Massé, G. Jouannic, M.R. Balme, F. Costard, and M. Vincendon. Are different martian gully morphologies due to different processes on the kaiser dune field? *Geological Society, London, Special Publications*, 467, 2018.

J. D. Pelletier, K. J. Kolb, A. S. McEwen, and R. L. Kirk. Recent bright gully deposits on mars: Wet or dry flow? *Geology*, 36(3):211–214, 2008.

R.J. Phillips, B.J. Davis, K.L. Tanaka, S. Byrne, M.T. Mellon, and et al. Massive co2 ice deposits sequestered in the south polar layered deposits of mars. *Science*, 332 (6031):838–841, 2011.

C. Pilorget and F. Forget. Formation of gullies on Mars by debris flows triggered by CO_2 sublimation. *Nature Geoscience*, 9:65–69, 2016.

S. Piqueux and P. R. Christensen. North and south subice gas flow and venting of the seasonal caps of Mars: A major geomorphological agent. *Journal of Geophysical Research (Planets)*, 113, 2008.

S. Piqueux, S. Byrne, and M. I. Richardson. Sublimation of Mars's southern seasonal CO_2 ice cap and the formation of spiders. *Journal of Geophysical Research (Planets)*, 108:3–1, 2003.

Piqueux, S. and Kleinbahl, A. and Hayne, P.O. and Kass, D.M. and Schofield, J.T. and McCleese, D.J. Variability of the martian seasonal CO2 cap extent over eight Mars Years. *Icarus*, 251:164 – 180, 2015.

Knauth P.L. and D.M. Burt. Eutectic brines on mars: Origin and possible relation to young seepage features. *Icarus*, 158(1):267 – 271, 2002.

G. Portyankina, W.J. Markiewicz, N. Thomas, C.J. Hansen, and M. Milazzo. Hirise observations of gas sublimation-driven activity in mars's southern polar regions: Iii. models of processes involving translucent ice. *Icarus*, 205(1):311 – 320, 2010.

G. Portyankina, K.-M. Aye, and C. J. Hansen. Diffusion-Limited Aggregation Model for Araneiform Pattern Formation. In *Lunar and Planetary Science Conference*, volume 48, page 2441, 2017a.

G. Portyankina, C. J. Hansen, and K.-M. Aye. Present-day erosion of Martian polar terrain by the seasonal CO_2 jets. *Icarus*, 282:93–103, 2017b.

G. Portyankina, J. Merrison, J.J. Iversen, Z. Yoldi, C.J. Hansen, K.-M. Aye, A. Pommerol, and N. Thomas. Laboratory investigations of the physical state of co_2 ice in a simulated martian environment. *Icarus*, 2018.

Portyankina, G. and Merrison, J. and Iversen, J.J. and Yoldi, Z. and Hansen, C.J. and Aye, K.-M. and Pommerol, A. and Thomas, N. Laboratory investigations of the physical state of co2 ice in a simulated martian environment. *Icarus*, 322:210 – 220, 2019.

J. Raack, D. Reiss, T. Appéré, M. Vincendon, O. Ruesch, and H. Hiesinger. Present-day seasonal gully activity in a south polar pit (Sisyphi Cavi) on Mars. *Icarus*, 251: 226–243, 2015.

D. Reiss and R. Jaumann. Recent debris flows on mars: Seasonal observations of the russell crater dune field. *Geophysical Research Letters*, 30(6), 2003.

D. Reiss, S. van Gasselt, G. Neukum, and R. Jaumann. Absolute dune ages and implications for the time of formation of gullies in nirgal vallis, mars. *Journal of Geophysical Research: Planets*, 109, 2004.

D. Reiss, G. Erkeling, K. E. Bauch, and Hiesinger H. Evidence for present day gully activity on the russell crater dune field, mars. *Geophysical Research Letters*, 37(6), 2010.

J.R Royer, D.J Evans, L. Oyarte, Q. Guo, E. Kapit, M.E Möbius, S.R Waitukaitis, and H.M Jaeger. High-speed tracking of rupture and clustering in freely falling granular streams. *Nature*, 459(7250):1110–1113, 2009.

S.C. Schon, J.W. Head, and C.I. Fassett. Unique chronostratigraphic marker in depositional fan stratigraphy on mars: Evidence for ca. 1.25 ma gully activity and surficial meltwater origin. *Geology*, 37(3):207, 2009.

N. Schorghofer, O. Aharonson, and S. Khatiwala. Slope streaks on mars: Correlations with surface properties and the potential role of water. *Geophysical Research Letters*, 29(23):41–1–41–4, 2002.

N. Schorghofer, O. Aharonson, M.F. Gerstell, and L. Tatsumi. Three decades of slope streak activity on mars. *Icarus*, 191(1):132 – 140, 2007.

M. E. Schwamb, K.-M. Aye, G. Portyankina, C. J. Hansen, C. Allen, S. Allen, F. J. Calef, S. Duca, A. McMaster, and G. R. M. Miller. Planet Four: Terrains - Discovery of araneiforms outside of the South Polar layered deposits. *Icarus*, 308:148–187, 2018.

D.H Scott and M.H Carr. Geologic map of Mars, 1978.

J. E. C. Scully, C. T. Russell, A. Yin, R. Jaumann, E. Carey, J. Castillo-Rogez, H. Y. McSween, C. A. Raymond, V. Reddy, and L. Le Corre. Geomorphological evidence for transient water flow on Vesta. *Earth and Planetary Science Letters*, 411:151–163, 2015.

A. Séjourné, F. Costard, J. Gargani, R. J. Soare, and C. Marmo. Evidence of an eolian ice-rich and stratified permafrost in Utopia Planitia, Mars. *Planetary and Space Science*, 60:248–254, 2012.

A. Shields. *Application of similarity principles and turbulence research to bed-load movement*. PhD thesis, CalTech, Soil Conservation Service, 1936.

T. Shinbrot, N.-H. Duong, L. Kwan, and M. M. Alvarez. Dry granular flows can generate surface features resembling those seen in martian gullies. *Proceedings of the National Academy of Sciences*, 101(23):8542–8546, 2004.

S. Silvestro, L. K. Fenton, D. A. Vaz, N. T. Bridges, and G. G. Ori. Ripple migration and dune activity on mars: Evidence for dynamic wind processes. *Geophysical Research Letters*, 37(20), 2010.

D.E. Smith, M.T. Zuber, S.C. Solomon, R.J. Phillips, J.W. Head, and et al. The global topography of mars and implications for surface evolution. *Science*, 284 (5419):1495–1503, 1999.

D.E. Smith, M.T. Zuber, and G.A. Neumann. Seasonal variations of snow depth on Mars. *Science*, 294(5549):2141–2146, 2001.

Soare, R.J. and Conway, S.J. and Godin, E. and Hawkswell, J. and Osinski, G. and Bina, A. Possible ice-wedge polygonisation in Utopia Planitia, Mars, and its Poleward Latitudinal Gradient. 2018.

Soare, R.J. and Conway, S.J. and Williams, J.-P. and Gallagher, C. and Mc Keown, L.E. Possible (closed system) pingo and ice-wedge/thermokarst complexes at the mid latitudes of Utopia Planitia, Mars. *Icarus*, 2019.

M. E. Sylvest, S. J. Conway, M. R. Patel, J. C. Dixon, and A. Barnes. Mass wasting triggered by seasonal CO_2 sublimation under Martian atmospheric conditions: Laboratory experiments. *Geophysical Research Letters*, 43:12, 2016.

M.E. Sylvest, J.C. Dixon, S.J. Conway, M.R. Patel, J.N. McElwaine, A. Hagermann, and A. Barnes. Co_2 sublimation in martian gullies: laboratory experiments at varied slope angle and regolith grain sizes. *Geological Society, London, Special Publications*, 467, 2018. doi: 10.1144/SP467.11.

N. Thomas, C. J. Hansen, G. Portyankina, and P. S. Russell. HiRISE observations of gas sublimation-driven activity in Mars's southern polar regions: II. Surficial deposits and their origins. *Icarus*, 205:296–310, 2010.

N. Thomas, G. Portyankina, C. J. Hansen, and A. Pommerol. HiRISE observations of gas sublimation-driven activity in Mars's southern polar regions: IV. Fluid dynamics models of CO_2 jets. *Icarus*, 212:66–85, 2011.

P. C. Thomas, M. C. Malin, K. S. Edgett, M. H. Carr, W. K. Hartmann, A. P. Ingersoll, P. B. James, L. A. Soderblom, J. Veverka, and R. Sullivan. North-south geological differences between the residual polar caps on Mars. *Nature*, 404:161–164, 2000.

P.C. Thomas, Malin M.C., P.B. James, B.A. Cantor, R.M.E. Williams, and P. Gierasch. South polar residual cap of mars: Features, stratigraphy, and changes. *Icarus*, 174:535 – 559, 2005.

P.C. Thomas, W. Calvin, B. Cantor, R. Haberle, P.B. James, and S.W. Lee. Mass balance of mars's residual south polar cap from ctx images and other data. *Icarus*, 268:118 – 130, 2016.

T.N. Titus, H.H. Kieffer, K.F. Mullins, and P.R. Christensen. Tes premapping data: Slab ice and snow flurries in the martian north polar night. *Journal of Geophysical Research: Planets*, 106:23181–23196, 2001.

T.N. Titus, H.H. Kieffer, and P.R. Christensen. Exposed water ice discovered near the south pole of mars. *Science*, 299(5609):1048–1051, 2003. doi: 10.1126/science.1080497.

J. Touma and J. Wisdom. The chaotic obliquity of mars. *Science*, 259(5099):1294–1297, 1993.

A.H. Treiman. Geologic settings of martian gullies: Implications for their origins. *Journal of Geophysical Research: Planets*, 108, 2003.

E. Védie, F. Costard, M. Font, and J. L. Lagarde. Laboratory simulations of martian gullies on sand dunes. *Geophysical Research Letters*, 35(21), 2008.

A.K. Verma and M.C. Bourke. A structure from motion photogrammetry-based method to generate sub-millimetre resolution digital elevation models for investigating rock breakdown features. *Earth Surface Dynamics Discussions*, pages 1–34, 2018.

M. Vincendon. Identification of Mars gully activity types associated with ice composition. *Journal of Geophysical Research (Planets)*, 120:1859–1879, 2015.

W.R. Ward. Climatic variations on mars: 1. astronomical theory of insolation. *Journal of Geophysical Research*, 79(24):3375–3386, 1974.

W.R. Ward, B.C. Murray, and M.C. Malin. Climatic variations on mars: 2. evolution of carbon dioxide atmosphere and polar caps. *Journal of Geophysical Research*, 79 (24):3387–3395, 1974.

M.J. Westoby, J. Brasington, N.F. Glasser, M.J. Hambrey, and J.M. Reynolds. Structure-from-Motion photogrammetry: A low-cost, effective tool for geoscience applications. *Geomorphology*, 179:300 – 314, 2012.

M.T. Zuber, R.J. Phillips, J.C. Andrews-Hanna, S.W. Asmar, A.S. Konopliv, F.G. Lemoine, J.J. Plaut, D.E. Smith, and S.E. Smrekar. Density of Mars's South Polar Layered Deposits. *Science*, 317(5845):1718–1719, 2007.

R. W. Zurek and S. E. Smrekar. An overview of the Mars Reconnaissance Orbiter (MRO) science mission. *Journal of Geophysical Research (Planets)*, 112, 2007.